UNIVERSIDAD DE CONCEPCIÓN
FACULTAD DE CIENCIAS FÍSICAS Y MATEMÁTICAS

NEUTRON STARS MODELS IN 4D EINSTEIN-GAUSS-BONNET GRAVITY

Por: Alejandro Andrés Saavedra San Martín

Tesis presentada a la Facultad de Ciencias Físicas y Matemáticas de la Universidad de Concepción para optar al grado académico de Magíster en Ciencias con Mención en Física

Enero 2025
Concepción, Chile

Profesor Guía: Dr. Guillermo Rubilar Alegría
Dr. Octavio Fierro Mondaca

A mis hermanos.

AGRADECIMIENTOS

Antes de entrar en contenido, quisiera tomarme un momento para expresar mi gratitud a las personas que han sido fundamentales durante el transcurso de mi carrera y el magíster.

En primer lugar, quiero agradecer especialmente a mis hermanos por su apoyo incondicional durante estos seis años, que no han sido sencillos. También agradezco profundamente el apoyo de mi tía Katty y mi abuelita.

En este arduo camino de aprendizaje, tuve la fortuna de contar con la guía y el apoyo de varios profesores. En particular, agradezco a mi profesor guía, el Dr. Guillermo Rubilar, por aceptarme como estudiante, por su paciencia y claridad al enseñar física, por las interesantes discusiones acompañadas de un buen café, por confiar en mí y por sus constantes consejos y apoyo, incluso en los momentos más difíciles. Por supuesto, también agradecer los almuerzos compartidos junto a mi profesor co-guía, el Dr. Octavio Fierro, a quien agradezco su apoyo, enseñanzas, consejos y dedicación dado durante este proyecto.

Mi gratitud también al Dr. Julio Oliva por lo mucho que aprendí en sus cursos, por su apoyo constante y por su compromiso con sus estudiantes; al Dr. Pablo Solano, por los conocimientos adquiridos en sus cursos, en especial por su visión fenomenológica en el curso de Física Estadística, que contribuyeron significativamente a mi formación científica; y al Dr. Robert Mann, por su valiosa colaboración y comentarios iluminadores en este proyecto, así como al MSc. Michael Gammon por su aporte en esta colaboración. Agradezco enormemente a todos los miembros de la comisión por su tiempo y consideración al formar parte de mi defensa de tesis. Asimismo, extiendo un especial agradecimiento al Dr. Joaquín Díaz De Valdés por sus motivadoras clases, en particular las de Electromagnetismo.

Quisiera dedicar este párrafo especialemente a mis amigos, futuro de la física: Luis U. (Lucho), Adheris C., Tomás M. (Tomi), Lilianne T. (Lily), Constanza R. (Connie), Constanza V., Daniel J., Cielo R. y Evángelo D. Gracias por acompañarme durante estos años de carrera, especialmente en los dos años de magíster, por su amistad, su apoyo en los buenos y malos momentos, por las salidas, las alegrías, las risas y, sobre todo, por ser un espacio seguro para mí. Les

deseo lo mejor; los quiero mucho.

Sin olvidar a mis amigos del colegio, a quienes agradezco desde la distancia: Mabel L., Matías M. y Cristóbal N.

A las personas de la sala de posgrado y de la carrera, fue un placer compartir estos años con ustedes. En especial, agradezco con cariño a: Danilo R., Nicole G., Pedro C., Martín Q., Benjamín H., Francisco J., Aníbal N., María Ignacia E., Florencia F., Martín G. y Martín S.

También quiero expresar mi gratitud a las secretarias y pilares del Departamento de Física: Nilsa G., Julia H. y Yarerla Soledad D., por su constante ayuda y gestión tanto durante la carrera como en el magíster.

Agradezco también a todos los estudiantes de Física, Astronomía, Ingeniería y Pedagogía en Matemática con quienes tuve el placer de realizar ayudantías, ya sea en ramos de física o matemáticas. Espero haberlos ayudado, aunque sea un poco, en su proceso de aprendizaje.

Finalmente, agradezco a mi pareja Vicente C. por su apoyo constante y amor durante este último año de tesis.

Agradezco a la Dirección de Postgrado por otorgarme la beca de estipendio.

Resumen

El estudio de objetos compactos en teorías modificadas de la gravedad expande nuestra descripción de la física gravitacional más allá de la Relatividad General (RG). En particular, las estrellas de neutrones son objetos con altas densidades y fuertes campos gravitacionales, lo que las convierte en laboratorios ideales para testear los límites de la teoría de Einstein en condiciones extremas. En esta tesis, encontramos soluciones numéricas de estrellas de neutrones en gravedad 4D Einstein-Gauss-Bonnet (4DEGB) usando ecuaciones de estado (EdEs) realistas para describir todas las regiones en el interior de una estrella de neutrones. En particular, usamos la EdE SLy (Skyrme Lyon) y MS2 (Müller and Serot), previamente utilizadas por Charmousis et al. (2022), en conjunto con la familia de EdEs BSk (Brussels-Montreal Skyrme functionales), la cual incorpora refinamientos a la EdE SLy para mejorar el ajuste tanto a las propiedades de la materia nuclear como a las observaciones de estrellas de neutrones. Con el fin de proporcionar las condiciones necesarias para la existencia de dichas soluciones, analizamos la estabilidad de las mismas a través de perturbaciones radiales adiabáticas. Encontramos que el cambio de estabilidad ocurre en la configuración de masa máxima, como en RG, obteniendo estrellas de neutrones estables con masas más grandes comparadas con las de la teoría de Einstein. Además, la brecha de masa entre las estrellas de neutrones y los agujeros negros de los mismos radios se reduce a medida que aumentamos la constante de acoplamiento de la teoría 4DEGB. La reducción de esta brecha de masa indica que algunos objetos astrofísicos (dentro de esta teoría) podrían ser estrellas de neutrones masivas u objetos más exóticos en lugar de agujeros negros. Nuestros hallazgos ofrecen valiosas contribuciones a la comprensión de los objetos compactos en el marco de la gravedad 4DEGB.

Abstract

The study of compact objects in modified theories of gravity expands our description of gravitational physics beyond General Relativity (GR). In particular, neutron stars (NS) are objects with high densities and strong gravitational fields, establishing them as ideal laboratories to test the limits of Einstein's theory under extreme conditions. In this thesis, we find numerical solutions of NS in 4D Einstein-Gauss-Bonnet (4DEGB) gravity using realistic equations of state (EOSs) to describe all regions inside a NS. In particular, we employ the SLy (Skyrme Lyon) and MS2 (Müller and Serot) EOSs, previously used by Charmousis et al. (2022), along with the BSk (Brussels-Montreal Skyrme functionals) family of EOSs, which incorporate refinements to SLy EOS to improve the fit to both nuclear matter properties and neutron star observations. In order to provide necessary conditions for the existence of such solutions, we analyzed the stability of these configurations by adiabatic radial perturbations. We found that the change of stability occurs at the maximum mass configuration, as in GR, obtaining stable neutron stars with greater mass compared to neutron stars in Einstein's theory. In addition, the mass gap between neutron stars and black holes of the same radii is reduced as we increase the coupling constant of the 4DEGB theory. The reduction of this mass gap indicates that some astrophysical objects (within this theory) could be massive neutrons stars or more exotic objects instead of black holes. Our findings offer valuable contributions to the understanding of compact objects within the framework of 4DEGB gravity.

Contents

List of Tables

List of Figures

Chapter 1

Introduction

1.1 Compact objects

When a star consumes most of its nuclear fuel, it approaches the final stage of its life cycle. Depending on the size and mass of the star, its life will end in one of two ways: either as a white dwarf (WD) or as a supernova explosion. In the latter case, the implosion of the core will leave behind a small, dense core of tightly packed neutrons called a neutron star (NS) or, a black hole with a gravitational field so powerful that not even light can escape it. In this work, we focus on neutron stars, but we briefly discuss white dwarfs.

The possible states of compact objects such as white dwarfs and neutron stars can be modeled given a model of the gravitational interaction and an equation of state (EOS), which amounts to a relation between the pressure and the density inside the star considering their composition and interactions. Polytropes are self-gravitating gaseous spheres that were very useful as a crude approximation to more realistic stellar models. The polytropic EOS is

$$P = K\rho^{\Gamma}, \tag{1.1.1}$$

where K and Γ are constants, the latter being the adiabatic or polytropic index [1]. Chandrasekhar [2] found that for the polytropic index $\Gamma = 4/3$, white dwarfs can only exist below a maximun mass $M_{\max} = 1.42\ \mathrm{M}_{\odot}$, known as the Chandrasekhar limit. This EOS does not contain information about the physical origin of the pressure that prevents the stellar collapse. Fowler [3] was the first who realized

that for studying highly dense matter, in particular white dwarfs, one needs to go beyond classical physics, i.e. to quantum physics. He understood that white dwarfs owe their stability to the quantum pressure of the degenerate electron gas resulting from the Pauli exclusion principle. Therefore, a first good approximation for a stellar model is to consider the star as gaseous sphere of non-interacting fermions at zero temperature, based on the fact that the temperature in white dwarfs is much smaller than the Fermi temperature, according to Newtonian gravity theory [4]. Using this EOS we also obtain the Chandrasekhar mass limit, because if we take the non-relativistic and ultra-relativistic limits, the Fermi EOS reduces to a polytropic one with polytropic index $\Gamma = 5/3$ and $\Gamma = 4/3$, respectively [1], see figure 1.1.1a.

As the density of a white dwarf enters the relativistic (electron) domain ($\rho \sim 10^6$ g/cm^3), we could expect to approach the Chandrasekhar limit. However, this never happens because, before that, the high densities inside the stellar core allow for a nuclear reaction known as inverse beta decay,

$$p + e^- \longrightarrow n + \nu_e, \tag{1.1.2}$$

where a neutron is created by capture of an electron in the nucleus (and an electron neutrino is emitted). This process changes the composition of the white dwarf before its total collapse to a star mainly composed of neutrons, there the new equilibrium state is reached due to the degeneration pressure of these fermions, thus forming neutron stars. If the Fermi EOS at zero temperature is used, we obtain that the Chandrasekhar mass limit is $M_{\max} = 5.73\ \mathrm{M}_\odot$ [5], see figure 1.1.1b.

If the gravitational theory is changed to General Relativity (GR), the hydrostatic equilibrium equation is replaced by the Tolman-Oppenheimer-Volkoff equation (T.O.V.) [6]:

$$\frac{dP}{dr} = -\frac{G\mathcal{M}(r)\rho(r)}{r^2}\left[1+\frac{P(r)}{\rho c^2}\right]\left[1+\frac{4\pi r^3 P(r)}{\mathcal{M}(r)c^2}\right]\left[1-\frac{2G\mathcal{M}(r)}{c^2 r}\right]^{-1}. \tag{1.1.3}$$

The last three factors are general relativistic corrections. For instance, a typical white dwarf has $GM/c^2R \approx 10^{-4}$ and a neutron star has $GM/c^2R \approx 10^{-1}$. Therefore, the general relativistic (or from other modified gravitational theory) effects are more significant in neutron star than in white dwarfs, see figures 1.1.1a

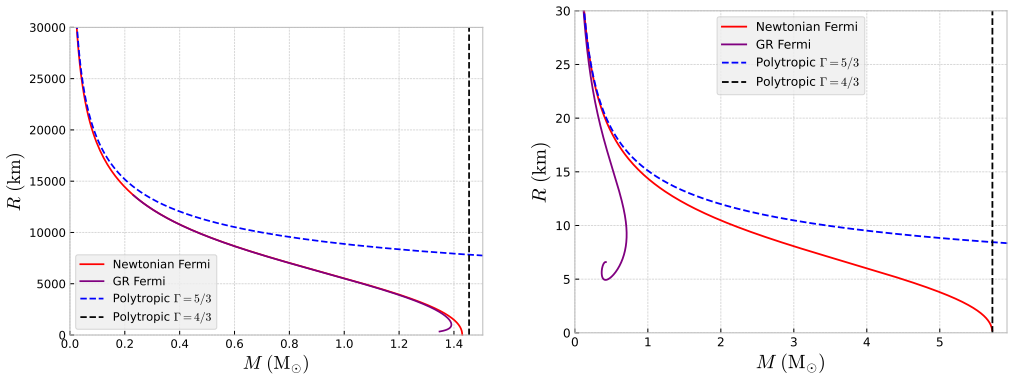

(a) White dwarfs **(b)** Neutron stars

Figure 1.1.1: Mass-radius relation for neutron stars in the cases of the Fermi, non-relativistic ($\Gamma = 5/3$) and ultra-relativistic ($\Gamma = 4/3$) polytropic EOS in Newtonian gravity and in General Relativity.

and 1.1.1b for an illustration.

Oppenheimer and Volkoff [6] made the first calculation of a neutron star model. They assumed that matter was composed of an ideal gas of free neutrons at high density. They found that equilibrium configurations exist only below a maximum mass $M_{\max} = 0.710\ \mathrm{M}_\odot$ and radius $R = 9.16$ km (4.37 times the corresponding Schwarzschild radius), now known as the Oppenheimer–Volkoff mass limit. However, current observations show that neutron stars can have masses in the range $1\ \mathrm{M}_\odot - 2\ \mathrm{M}_\odot$ and radius of about $10\ \mathrm{km} - 15\ \mathrm{km}$ [5]. Therefore, they must avoid the gravitational collapse by pressure originating, for example, from nuclear forces. The arising problem is that for neutron star densities the reliability of many-body nuclear theory decreases and there is little experimental information on the contributions of hyperons, quarks, phase transitions, etc. Thus, the EOS at these densities requires to extrapolate calculations based on phenomenological models of the nuclear force as well as in effective field theory models of quantum chromodynamics (QCD) [7].

Among possible observables regarding neutron stars, the mass and radius are the most important, since they can be used to constrain the neutron star EOS within a certain observational uncertainty. The masses of several neutron stars are known with good precision, but the information on their radii is less accurate. One of the most precise measurements of neutron star masses come from pulsar timing. For radii, the approaches can broadly be divided into spectroscopic and timing measurements where data sets come from X-ray and γ-ray satellites [8].

Nevertheless, both measurements are crucial to constrain the EOS. In 2017, the observations of gravitational waves (GW170817) emitted during the merger of a neutron star binary [9–11] has given a new way of obtaining information on their masses and radii, by measuring the tidal deformability, allowing to deduce upper and lower limits for the masses and radii [8]. This allowed to impose constraints on the EOS of matter at supranuclear densities.

1.2 A modified theory of gravity

General Relativity is doubtlessly a very successful theory of gravity that has passed all observational tests to date. Nonetheless, modified theories of gravity have been explored for several reasons. For instance, the current accelerated expansion of the Universe, which according to the classical cosmological models is caused by the cosmological constant. There is, however, no consistent explanation of the value of the cosmological constant [12]. For this and other reasons it is theorized that GR could be modified at the large scale regime. We also have the theoretical problem of finding a consistent quantum gravity theory. Such a pursuit of modified gravitational models can help us understand GR and gravity more deeply and have more confidence in that theory.

An approach to confront these problems is to propose modifications to the theory of General Relativity by modifying the 4D Einstein-Hilbert action with cosmological constant either by adding i) nonlinear curvature terms, such as $f(R)$ theories, critical gravity [13], Einstenian cubic gravity [14], quasitopological gravities, etc, and/or ii) including scalar fields, as in Horndeski theories [15], Dilaton Einstein theories, Einstein conformally coupled to scalar fields, etc.

Lovelock's theorem [16] states that the only $(3+1)$-dimensional gravity theory which possesses diffeomorphism invariance, metricity, and second order equations of motion is Einstein's theory of gravity. Higher order terms vanish identically in 4 spacetime dimensions or less ($D \leq 4$). The first of these higher terms is the Gauss Bonnet (GB) term which is quadratic in the curvature and is the integral of a total derivative in $D = 4$, thus contributing nothing to the system's dynamics. However, it was recently shown [17] that the Gauss-Bonnet contribution to solutions to the D-dimensional field equations can be non-trivial for $D \to 4$ under a rescaling of the GB coupling constant. Despite this apparent violation of the Lovelock

theorem, a number of sensible 4-dimensional metrics can be obtained. This was done for spherical black holes [17–21], cosmological solutions [17, 22, 23], star-like solutions [24, 25], radiating solutions [26], collapsing solutions [27], etc.

In reality the existence of such solutions does not actually imply the existence of a well-defined 4D theory, and a number of objections in this vein quickly appeared [28–30]. Two independent groups [31, 32] derived consistent versions of what has come to be known as 4D Einstein-Gauss-Bonnet (4DEGB) gravity, making use of the same rescaling first introduced by Glavan and Lin [17]. In both cases a scalar field is introduced into the action making 4DEGB gravity a Horndeski theory of gravity.

This 4DEGB gravity has been shown to be an interesting phenomenological competitor to GR [25, 33, 34]. One important test of modified theories against standard General Relativity is via observations of compact astrophysical objects like neutron stars. The correct theory should be able to accurately describe recent and future gravitational wave observations of astrophysical objects existing in the mass gap between the heaviest compact stars and the lightest black holes. A number of such objects have been recently observed that are inconsistent with standard GR and a simple neutron star EOS. Recently it was shown that the secondary component of the merger GW190814 [35] is well described as a slowly-rotating neutron star in the 4DEGB theory without resorting to exotic EOSs, while also demonstrating that the equilibrium sequence of neutron stars asymptotically matches the minimum mass black hole solution, thus closing the mass gap between NS and black holes of the same radius [25]. Such solutions beg the question of stability since if we analyze the radial oscillations in GR of an uncharged, spherical, gravitating compact star, it is stable in the part of the solution branch where $dM/d\rho_c \geq 0$ and the transition to instability happens at the maximum mass solution [36]. In the literature, it has been unclear whether including non-vanishing coupling to the 4DEGB theory will have a similar offsetting effect, and whether the parts of the solution curves corresponding to extreme compact objects could exist in a universe described by the 4DEGB theory. If there are indeed stable solutions that approach the black hole horizon, then for that set of parameters we can expect an universe with compact stars with radii arbitrarily close to the horizon size of black holes.

1.3 Hypothesis and Objectives

Our hypothesis is that neutron stars solutions obtained in 4DEGB gravity deviate from those predicted by General Relativity, obtaining more massive stars. However, the change of stability also occurs at the maximum mass solution.

To verify this hypothesis, our main objective is to study neutron stars in 4DEGB using realistic equations of state at zero temperature. Specifically, we aim to:

1. Derive the hydrostatic equilibrium equations in 4DEGB.
2. Determine the eigenvalue problem for the radial oscillations in 4DEGB.
3. Find numerical solutions of the hydrostatic equilibrium equations and the eigenfrequencies of the radial oscillation modes.
4. Contrast the results with the predictions of General Relativity.

This thesis is organized as follows:

- In chapter 2 we provide a review of the structure of neutron stars and the EOSs for highly dense matter. The analytical representations of the EOSs that we will use through this thesis are also discussed in this chapter.
- In chapter 3 we review the theory of General Relativity, starting from the Einstein-Hilbert action (and omitting the mathematical preliminaries, as it is assumed the reader already has a basic understanding of differential geometry). Next, we review the Schwarzschild solution and the derivation of the hydrostatic equilibrium equation for GR, the T.O.V. equation. We conclude with numerical solutions of static NS configurations, followed by an analysis of the stability of these solutions through adiabatic radial oscillations, following the approach by Chandrasekhar [37].
- In chapter 4 we introduce the 4DEGB gravity theory derived in Ref. [31] and [32], followed by an exact solution of the field equations which represents the spacetime of a non-rotating black hole in this theory. We also derive the hydrostatic equilibrium equations and the radial oscillation equations. We compute numerical solutions of the hydrostatic equilibrium equations and the radial oscillation equations in 4DEGB. Finally, we conclude with an analysis of these solutions comparing their stability in GR and 4DEGB.

Chapter 2

Equations of State for Neutron Stars

2.1 Thermodynamics in curved spacetime

Consider the equilibrium thermodynamics of a **perfect fluid**, that is, a fluid that can be completely characterized by its rest frame energy density ϵ and isotropic pressure P, neglecting the shear stresses, viscosity and heat conduction that the fluid may have. The thermodynamic state of a fluid element can be characterized by various thermodynamic potential n, ϵ, P, T and s. All of these quantities are referred to a local reference frame comoving with the fluid element. The formal definitions of these thermodynamic potentials are as follows:

- n, baryon number density, i.e., the number of baryons per unit comoving three-dimensional volume.
- ϵ, total energy density, i.e., the total energy (including rest energy, thermal energy, etc.) contained in a unit comoving three-dimensional volume.
- P, isotropic pressure in the rest frame.
- T, temperature in the rest frame.
- s, entropy per baryon in the rest frame.

The most fundamental law of thermodynamics is baryon conservation. Consider a fluid element whose moving walls are attached to the fluid so that baryons flow in or out. As the fluid element moves, it deforms along the way changing its volume,

but the number of baryons remains fixed, thus

$$\frac{d}{d\tau}(nV) = 0, \tag{2.1.1}$$

where τ is the time measured by a comoving observer with the fluid element. The changes in volume are produced by the flow of neighboring fluid pieces moving away from or toward each other, explicitly, [38]

$$\frac{dV}{d\tau} = (\nabla_\mu u^\mu)V, \tag{2.1.2}$$

where $u^\mu := dx^\mu/d\tau$ is the 4-velocity of the fluid. Consequently, the baryon conservation equation (2.1.1) can be expressed as

$$\begin{aligned} 0 = \frac{dn}{d\tau} + \frac{n}{V}\frac{dV}{d\tau} &= \frac{dx^\mu}{d\tau}\partial_\mu n + n\nabla_\mu u^\mu \\ &= u^\mu \nabla_\mu n + n\nabla_\mu u^\mu \\ &= \nabla_\mu (nu^\mu); \end{aligned} \tag{2.1.3}$$

that is,

$$\nabla_\mu S^\mu = 0, \tag{2.1.4}$$

with $S^\mu := nu^\mu$ the baryon number flux 4-density. Equation (2.1.4) is known as the **baryon conservation law**.

The **first law of thermodynamics**, in the proper reference frame of a fluid element, is identical to the first law in flat spacetime because of the *principle of equivalence*. Thus, we can write

$$d\left(\frac{\epsilon}{n}\right) = -Pd\left(\frac{1}{n}\right) + đQ, \tag{2.1.5}$$

where $đQ$ is the heat gained per baryon. It is convenient to define these quantities in terms of n, since it is a conserved quatity.

If a process occurs in a fluid element that is in equilibrium at all times (quasi-static process), then $đQ = Tds$. Under this condition, we can write the equation (2.1.5) as follow:

$$d\left(\frac{\epsilon}{n}\right) = -Pd\left(\frac{1}{n}\right) + Tds. \tag{2.1.6}$$

By developing equation (2.1.6) a little further, we can write the first law of thermodynamics as

$$d\epsilon = \frac{\epsilon + P}{n} dn + nT ds. \tag{2.1.7}$$

In writing equation (2.1.6), we are assuming that ϵ/n is a function only of n and s, i.e., $\epsilon = \epsilon(n, s)$. In addition, it allows us to express the thermodynamic potentials P and T as derivaties of the energy per baryon:

$$P = -\frac{\partial(\epsilon/n)}{\partial(1/n)} = n^2 \frac{\partial(\epsilon/n)}{\partial n}, \tag{2.1.8}$$

$$T = \frac{\partial(\varepsilon/n)}{\partial s}. \tag{2.1.9}$$

From equation (2.1.8) we can conclude that, in general, $P = P(n, s)$ or $P = P(n, T)$. Moreover, if we consider the mass density $\rho = \epsilon/c^2$, then ρ is a function of the baryon number density n and the entropy per baryon, in this case, the **equation of state** (EOS) for the star, modeled as a perfect fluid, is given by

$$P = P(n, s), \qquad \rho = \rho(n, s), \tag{2.1.10}$$

or,

$$P = P(n, T), \qquad \rho = \rho(n, T). \tag{2.1.11}$$

Nevertheless, if the temperature of the star is negligible, which it will be the case of a neutron star, the entropy per baryon will be constant for the whole star according to Nernst's heat theorem [39]. The EOS in this scenario is simply a relation between P and ρ of the form $P = P(\rho)$.

An important quantity that characterizes the relationship between pressure and density (e.g. the stiffness) under adiabatic conditions is the **adiabatic index**, denoted by Γ and defined as [38]

$$\Gamma := \frac{n}{P} \left(\frac{\partial P}{\partial n} \right)_s. \tag{2.1.12}$$

Using the first law of thermodynamics (2.1.7), we have

$$\left(\frac{\partial \epsilon}{\partial n} \right)_s = \frac{\epsilon + P}{n}. \tag{2.1.13}$$

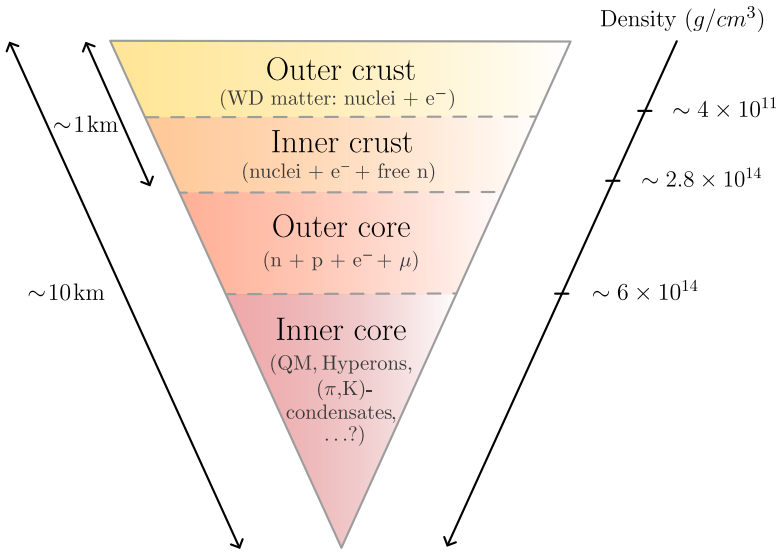

Figure 2.2.1: Internal structure of a neutron star.

Thus, if we suppose that $P = P(\epsilon(n))$, we can write the adiabatic index as

$$\Gamma = \frac{\epsilon + P}{P} \left(\frac{\partial P}{\partial \epsilon} \right)_s . \tag{2.1.14}$$

Another quantity with the same importance for the EOS is the speed of sound [40]

$$v_s := \sqrt{\frac{dP}{d\rho}}. \tag{2.1.15}$$

2.2 The structure of a Neutron Star

Before discussing the equations of state for matter inside a neutron star, we start with a brief overview of the structure of a neutron star. The cross section of a typical neutron star can be divided into the following regions (see figure 2.2.1) [5, 40, 41]:

1. The **outer crust** which is found underneath an atmosphere of just about 1 cm thickness. It consists of a lattice of completely ionized nuclei with a degenerate electron gas, i.e., white dwarf matter. In this layer the density increases to about 4×10^{11} g/cm^3; its thickness is typically a few hundred meters.

2. The **inner crust** starts at $\rho \sim 4 \times 10^{11}$ g/cm^3 and is less than 1 km thick, at which point the density has reached the value $\rho \sim 2.8 \times 10^{14}$ g/cm^3. In addition to a increasingly neutron-rich nuclei and degenerate relativistic electrons, it contains also a degenerate neutron gas, which may be a superfluid.

3. The **outer core** starts at $\rho \sim 2.8 \times 10^{14}$ g/cm^3 to $\rho \sim 6 \times 10^{14}$ g/cm^3. This layer consists mainly of neutrons, which are possibly superfluid in a certain density domain. In order to maintain the balance of the weak interaction processes, a few percents of the nucleons have to be protons, which are neutralized by electrons and muons.

4. The **inner core** starts at $\rho \sim 6 \times 10^{14}$ g/cm^3, where all atomic nuclei have been dissolved into their constituents, neutrons and protons. Due to the high Fermi pressure, the core might also contain hyperons, more massive baryon resonances, and possibly a gas of free up, down and strange quarks. Finally, π- and K-meson condensates may be found there too.

The composition of the central core is still unclear, but certainly consists in the outer part only of neutrons, protons, electrons and muons. Today, neutron stars come in various flavors depending on the composition of the core. In this respect, we speak now of traditional neutron stars (or **hadronic stars**), where the core mainly consists of neutrons, protons and electrons. At high densities, however, also heavier baryons are excited, the neutron star now becomes a **hyperon star**. Since these baryons are so densely packed, a quark bag could be formed, and quarks are probably in a color-superconducting state, forming a neutron star with a quark core. Finally, Bose condensates of pions and K mesons might occur [40].

2.3 Equations of state for highly dense matter

The state of matter at zero temperature is fully determined by its density and composition, and then the EOS reduces to a simple function $P = P(\rho)$. For low densities, $\rho < 500$ g/cm^3, the electrons cannot be treated as free and the pressure depends strongly on the electrostatic interactions between the atomic nuclei and the electrons, that is, it depends not only on the density but also on the atomic number Z [42]. This domain is of little interest to astrophysics (however, they are important for the physics of the Earth and other planets) because the lower

the pressure, the more we must consider the effect of the temperature upon the EOS at low temperatures: so that even at relatively low temperature the concept of cold matter is no longer applicable. All ordinary stars have central densities precisely in this region, for example, our Sun. In the case of compact stars such as white dwarfs and neutron stars, we need to go to a high density regime, where the effects of temperature are negligible. We will justify this statement as follows.

Cooling of neutron stars

When a neutron star is formed in the collapse of a stellar core it is very rapidly cooled by neutrino radiation. After about a day, the internal temperature drops to 10^9 K-10^{10} K. Photon emission overtakes neutrinos only when the internal temperature falls to $\sim 10^8$ K, with a corresponding surface temperature roughly two orders of magnitude smaller. Neutrino cooling dominates for at least the first three years, and typically for much longer [5].

For an ideal Fermi gas in equilibrium, the **Fermi-Dirac distribution function** f has the form [5]

$$f(E) = \frac{1}{e^{1+\frac{E-\mu}{kT}}}, \tag{2.3.1}$$

where $E = \sqrt{p^2c^2 + m^2c^4}$, m is the fermion mass, k is Boltzmann's constant, c the speed of light, p the magnitude of the momentum, T the temperature and μ is the chemical potential.

When temperatures are low, the fermions will go to the lowest available energy levels, being called **completely degenerate Fermi gas** in the limit $T \to 0$. For this case, the chemical potential $\mu = E_F$ is called **Fermi energy**, and the distribution function becomes a step function:

$$f(E) = \begin{cases} 1, & \text{if } E \leq E_F \\ 0, & \text{if } E > E_F \end{cases}. \tag{2.3.2}$$

The Fermi energy for a non-interacting ensemble of identical spin-1/2 fermions in a three-dimensional system is given by (relativistic limit) [43]

$$E_{\mathrm{F}} = \hbar c \left(\frac{3\pi^2 N}{V}\right)^{1/3}, \tag{2.3.3}$$

where N is the number of particles and V the volume of the system.

For a neutron star, suppose that $R = 10$ km and $\rho = 4.0 \times 10^{17}\,\mathrm{kg/m^3}$. Then,

$$\frac{N}{V} = \frac{\rho}{m} \approx 2.388 \times 10^{44}\ \mathrm{m^{-3}}. \tag{2.3.4}$$

Therefore, the Fermi energy is given by

$$E_\mathrm{F} \approx 6.0722 \times 10^{-11}\ \mathrm{J}. \tag{2.3.5}$$

and the Fermi temperature is

$$T_\mathrm{F} = \frac{E_\mathrm{F}}{k_\mathrm{B}} \approx 4.40 \times 10^{12}\ \mathrm{K}. \tag{2.3.6}$$

Thus, since the temperature of the neutron star shortly after its formation is lower by three (or more) orders of magnitude than the Fermi temperature, we can neglect the temperature of the neutron star.

There exist two main regimes of high density. As long as all nucleons are confined to nuclei, their contribution to the total pressure is negligible compared to that of the degenerate electrons. At some threshold density, ρ_drip, it becomes favorable for the nuclei to disintegrate, i.e. the neutrons drip out of the nuclei and form a nucleon gas. The standard EOS of Baym, Pethick and Sutherland (BPS) suggests that $\rho_\mathrm{drip} \lesssim 4 \times 10^{11}\ \mathrm{g/cm^3}$ [40]. One therefore distinguishes between the EOS below neutron drip and above the neutron drip density. For example, for WD we merely need the EOS below the neutron drip.

2.3.1 EOS below the neutron drip

In matter below the neutron drip, the EOS is governed mainly by an electron gas, and we may treat these electrons in a first approximation as an ideal fermion gas, where at extremely low densities Coulomb corrections have to be included. For high densities corrections enter through the neutronization just below the neutron drip.

This domain is subdivided into a region where the electrons are non-relativistic ($\rho < 10^6\ \mathrm{g/cm^3}$) and a region in which most of the electrons have an energy of the

order of, or larger than, its rest energy, i.e. relativistic ($\rho > 10^6$ g/cm^3). As the density increases in the relativistic domain, approaching neutron drip density for $\rho > 10^7$ g/cm^3 [5], electrons acquire enough energy to produce a type of nuclear reaction known as **inverse beta decay**:

$$p + e^- \quad \longrightarrow \quad n + \nu_e, \tag{2.3.7}$$

where a neutron is created by capturing an electron in the nucleus and an electron neutrino is simply emitted out of the system. The beta decay,

$$n \quad \longrightarrow \quad p + e^- + \overline{\nu}_e, \tag{2.3.8}$$

may interfere the creation of a star fully composed by neutrons. However, this reaction is blocked if the density is high enough that all electron energy levels in the Fermi sea are occupied up to the one that the emitted electron would fill.

The standard equations for cold, degenerate matter in white dwarfs (helium, carbon, oxygen, and possibly iron dominated models) have been derived by Chandrasekhar [1] and Hamada and Salpeter [44]. The Chandrasekhar EOS considers a star consisting only of an ideal, non-interacting electron gas (following the distribution function (2.3.2)), but the Hamada and Salpeter EOS refines the Chandrasekhar EOS by including Coulomb interactions, inverse beta decay and relativistic corrections, making it necessary to specify the chemical composition of the star. Models for matter for low densities, $\rho \leq 10^4$ g/cm^3, have been derived by Dirac (1930) and Feynman, Metropolis and Teller (1932). The matter is described in nuclear equilibrium and it is composed mainly by $^{56}_{26}$Fe nuclei with electrons model by the Thomas-Fermi-Dirac atomic model [5, 40].

The matter in neutron stars, below the neutron drip but above $\rho \geq 10^7$ g/cm^3 (where the neutronization begins), become progressively neutron rich (because of the inverse beta decay) until they begin losing neutrons (neutron drip). The parameters which characterize the nuclei, i.e. their mass and charge numbers (A, Z), are now functions of the density and are obtained by minimizing the total energy, that is, the sum of nuclear, lattice and electron energies. To identify the nuclei that are present at different density layers of the crust, experimental mass tables for known nuclei have been used. Two well-known EOSs for this regime are: the Harrison-Wheeler (HW) EOS and the Baym-Pethick-Sutherland (BPS) EOS

[45]. The latter considers the correction of Coulomb lattice energy in addition to the inverse beta decay.

2.3.2 EOS above the neutron drip

The EOSs above neutron drip can be divided into two regions. The first region covers the intermediate density regime from ρ_{drip} to nuclear density, $\rho_{\text{nuc}} = 2.8 \times 10^{14}$ g/cm^3, the density at which nuclei begin to dissolve and merge together [5]. The properties of dense matter are reasonably well understood in this density regime. In the second region above ρ_{nuc} (high density range), the physical properties of matter are still uncertain.

Below nuclear density

Above the neutron drip the electrons and nuclei coexist with free neutrons. The nuclei disappear at the upper end of this density range because their binding energy decreases with increasing density. Therefore, in this regime, the first approximation is to consider a neutron star as an ideal degenerate neutron gas following the distribution function (2.3.2), making the contribution of the nuclei to the total pressure negligible compared to that of the degenerate neutrons. Oppenheimer and Volkoff [6] were the first to do calculations in GR using this model which possesses a fully analytic expression given by [6]

$$P = \frac{K}{3}\left(\sinh(t) - 8\sinh\left(\frac{t}{2}\right) + 3t\right), \tag{2.3.9}$$

$$\rho = \frac{K}{c^2}\left(\sinh(t) - t\right), \tag{2.3.10}$$

where the constant K is

$$K := \frac{\pi m_{\text{n}}^4 c^5}{4h^3} \tag{2.3.11}$$

and the parameter t is defined as follows

$$t := 4\ln\left|x_{\text{F}} + \sqrt{1 + x_{\text{F}}^2}\right|, \quad x_{\text{F}} = \frac{p_{\text{F}}}{m_{\text{n}}c}. \tag{2.3.12}$$

Here we have denoted m_{n} the neutron mass and p_{F} the Fermi momentum defined by the Fermi energy $E_{\text{F}} = \sqrt{p_{\text{F}}^2 c^2 + m_{\text{n}}^2 c^4}$.

The EOS can be written in the polytropic form:

$$P = K\rho^{\Gamma}, \tag{2.3.13}$$

where Γ is the adiabatic index and K is a constant, in two limiting cases [5]:

1. Non-relativistic neutrons, $x_{\rm F} \ll 1$ or $\rho \ll 6 \times 10^{15}$ g/cm^3,

$$\Gamma = \frac{5}{3}, \quad K = \frac{3^{2/3}\pi^{4/3}}{5}\frac{\hbar^2}{m_{\rm n}^{8/3}}. \tag{2.3.14}$$

2. Extremely relativistic neutrons, $x_{\rm F} \gg 1$ or $\rho \gg 6 \times 10^{15}$ g/cm^3,

$$\Gamma = \frac{4}{3}, \quad K = \frac{3^{1/3}\pi^{2/3}}{4}\frac{\hbar c}{m_{\rm n}^{4/3}}. \tag{2.3.15}$$

For a more realistic treatment, the Baym, Bethe and Pethick (BPP) EOS is used. This EOS improved the approach made by HW and BPS in the determination of the mass of the atomic nuclei, incorporating results obtained from detailed many-body computations. One must account for the effects of the surrounding gas of free nucleons on the nuclei, as well as other effects such as nuclei surface and Coulomb energies making it a complicated calculation. Nonetheless, the properties of matter in this range of densities can still be derived by a natural extrapolation from ordinary nuclei. This EOS are based on the compressible liquid-drop model. For problems where a more accurate description of the neutron star inner crust is required, attention must be given to lattice effects, as the nuclei and free nucleons arrange in a distinct spatial structure (where the nuclei settle into bubbles, slabs or rods, depending on density). It is expected that at $\rho \approx \rho_{\rm nuc}/2$ all nuclei will have dissolved so that the matter is completely uniform [46].

Above nuclear density

The non-interacting gas approximation is not reliable for deriving the EOS above nuclear density. Unlike electrostatic perturbations, nucleon-nucleon interactions are not negligible, and the interaction energies are comparable to the Fermi energies of the degenerate nucleons (electrons do not feel the strong interaction, and may still be treated as noninteracting). Modeling of the nucleon-nucleon interaction is one of the longest-standing problems in nuclear physics, still only partially

solved. Profound difficulties exist due to the absence of a comprehensive theory of the interactions and the difficulty of obtaining experimental data. Moreover, the description of nuclear matter in the core of neutron stars ($\rho \approx \rho_{\text{nuc}}$) eludes the main tools of investigation of QCD, such as perturbation theory and the lattice formulation of the theory. The perturbation theory does not apply, since at the densities found in neutron star cores, QCD remains in a strongly coupled regime and lattice QCD works well only for vanishing or small baryon chemical potentials [47]. Instead, the most useful approaches are still based on phenomenological potential formalisms, because not only is the correct form of the nuclear potential still uncertain, but a totally satisfactory many-body computational method for solving the Schrödinger equation, given the potential, remains to be developed.

Current models for the EOS in this regime fall into two categories: **nonrelativistic variational approximation** and **relativistic field-theoretic approaches**. The first approach leads in general to acausal behavior at high densities, due to its basis on the nonrelativistic Schrödinger equation (we will see this when we plot the speed of sound).

Nonrelativistic approach

In this traditional approach one uses two-body potentials which are fitted to nucleon-nucleon scattering and three-body terms whose form is suggested in part by theory (two-pion exchange interaction) and purely phenomenological contributions, whose parameters are determined by the binding of few-body nuclei and saturation properties of nuclear matter. The effective nuclear Hamiltonian can be written as [41]

$$H = -\sum_i \frac{\hbar^2}{2m}\nabla_i^2 + \sum_{i<j} \mathcal{V}_{ij} + \sum_{i<j<k} V_{ijk}, \tag{2.3.16}$$

where $\mathcal{V}_{ij}$ is the potential of the nucleon-nucleon interactions and V_{ijk} is the potential of the three-nucleon interactions.

The most realistic EOS based on nonrelativistic potentials are listed below (only neutrons, protons, electrons and muons are considered):

1. **AP family**:

   The AP (Akmal and Pandharipande) family of EOSs [48] are:

- The AP1 EOS, where the only potential that describes the interaction between a nucleon-nucleon pair is the Argonne $\mathcal{V}_{18}$ (or AV18) potential, which consists of sums of 18 operators like $\hat{\sigma}_i \cdot \hat{\sigma}_j$, etc., with $\hat{\sigma}_i$ the Pauli spin operators [49].
- The AP2 EOS, which considers the same AV18 potential plus relativistic corrections (so-called boost interactions) [49].
- The AP3 EOS, which considers the AV18 potential plus the Urbana IX (UIX) potential that describes three-nucleon interaction [49]. One of the reasons to include three-nucleon interactions potentials is that nucleon-nucleon potentials underbind the triton and other light nuclei and predict too high equilibrium density for symmetric nuclear matter [41].
- The AP4 EOS, which considers the AV18 potential plus the UIX potential plus relativistic corrections [49].

2. **SLy**:

   The Skyrme Lyon (SLy) effective nucleon-nucleon interaction [50] consists in a effective nuclear hamiltonian obtained from many-body calculations with a simple two-nucleon potential. The nuclei in the neutron star crust are described by the compressible liquid drop model.

3. **FPS**:

   In the FPS (Friedman, Pandharipande and Smith) model [51], different from SLy model, the crust-core transition takes place through a sequence of phase transitions involving changes in nuclear shapes (from spheres to spaghetti and lasagna, and finally to bubbles).

4. **BSk**:

   The BSk (Brussels-Montreal Skyrme functionals) family of EOSs (BSk19-26) [52, 53] are based on the nuclear energy-density functional theory with generalized Skyrme effective forces that have been fitted with great precision to essentially all the available mass data. At the same time, these forces were constrained to reproduce microscopic calculations of homogeneous neutron matter based on realistic two- and three-nucleon forces. This family of

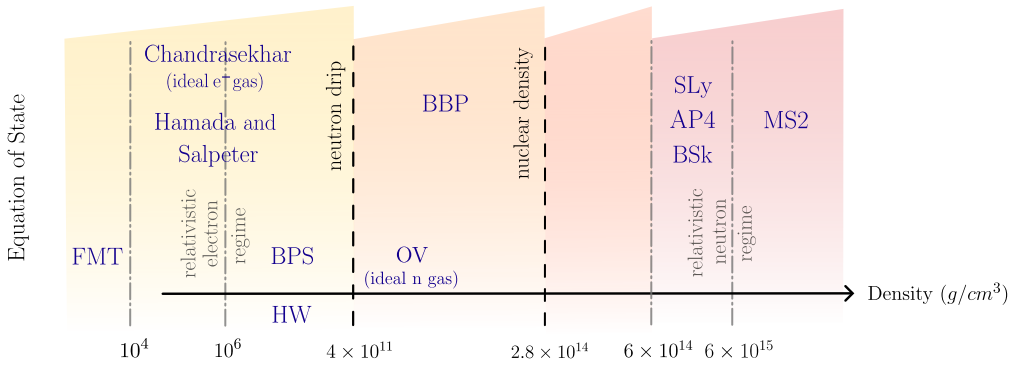

Figure 2.3.1: Density regimes inside a neutron star with their respective equations of state.

EOSs incorporates refinements to the SLy EOS that improve the fit to both nuclear matter properties and neutron star observations.

Relativistic approach

In this approach one starts from a local relativistic mean field theory with baryon and meson degrees of freedom. Such models have the advantage to be relativistic but sacrifice the connection to the large body of nucleon-nucleon scattering data. The coupling constants and mass parameters of the effective Lagrangian are constraint by empirical properties of nuclear matter at saturation.

We will focus on the non-relativistic approach, but one example of EOS using this relativistic formalism is the MS2 (Müller and Serot) EOS [54], which incorporate other constituents such as hyperons, pions and condensates. In specific they used the relativistic Dirac–Brueckner–Hartree–Fock formalism and a relativistic mean field theory, accounting for the energetic contributions due to the exchange between pions and mesons.

A summary of the EOS in all the density regimes is represented in figure 2.3.1.

2.4 Analytical fits to EOS

A particular EOS is usually presented in the form of a table containing a grid of calculated values of matter density ρ, baryon number density n and pressure P. The EOS is then interpolated between the tabulated forms to obtain a one-paremeter form $P = P(n)$ and $\rho = \rho(n)$. Depending on the interpolation schemes,

different results for the mass–radius relation are in general obtained. For numerical purposes, it is sometimes useful to have analytical fits to the EOS. In what follows, the analytical fits to the EOSs that will be used in this work will be discussed.

SLy

Haensel and Potekhin [55] proposed an analytical representation for the SLy EOS (and FPS EOS). In the fitting, they neglect the small discontinuities that appear at the interfaces between the crust and the core. However, the different character of the EOS in the different domains is reflected by the complexity of the fit, which consists of several fractional-polynomial parts, matched together by virtue of the function

$$f_0(x) = \frac{1}{1+e^x}. \tag{2.4.1}$$

They rely on a tabulated unified SLy EOS at $\rho > 5 \times 10^{10}$ g/cm^3 found in the following website. At lower densities, 10^8 g/cm$^3 \lesssim \rho < 5 \times 10^{10}$ g/cm^3, the crustal matter is described by the EOS of Haensel and Pichon (HP94) [56] based on experimental nuclear data, supplemented by the EOS for cold catalyzed matter due to BPS [45] at still lower density $\rho \lesssim 10^8$ g/cm^3. At extremely low densities, the EOS would depend on temperature, this can however be neglected for fitting.

If we denote $\zeta = \log_{10}(P/\text{dyn cm}^{-2})$ and $\xi = \log_{10}(\rho/\text{g cm}^{-3})$, the parametrization is given by [55]

$$\begin{aligned}\zeta = {} & \frac{a_1 + a_2\xi + a_3\xi^3}{1 + a_4\xi} f_0(a_5(\xi - a_6)) + (a_7 + a_8\xi) f_0(a_9(a_{10} - \xi)) \\ & + (a_{11} + a_{12}\xi) f_0(a_{13}(a_{14} - \xi)) + (a_{15} + a_{16}\xi) f_0(a_{17}(a_{18} - \xi)),\end{aligned} \tag{2.4.2}$$

where the (dimensionless) coefficients $\{a_1, \ldots, a_{18}\}$ are tabulated in the table 2.4.1. The typical fit error of P is $1 - 2\%$ (for $\xi \gtrsim 5$). The maximum error is determined by the jumps near the neutron drip and crust–core phase transitions in the tabulated EOSs, which are smoothed by the fit (2.4.2). The maximum error is 2.9% at $\xi = 8.42$ [55].

Figure 2.4.1 shows the tabulated EOS (symbols) and the corresponding fit (solid line). Triangles correspond to BPS, stars to HP94, and dots to SLy data.

n	a_n	n	a_n
1	6.22	10	11.4950
2	6.121	11	-22.775
3	0.005925	12	1.5707
4	0.16326	13	4.3
5	6.48	14	14.08
6	11.4971	15	27.80
7	19.105	16	-1.653
8	0.8938	17	1.50
9	6.54	18	14.67

Table 2.4.1: Parameters of the fit (2.4.2), according to Ref. [55].

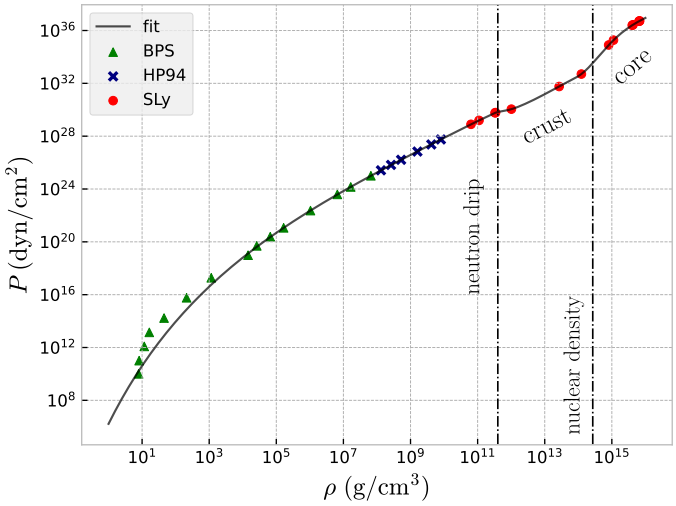

Figure 2.4.1: Pressure-density relation for the analytical representation of the SLy EOS (black solid line). The tabulated EOS used are: BPS (triangles), HP94 (stars) and SLy (circles). The vertical dash-dotted lines mark the main regimes inside the NS. Adapted from Ref. [55].

BSk

The analytic parametrization of the BSk family of EOS is

$$\begin{aligned}\zeta = &\frac{a_1 + a_2\xi + a_3\xi^3}{1 + a_4\xi} f_0(a_5(\xi - a_6)) + (a_7 + a_8\xi) f_0(a_9(a_6 - \xi)) \\ &+ (a_{10} + a_{11}\xi) f_0(a_{12}(a_{13} - \xi)) + (a_{14} + a_{15}\xi) f_0(a_{16}(a_{17} - \xi)) \\ &+ \frac{a_{18}}{1 + [a_{19}(\xi - a_{20})]^2} + \frac{a_{21}}{1 + [a_{22}(\xi - a_{23})]^2},\end{aligned} \tag{2.4.3}$$

where the (dimensionless) coefficients $\{a_1, \ldots, a_{23}\}$ for the BSk19 and BSk22 EOSs are tabulated in the table 2.4.2. The typical fit error of P is $\approx 1\%$ for $\xi \gtrsim 6$.

The maximum error is 3.7% at $\xi = 9.51$; it is determined by the jumps at the interfaces between layers containing different nuclides in the tabulated EOS. The fit (2.4.3) smoothly interpolates across these jumps.

n	a_n (BSk19)	a_n (BSk22)
1	3.916	6.682
2	7.701	5.651
3	0.00858	0.00459
4	0.22114	0.14359
5	3.269	2.681
6	11.964	11.972
7	13.349	13.993
8	1.3683	1.2904
9	3.254	2.665
10	-12.953	-27.787
11	0.9237	2.0140
12	6.20	4.09
13	14.383	14.135
14	16.693	28.03
15	-1.0514	-1.921
16	2.486	1.08
17	15.362	14.89
18	0.085	0.098
19	6.23	4.75
20	11.68	11.67
21	-0.029	-0.037
22	20.1	11.9
23	14.19	14.10

Table 2.4.2: Parameters of the fit (2.4.3), according to Ref. [52] and [53].

Compared to equation (2.4.2), equation (2.4.3) contains additional terms in the last line with coefficients $a_{18} - a_{23}$. These terms improve the fit near the boundaries between the outer and inner crust and between the crust and the core, where the slope of $P(\rho)$ sharply changes. In SLy the analogous changes are less abrupt. However, in the case of BSk models, the residuals of the fit without these additional terms may reach about 10% [52].

MS2

Gungor and Eksi [57] proposed an extension of the parameterization (2.4.2) made by Haensel and Potekhin. This new analytical representation has 23 parameters,

12 of which are fixed to represent low density regimes of BPS EOS and NV (Negele and Vautherin) [58]. The remaining 11 free parameters are used to fit the different EOS at high-density regimes and to match them. The analytic parametrization of the MS2 of EOS is

$$\zeta = \zeta_{\text{low}} f_0(a_1(\xi - c_{11})) + f_0(a_2(c_{12} - \xi))\zeta_{\text{high}}, \tag{2.4.4}$$

where

$$\zeta_{\text{low}} = [c_1 + c_2(\xi - c_3)^{c_4}] f_0(c_5(\xi - c_6)) + (c_7 + c_8\xi) f_0(c_9(c_{10} - \xi)) \tag{2.4.5}$$

and

$$\zeta_{\text{high}} = (a_3 + a_4\xi) f_0(a_5(a_6 - \xi)) + (a_7 + a_8\xi + a_9\xi^2) f_0(a_{10}(a_{11} - \xi)) \tag{2.4.6}$$

describe the low and high density regimes, respectively. The (dimensionless) coefficients $\{c_1, \ldots, c_{12}\}$ and $\{a_1, \ldots, a_{11}\}$ for the MS2 EOS are tabulated in the table 2.4.3.

n	c_n	a_n
1	10.6557	14.0084
2	3.7863	13.8422
3	0.8124	16.5970
4	0.6823	-1.0943
5	3.5279	5.6701
6	11.8100	14.8169
7	12.0584	-56.3794
8	1.4663	9.6159
9	3.4952	-0.2332
10	11.8007	-3.8369
11	14.4114	23.1860
12	14.4081	—

Table 2.4.3: Parameters of the fit (2.4.4) , according to Ref. [57].

In figure 2.4.2 the SLy, BSk19, BSk22, MS2 and Fermi EOSs are plotted. For low densities, the curves are similar, but for higher densities, above the nuclear density, the curves are quite different.

For the analytical representations of the EOS, we can express the adiabatic index

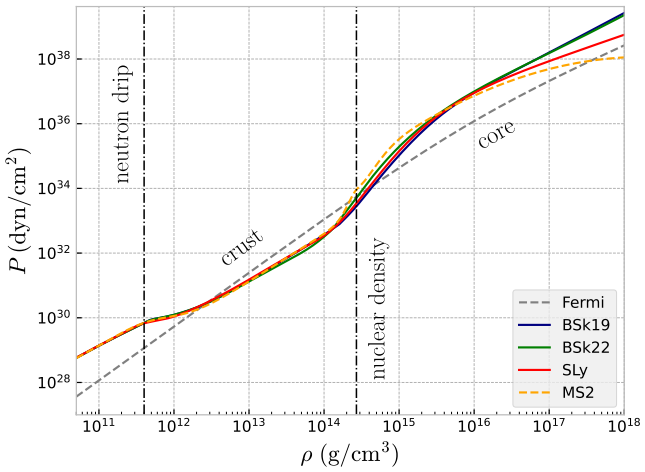

Figure 2.4.2: Pressure-density relation for the EOS: SLy (red line), BSk19-22 (blue and green lines), and Fermi (gray dashed line) used by Oppenheimer and Volkoff. The vertical dashed-dotted lines mark the main regimes inside the NS.

as a function of ξ, i.e.

$$\Gamma = \frac{\partial \zeta}{\partial \xi}\left(1 + \frac{10^{\zeta-\xi}}{c^2/(\mathrm{cm}^2\ \mathrm{s}^{-2})}\right). \tag{2.4.7}$$

The adiabatic index as a function of the density is plotted in figure 2.4.3 for different EOSs. One can see that the adiabatic index for SLy and BSk EOSs falls below the line $\Gamma = 4/3$ for lower densities ($\leq 10^{13}$ g/cm^3). This is because for these EOS models, the pressure at this density is mainly determined by the pressure of ultrarelativistic electron gas. On the other hand, the adiabatic index Γ for the Fermi EOS approaches asymptotically 5/3 for lower densities and 4/3 for higher densities, which is compatible with equations (2.3.14) and (2.3.15), respectively.

The speed of sound can also be written as follows

$$v_\mathrm{s} = \sqrt{10^{\zeta-\xi}\frac{d\zeta}{d\xi}}\ \frac{\mathrm{cm}}{\mathrm{s}}. \tag{2.4.8}$$

An illustration for this expression is found in figure 2.4.4. One can see that for the SLy, BSk19 and BSk22 EOSs, from a value of density, the speed of sound will be greater than the speed of light and causality will be violated. This is because of the non-relativistic formalism at high densities that these EOSs present. However,

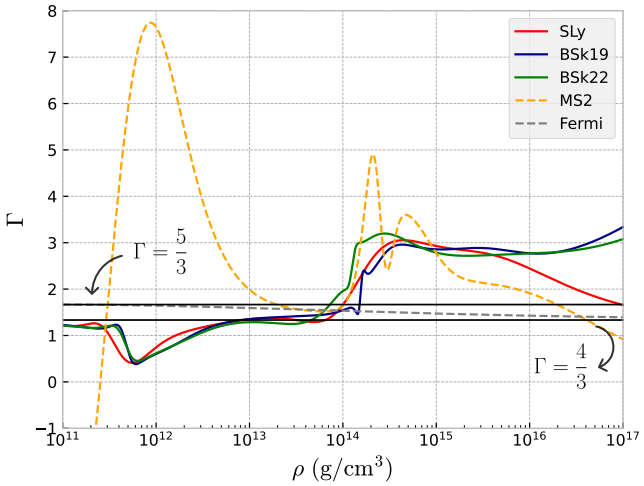

Figure 2.4.3: The adiabatic index Γ as a function of the density ρ for the Fermi, SLy, BSk19, BSk22, and MS2 EOSs. The horizontal lines mark $\Gamma = 4/3$ and $\Gamma = 5/3$.

the MS2 does not exhibit this problem. Thus, the causal limit puts constraints on the density for the EOSs considered. The maximum densities allowed are found to be 3.007, 3.381, and 2.737 (in units of 10^{15} g/cm^3) for the SLy, BSk19, and BSk22 EOSs, respectively. Finally, the speed of sound for the SLy EOS is again smaller than the speed of light at $\rho = 3.747 \times 10^{16}$ g/cm^3.

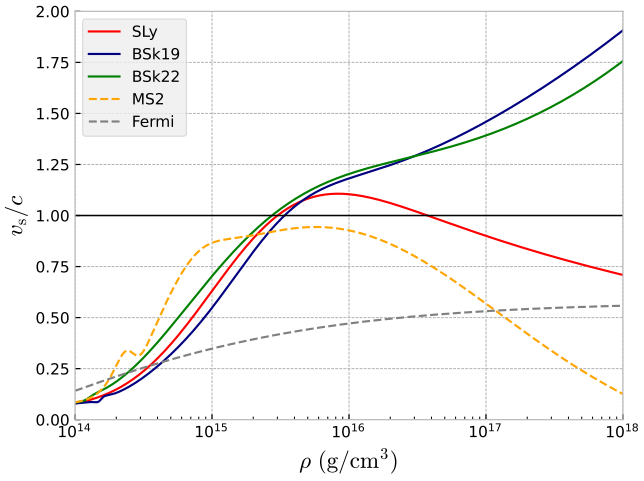

Figure 2.4.4: The speed of sound v_s as a function of the density ρ for the Fermi, SLy, BSk19, BSk22, and MS2 EOSs. The horizontal line marks the causal limit $v_s = c$.

Chapter 3

Relativistic Star Models

3.1 Schwarzschild solution

General Relativity is the most successful theory of gravity we have nowadays. This theory was published by Albert Einstein in 1915 [59] changing the Newtonian concept of gravity from a force at a distance between two massive bodies to a unified description of gravity as the curvature of spacetime due to a matter distribution. Precisely, GR is a (classical) field theory for the metric tensor $g_{\mu\nu}$, which describes the geometry of spacetime. The dynamic of this tensor is given by the Einstein field equations [1],

$$R_{\mu\nu} - \frac{1}{2}Rg_{\mu\nu} + \Lambda g_{\mu\nu} = \frac{8\pi G}{c^4}T_{\mu\nu}, \tag{3.1.1}$$

where $R_{\mu\nu}$ is the Ricci tensor, R the curvature scalar, Λ the cosmological constant (introduced by Einstein in 1917 [60]), and $T_{\mu\nu}$ the energy-momentum tensor of the matter distribution.

These field equations can be derived from the Einstein-Hilbert action [61]

$$S_{\mathrm{EH}} = \frac{1}{2\kappa}\int d^4x\sqrt{-g}(R - 2\Lambda) + S_{\mathrm{m}}, \tag{3.1.2}$$

where $\kappa = 8\pi G c^{-4}$ and S_{m} is the action for matter. The field equations can be obtained requiring that the variation δS_{EH} be zero for any variation of the metric $\delta g_{\mu\nu}$ that vanishes at the boundary and that the energy-momentum tensor is

[1] We adopt the sign conventions $(-,+,+,+)$.

defined by

$$T_{\mu\nu} := -\frac{2}{\sqrt{-g}}\frac{\delta S_{\mathrm{m}}}{\delta g^{\mu\nu}}. \tag{3.1.3}$$

The first non-trivial exact solution of the Einstein equations in vacuum ($T_{\mu\nu} = 0$ and $\Lambda = 0$) was derived by Karl Schwarzschild in 1916 [62]. This solution describes the gravitational field outside a non-rotating spherical body of mass M. In Schwarzschild coordinates, $x^\mu = (ct, r, \theta, \varphi)$, the solution can be written as

$$ds^2 = -f(r)(cdt)^2 + \frac{dr^2}{f(r)} + r^2(d\theta^2 + \sin^2\theta d\varphi^2), \tag{3.1.4}$$

where

$$f(r) = 1 - \frac{r_{\mathrm{s}}}{r} \tag{3.1.5}$$

and $r_{\mathrm{s}} := 2GM/c^2$ is the **Schwarzschild radius**. There are two singularities for the coordinate r, when $r \to 0$ and $r \to r_{\mathrm{s}}$. Therefore, the metric is only defined for the exterior region $r > r_{\mathrm{s}}$. However, $r = r_{\mathrm{s}}$ is not a curvature singurality, and it can be removed with a change of coordinates, first introduced by Eddington and Finkelstein [63, 64].

It is natural to wonder whether the Schwarzschild metric is the unique spherically symmetric solution in vacuum. According to Birkhoff's theorem [65], any spherically symmetric solution of the vacuum field equations must be static and asymptotically flat. This means that the equation (3.1.4) is the most general spherically symmetric vacuum solution to the Einstein field equations without cosmological constant.

3.2 Tolman-Oppenheimer-Volkoff equation

In this section, we will find solutions for the Einstein field equations inside a star modeled as a spherical, static perfect fluid in hydrostatic equilibrium. These solutions complement the Schwarzschild solution (3.1.4), since the latter describes the gravitational field outside a spherically symmetric mass, while the solutions we will found describe the spacetime inside of the matter distribution.

It will be convenient to rewrite the field equations (3.1.1) as follows

$$R_{\mu\nu} = \frac{8\pi G}{c^4}\left[T_{\mu\nu} - \frac{1}{2}T g_{\mu\nu}\right] + \Lambda g_{\mu\nu}, \tag{3.2.1}$$

where $T := T^{\mu}_{\ \mu} = g^{\mu\nu}T_{\mu\nu}$ is the trace of the energy-momentum tensor.

Consider the line element for a spherically symmetric, static spacetime in Schwarzschild coordinates:

$$ds^2 = -e^{\alpha}(cdt)^2 + e^{\beta}dr^2 + r^2(d\theta^2 + \sin^2\theta d\varphi^2), \tag{3.2.2}$$

where $\alpha = \alpha(r)$ and $\beta = \beta(r)$ are the metric functions.

The non-trivial components of the Ricci tensor are:

$$R_{00} = \frac{1}{2}e^{(\alpha-\beta)}\left[\alpha'' - \frac{\beta'\alpha'}{2} + \frac{2\alpha'}{r} + \frac{\alpha'^2}{2}\right], \tag{3.2.3}$$

$$R_{rr} = -\frac{1}{2}\left[\alpha'' - \frac{\beta'\alpha'}{2} - \frac{2\beta'}{r} + \frac{\alpha'^2}{2}\right], \tag{3.2.4}$$

$$R_{\theta\theta} = 1 - e^{-\beta}\left[1 - \frac{1}{2}r\beta' + \frac{1}{2}r\alpha'\right], \tag{3.2.5}$$

$$R_{\varphi\varphi} = \sin^2\theta R_{22}. \tag{3.2.6}$$

The matter inside the star will be described in terms of the energy-momentum tensor of a perfect fluid given by

$$T_{\mu\nu} = \left(\rho + \frac{P}{c^2}\right)u_\mu u_\nu + P g_{\mu\nu}, \tag{3.2.7}$$

where the pressure and the density are functions of the coordinate r, $u^\mu = dx^\mu/d\tau$ is the 4-velocity of a fluid element, and τ its proper time.

Since we are considering the static case, the only non-vanishing component of the 4-velocity is u_0 so that $u_\mu = (u_0, 0, 0, 0)$. Using the identity $g_{\mu\nu}u^\mu u^\nu \equiv -c^2$, we can obtain

$$u_0 = -ce^{\alpha(r)/2}. \tag{3.2.8}$$

Thus, replacing the components of the metric and components of the 4-velocity (3.2.8) in the energy-momentum tensor (3.2.7), we can write

$$T_{\mu\nu} = \mathrm{diag}(\rho c^2 e^{\alpha}, Pe^{\beta}, Pr^2, Pr^2\sin^2\theta). \tag{3.2.9}$$

Taking the trace of (3.2.9), we have

$$\begin{aligned} T = T_{\mu\nu}g^{\mu\nu} &= \left(\rho + \frac{P}{c^2}\right) u_\mu u_\nu g^{\mu\nu} + P g_{\mu\nu} g^{\mu\nu} \\ &= -\left(\rho + \frac{P}{c^2}\right) c^2 + P\delta^\mu{}_\mu \\ &= -\rho c^2 + 3P. \end{aligned} \tag{3.2.10}$$

Replacing the values for the components of the Ricci tensor (3.2.3)-(3.2.6) in the field equations (3.2.1), we obtain three relevant field equations (since $R_{\varphi\varphi}$ only differs by a factor $\sin^2\theta$ from $R_{\theta\theta}$) for a vanishing cosmological constant:

$$R_{00} = \frac{1}{2}e^{(\alpha-\beta)}\left[\alpha'' - \frac{\beta'\alpha'}{2} + \frac{2\alpha'}{r} + \frac{\alpha'^2}{2}\right] = \frac{4\pi G}{c^4}(\rho c^2 + 3P)e^\alpha, \tag{3.2.11}$$

$$R_{rr} = -\frac{1}{2}\left[\alpha'' - \frac{\beta'\alpha'}{2} - \frac{2\beta'}{r} + \frac{\alpha'^2}{2}\right] = \frac{4\pi G}{c^4}(\rho c^2 - P)e^\beta, \tag{3.2.12}$$

$$R_{\theta\theta} = 1 - e^{-\beta}\left[1 - \frac{1}{2}r\beta' + \frac{1}{2}r\alpha'\right] = \frac{4\pi G}{c^4}(\rho c^2 - P)r^2. \tag{3.2.13}$$

Let us solve this system of equations. First, we will determine the function $\beta(r)$ of the metric by performing the following combination:

$$\frac{1}{2}e^{-\alpha}R_{00} + \frac{1}{2}e^{-\beta}R_{rr} + r^{-2}R_{\theta\theta} = e^{-\beta}\left(\frac{\beta'}{r} - \frac{1}{r^2}\right) + \frac{1}{r^2} = \frac{8\pi G}{c^2}\rho. \tag{3.2.14}$$

Multiplying the equation (3.2.14) by r^2, then integrating from $\bar{r} = 0$ to $\bar{r} = r$, we obtain the following

$$e^{-\beta}\beta' r - e^{-\beta} + 1 = \frac{8\pi G}{c^2}\rho r^2, \tag{3.2.15}$$

$$\frac{d}{dr}\left(e^{-\beta}r\right) = 1 - \frac{8\pi G}{c^2}\rho r^2, \tag{3.2.16}$$

$$\int_0^r \frac{d}{d\bar{r}}\left(e^{-\beta(\bar{r})}\bar{r}\right)d\bar{r} = \int_0^r \left(1 - \frac{8\pi G}{c^2}\rho(\bar{r})\bar{r}^{\,2}\right)d\bar{r}, \tag{3.2.17}$$

$$re^{-\beta(r)} - \lim_{r\to 0} re^{-\beta(r)} = r - \int_0^r \frac{8\pi G}{c^2}\rho(\bar{r})\bar{r}^2 d\bar{r}, \tag{3.2.18}$$

$$e^{-\beta(r)} = 1 + \frac{1}{r}\lim_{r\to 0} re^{-\beta(r)} - \frac{1}{r}\int_0^r \frac{8\pi G}{c^2}\rho(\bar{r})\bar{r}^2 d\bar{r}, \tag{3.2.19}$$

$$e^{\beta(r)} = \left(1 - \frac{1}{r}\lim_{r\to 0} re^{-\beta(r)} - \frac{2G\mathcal{M}(r)}{c^2 r}\right)^{-1}, \tag{3.2.20}$$

where in the last line we have used the same definition of the mass function $\mathcal{M}(r)$ for the Newtonian case (see appendix A), i.e.,

$$\mathcal{M}(r) = 4\pi \int_0^r \rho(\bar{r})\bar{r}^{\,2} d\bar{r}, \tag{3.2.21}$$

or

$$\frac{d\mathcal{M}}{dr} = 4\pi r^2 \rho. \tag{3.2.22}$$

The difference is that this function does not correspond to the rest mass contained in a r radius of the star because it is a coordinate-dependent quantity (non-invariant). Therefore, its interpretation is not trivial. The reader can find a discussion of its meaning in chapter 23: spherical stars in Ref. [38].

Continuing with the calculation, let us assume that the metric function $g_{rr} = e^{\beta}$ is not singular at $r = 0$ so that

$$\lim_{r\to 0} r e^{-\beta(r)} = 0, \tag{3.2.23}$$

and not other finite value, so that the expression (3.2.20) does not present divergences when r tends to zero. Thus, the metric coefficient g_{rr} is given by

$$e^{\beta(r)} = \frac{1}{1 - \frac{2G\mathcal{M}(r)}{c^2 r}}. \tag{3.2.24}$$

Let us find the metric function α, for this, it is useful to use the conservation equation for the energy-momentum tensor:

$$\nabla_\nu T^{\mu\nu} := \partial_\nu T^{\mu\nu} + \Gamma^{\mu}{}_{\nu\lambda} T^{\lambda\nu} + \Gamma^{\nu}{}_{\nu\lambda} T^{\mu\lambda} = 0. \tag{3.2.25}$$

Equation (3.2.25) is a consequence of the Einstein field equations (3.1.1) and represents the relativistic version of the continuity and Euler equations for a perfect fluid. In other words, it is the generalization to non-zero gravitational fields of the law of conservation of energy and momentum of a system. Evaluating the component $\mu = r$ of equation (3.2.25), we obtain

$$\nabla_\nu T^{r\nu} = \frac{1}{2} e^{-\beta} \left[(\rho c^2 + P)\alpha' + 2P' \right]. \tag{3.2.26}$$

Thus, solving for α' gives

$$\alpha' = -\frac{2P'}{\rho c^2 + P}. \tag{3.2.27}$$

Replacing the equation (3.2.24) for β in the field equation (3.2.13), we can express P' only in terms of the properties of the matter (ρ, P and $\mathcal{M}$):

$$\begin{aligned}
R_{22} &= \frac{4\pi G}{c^4}(\rho c^2 - P)r^2 \\
&= 1 - e^{-\beta}\left[1 - \frac{1}{2}r\beta' + \frac{1}{2}r\alpha'\right] \\
&= 1 - \left(1 - \frac{2G\mathcal{M}}{c^2 r}\right)\left[1 - \frac{1}{2}r\frac{d}{dr}\left\{-\ln\left(1 - \frac{2G\mathcal{M}}{c^2 r}\right)\right\} + \frac{1}{2}r\left(\frac{-2P'}{P + \rho c^2}\right)\right] \\
&= 1 - \left(1 - \frac{2G\mathcal{M}}{c^2 r}\right)\left[1 + \frac{1}{2}r\left(1 - \frac{2G\mathcal{M}}{c^2 r}\right)^{-1}\left(\frac{2G\mathcal{M}}{c^2 r^2} - \frac{2G\mathcal{M}'}{c^2 r}\right) - \frac{r}{P + \rho c^2}P'\right] \\
&= \frac{G\mathcal{M}}{c^2 r} + \frac{4\pi G}{c^2}\rho r^2 + \left(1 - \frac{2G\mathcal{M}}{c^2 r}\right)\frac{r}{P + \rho c^2}P'.
\end{aligned} \tag{3.2.28}$$

Solving for P', we can write

$$\left(1 - \frac{2G\mathcal{M}}{c^2 r}\right)\frac{r}{P + \rho c^2}P' = \frac{4\pi G}{c^4}(\rho c^2 - P)r^2 - \frac{G\mathcal{M}}{c^2 r} - \frac{4\pi G r^2 \rho}{c^2}, \tag{3.2.29}$$

$$\left(r - \frac{2G\mathcal{M}}{c^2}\right)\frac{P'}{P + \rho c^2} = -\frac{G}{c^2 r}\left(\mathcal{M} + \frac{4\pi}{c^2}Pr^3\right). \tag{3.2.30}$$

Thus, we have found P' in terms of the three known fields: the pressure $P(r)$, the mass density $\rho(r)$ and the mass function $\mathcal{M}(r)$, leading to the so-called **Tolman-Oppenheimer-Volkoff equation** (T.O.V.) [6]:

$$\frac{dP}{dr} = -\frac{\rho c^2 + P}{r\left(r - \frac{2G\mathcal{M}}{c^2}\right)}\left[\frac{G\mathcal{M}}{c^2} + \frac{4\pi G}{c^4}r^3 P\right]. \tag{3.2.31}$$

If we want to see clearly the GR corrections of the hydrostatic equilibrium equation, we can rewrite equation (3.2.31) as follows

$$\frac{dP}{dr} = -\frac{G\mathcal{M}(r)\rho(r)}{r^2}\left[1 + \frac{P(r)}{\rho c^2}\right]\left[1 + \frac{4\pi r^3 P(r)}{\mathcal{M}(r)c^2}\right]\left[1 - \frac{2G\mathcal{M}(r)}{c^2 r}\right]^{-1}. \tag{3.2.32}$$

Comparing with equation (A.8) of appendix A, we see that the last three factors of (3.2.32) are the GR corrections and these are important when we are in a

relativistic regime.

If we replace the equation (3.2.31) in the expression (3.2.27) for α', we can obtain the explicit form of the metric function α:

$$\begin{aligned}\alpha' &= -\frac{2}{\rho c^2 + P}\frac{dP}{dr} \\ &= \frac{2}{r\left(r - \frac{2G\mathcal{M}}{c^2}\right)}\left[\frac{G\mathcal{M}}{c^2} + \frac{4\pi G}{c^4}r^3 P\right] \\ &= \frac{2G}{c^2 r^2}\left[\mathcal{M}(r) + \frac{4\pi r^3 P(r)}{c^2}\right]\left[1 - \frac{2G\mathcal{M}(r)}{c^2 r}\right]^{-1}. \end{aligned} \tag{3.2.33}$$

Integrating from $\bar{r} = r$ to $\bar{r} \to \infty$, we have

$$\int_r^\infty \alpha'(\bar{r})d\bar{r} = \int_r^\infty \frac{2G}{c^2\bar{r}^{\,2}}\left[\mathcal{M}(\bar{r}) + \frac{4\pi\bar{r}^{\,3}P(\bar{r})}{c^2}\right]\left[1 - \frac{2G\mathcal{M}(\bar{r})}{c^2\bar{r}}\right]^{-1} d\bar{r}. \tag{3.2.34}$$

Assuming that the metric is asymptotically flat, that is,

$$\lim_{r\to\infty}\alpha(r) = 0 \quad \Rightarrow \quad \lim_{r\to\infty} g_{00} = 1, \tag{3.2.35}$$

we obtain the metric function

$$\alpha(r) = -\frac{2G}{c^2}\int_r^\infty \frac{d\bar{r}}{\bar{r}^{\,2}}\left[\mathcal{M}(\bar{r}) + \frac{4\pi\bar{r}^{\,3}P(\bar{r})}{c^2}\right]\left[1 - \frac{2G\mathcal{M}(\bar{r})}{c^2\bar{r}}\right]^{-1}. \tag{3.2.36}$$

The exterior solution

Outside a star the density and pressure vanish, so only the metric functions α and β remain. From equation (3.2.21) one sees that the mass function $\mathcal{M}(r)$ stays constant for values of r greater than R (radius of the star). Therefore, for $r > R$, we have

$$\rho(r) = 0, \quad P(r) = 0, \quad \mathcal{M}(r) = M, \tag{3.2.37}$$

where we have denoted the constant $\mathcal{M}(R)$ by M. The first metric function α is determined by imposing the conditions (3.2.37) in equation (3.2.36):

$$\alpha(r) = -\frac{2G}{c^2}\int_r^\infty \frac{d\bar{r}}{\bar{r}^2}\frac{M}{1 - \frac{2GM}{c^2\bar{r}}} = \ln\left(1 - \frac{2GM}{c^2 r}\right), \quad r > R. \tag{3.2.38}$$

Using equation (3.2.24) to find the second metric function, we obtain the following line element:

$$ds^2 = -\left(1 - \frac{2GM}{c^2 r}\right)(cdt)^2 + \frac{dr^2}{\left(1 - \frac{2GM}{c^2 r}\right)} + r^2(d\theta^2 + \sin^2\theta d\varphi^2). \tag{3.2.39}$$

This solution is precisely the Schwarzschild metric (3.1.4). Thus, we can conclude that the quantity M must be the total mass of the star so that the interior metric solution will smoothly match the exterior Schwarzschild metric.

Equations of stellar structure

The system of equations to be integrated in order to obtain a complete stellar model are the following:

$$\frac{d\alpha}{dr} = \frac{2}{r\left(r - \frac{2G\mathcal{M}}{c^2}\right)}\left[\frac{G\mathcal{M}}{c^2} + \frac{4\pi G}{c^4} r^3 P\right], \tag{3.2.40}$$

$$\frac{d\mathcal{M}}{dr} = 4\pi r^2 \rho, \tag{3.2.41}$$

$$\frac{dP}{dr} = -\frac{\rho c^2 + P}{r\left(r - \frac{2G\mathcal{M}}{c^2}\right)}\left[\frac{G\mathcal{M}}{c^2} + \frac{4\pi G}{c^4} r^3 P\right], \tag{3.2.42}$$

$$P = P(\rho), \tag{3.2.43}$$

where the last one is the EOS. It remains for us to state the boundary conditions of the problem. First, when we write the equations (3.2.21) and (3.2.22), we implicitly assume that $\mathcal{M}(0) = 0$, which is physically acceptable. Indeed, following an argument given in Ref. [38], if $\mathcal{M}(0) \neq 0$, then near the origin, the spatial part of the metric remains

$$dl^2 = \left(1 - \frac{2G\mathcal{M}(0)}{c^2 r}\right)^{-1} dr^2 + r^2(d\theta^2 + \sin^2\theta d\varphi^2) \tag{3.2.44}$$

$$\approx \left(1 + \frac{2G\mathcal{M}(0)}{c^2 r}\right) dr^2 + r^2(d\theta^2 + \sin^2\theta d\varphi^2), \quad r \approx 0. \tag{3.2.45}$$

We have a singularity at the origin, which is physically unacceptable because we could not define a local inertial reference frame at $r = 0$. On the other hand, if

we fixed $\mathcal{M}(0) = 0$, then $\rho \approx \rho_c$ constant and

$$\mathcal{M}(r) = \int_0^r 4\pi \bar{r}^2 \rho(\bar{r}) d\bar{r} \approx \frac{4\pi}{3}\rho_c r^3. \tag{3.2.46}$$

Thus,

$$dl^2 = \left(1 - \frac{8\pi G}{3c^2}\rho_c r^2\right)^{-1} dr^2 + r^2(d\theta^2 + \sin^2\theta d\varphi^2) \tag{3.2.47}$$

$$\approx dr^2 + r^2(d\theta^2 + \sin^2\theta d\varphi^2), \quad r \approx 0 \tag{3.2.48}$$

which describes a smooth spacetime geometry near the origin.

Continuing with the other fields involved, the pressure at the center of the star has a given value $P(0) = P_c$. With this value we can determine the central density $\rho(0) = \rho_c$ using the EOS, or vice versa. The central value of α is arbitrary in the numerical integration, but later it is renormalized imposing the boundary condition at the radius of the star:

$$\alpha(R) = \ln\left(1 - \frac{2G\mathcal{M}(R)}{c^2 R}\right). \tag{3.2.49}$$

In short, the boundary conditions $P(0) = P_c$, $\alpha(0) = \alpha_c$ and $\mathcal{M}(0) = 0$ are sufficient to uniquely determine the solution to the coupled equations (3.2.40)-(3.2.43). We integrate these coupled equations from $r = 0$ until the pressure vanishes. The point at which the pressure reaches zero is the radius of the star.

3.3 Uniform density case and Buchdahl limit

For realistic EOSs, the equations of stellar structure (3.2.40)-(3.2.43) cannot be integrated analytically, numerical integration is necessary. However, analytic solutions exist for various idealized EOSs. One of the most useful analytic solutions describes a star of uniform density:

$$\rho(r) = \begin{cases} \rho_c = \text{const}, & r < R \\ 0, & r > R \end{cases}. \tag{3.3.1}$$

This EOS is independent of the pressure, so we are considering incompressible

matter. Replacing (3.3.1) in equation (3.2.21), we obtain

$$\mathcal{M}(r) = \begin{cases} \frac{4\pi}{3}\rho_c r^3, & r < R \\ \frac{4\pi}{3}\rho_c R^3, & r > R \end{cases} . \tag{3.3.2}$$

Replacing (3.3.1) and (3.3.2) in the T.O.V. equation (3.2.32), for $r \leq R$, we obtain:

$$\frac{dP}{dr} = -[\rho_c c^2 + P]\left[\frac{4\pi G}{3c^2}\rho_c r^3 + \frac{4\pi G}{c^4} P r^3\right] \tag{3.3.3}$$

$$= -\frac{4\pi G}{c^4} r\left[\rho_c c^2 + P\right]\left[P + \frac{1}{3}\rho_c c^2\right]\left[1 - \frac{8\pi G}{3c^2}\rho_c r^2\right]^{-1} . \tag{3.3.4}$$

Reordering the terms of the equation above, we can write

$$\frac{P'}{(P + \rho_c c^2)(P + \rho_c c^2/3)} = -\frac{4\pi G}{c^4} r\left[1 - \frac{8\pi G}{3c^2}\rho_c r^2\right]^{-1} . \tag{3.3.5}$$

If we change the variable

$$x := \sqrt{\frac{8\pi G \rho_c}{3c^2}}\, r, \tag{3.3.6}$$

the equation (3.3.5) gives us

$$\frac{-2\rho_c c^2 dP}{(P + \rho_c c^2)(3P + \rho_c c^2)} = \frac{x\, dx}{1 - x^2}. \tag{3.3.7}$$

Integrating with respect to r, we obtain

$$\ln\left(\frac{P + \rho_c c^2}{3P + \rho_c c^2}\right) = -\frac{1}{2}\ln(1 - x^2) - \frac{1}{2}\ln a = \ln[a(1 - x^2)]^{-1/2}, \tag{3.3.8}$$

where a is an integration constant. This constant can be found by considering vanishing pressure on the surface of the star, $P(R) = 0$. Thus,

$$a = \frac{1}{1 - x_R^2} = \frac{1}{1 - \frac{8\pi G}{3c^2}\rho_c R^2}. \tag{3.3.9}$$

Replacing the value of a in (3.3.8), we can write

$$\frac{P+\rho_c c^2}{3P+\rho_c c^2} = \left[\frac{1-8\pi G\rho_c R^2/3c^2}{1-8\pi G\rho_c r^2/3c^2}\right]^{1/2}, \qquad r \leq R. \tag{3.3.10}$$

Considering the Schwarzschild radius:

$$r_S = \frac{2GM}{c^2} = \frac{8\pi G}{3c^2}\rho_c R^3, \tag{3.3.11}$$

and solving for $P(r)$, we obtain

$$P(r) = \rho_c c^2 \frac{\sqrt{\frac{1-r_S/R}{1-r_S r^2/R^3}} - 1}{1 - 3\sqrt{\frac{1-r_S/R}{1-r_S r^2/R^3}}}. \tag{3.3.12}$$

Simplifying, we obtain an exact solution for the pressure in terms of the radial coordinate r, given by

$$P(r) = \rho_c c^2 \frac{\sqrt{1-\frac{r_S r^2}{R^3}} - \sqrt{1-\frac{r_S}{R}}}{3\sqrt{1-\frac{r_S}{R}} - \sqrt{1-\frac{r_S r^2}{R^3}}}, \qquad r \leq R. \tag{3.3.13}$$

Buchdahl's bound

The pressure is always maximum at the center of the star, and in the uniform density case it assumes the value

$$P(0) = \rho_c c^2 \frac{1-\sqrt{1-\frac{r_S}{R}}}{3\sqrt{1-\frac{r_S}{R}} - 1}. \tag{3.3.14}$$

The central pressure must be finite and positive to sustain equilibrium, so we need

$$3\sqrt{1-\frac{r_S}{R}} - 1 > 0 \quad \Leftrightarrow \quad R > \frac{9}{8}r_S. \tag{3.3.15}$$

Thus, it is necessary for the stability that the radius of the star is greater than

$$R > \frac{9}{8}r_S = \frac{9}{4}\frac{GM}{c^2}, \tag{3.3.16}$$

i.e., there is a lower bound for the radius R of a star of a given mass M. A rigorous analysis shows that the result (3.3.16) is independent of the EOS. It depends only on the structure of the relativistic equations for hydrostatic equilibrium and was obtained by Buchdahl [66], that is why the expression (3.3.16) is known as the **Buchdahl's bound**.

3.4 Neutron star solutions

In this section, numerical solutions to the relativistic stellar structure equations based on the T.O.V. equation for neutron stars will be determined using the EOS described in chapter 2. For this purpose, we will normalize the equations (3.2.40)-(3.2.43). First, we will write the dimensionless pressure $\overline{P}$ and the energy density $\bar{\epsilon}$ as follows

$$P =: K\overline{P}, \qquad \epsilon =: K\bar{\epsilon}, \tag{3.4.1}$$

where the constant K is defined in (2.3.11). Replacing (3.4.1) in the equations (3.2.40)-(3.2.42), we obtain

$$\frac{d\alpha}{dr} = \frac{2}{r\left(r - \frac{2G\mathcal{M}}{c^2}\right)}\left[\frac{G\mathcal{M}}{c^2} + \frac{4\pi GK}{c^4}r^3\overline{P}\right], \tag{3.4.2}$$

$$\frac{d\mathcal{M}}{dr} = \frac{4\pi K}{c^2}r^2\bar{\epsilon}, \tag{3.4.3}$$

$$\frac{d\overline{P}}{dr} = -\frac{\bar{\epsilon} + \overline{P}}{r\left(r - \frac{2G\mathcal{M}}{c^2}\right)}\left[\frac{G\mathcal{M}}{c^2} + \frac{4\pi GK}{c^4}r^3\overline{P}\right]. \tag{3.4.4}$$

It is also convenient to define the dimensionless radial coordinate x and mass m as

$$r =: ax, \qquad \mathcal{M} =: bm, \tag{3.4.5}$$

where a and b are constants. Replacing these definitions in (3.4.2)-(3.4.4), we find

$$\frac{d\alpha}{dx} = \frac{2}{x\left(x - \frac{2Gbm}{ac^2}\right)}\left[\frac{Gbm}{ac^2} + \frac{4\pi GKa^2}{c^4}x^3\overline{P}\right], \tag{3.4.6}$$

$$\frac{dm}{dx} = \frac{4\pi Ka^3}{bc^2}x^2\bar{\epsilon}, \tag{3.4.7}$$

$$\frac{d\overline{P}}{dx} = -\frac{\bar{\epsilon} + \overline{P}}{x\left(x - \frac{2Gbm}{ac^2}\right)}\left[\frac{Gbm}{ac^2} + \frac{4\pi GKa^2}{c^4}x^3\overline{P}\right]. \tag{3.4.8}$$

Here we see that it is convenient to choose a and b such that

$$\frac{4\pi K}{c^2}\frac{a^3}{b} \stackrel{!}{=} 1, \qquad \frac{bG}{ac^2} \stackrel{!}{=} 1. \tag{3.4.9}$$

Solving for a and b, we obtain

$$a = \sqrt{\frac{c^4}{4\pi KG}}, \qquad b = \frac{c^2}{G}a. \tag{3.4.10}$$

Thus, we have reduced the relativistic stellar equations to the following normalized equations:

$$\frac{d\alpha}{dx} = \frac{2}{x(x-2m)}(m + x^3\overline{P}) \tag{3.4.11}$$

$$\frac{dm}{dx} = x^2\overline{\epsilon}, \tag{3.4.12}$$

$$\frac{d\overline{P}}{dx} = -\frac{\overline{\epsilon}+\overline{P}}{x\,(x-2m)}(m + x^3\overline{P}), \tag{3.4.13}$$

where now the boundary conditions are:

$$\alpha(0) = \alpha_{\rm c}, \tag{3.4.14}$$

$$m(0) = 0, \tag{3.4.15}$$

$$\overline{P}(0) = \overline{P}_{\rm c}. \tag{3.4.16}$$

Since the pressure is monotonically decreasing from its maximum value at the center of the star, there will be a point $x = x_1$ such that $\overline{P}(x_1) = 0$, and this will be the dimensionless radius of the star, which then determine the radius as

$$R = ax_1 \approx 13.683\,x_1 \text{ km}. \tag{3.4.17}$$

Furthermore, the mass of the star will be obtain evaluating b in (3.4.10):

$$M = bm(x_1) \approx 9.2648\,m(x_1)\ \mathrm{M}_\odot. \tag{3.4.18}$$

Note that the value of $\alpha_{\rm c}$ is unknown, but it is fixed when the boundary condition (3.2.49) is imposed, which is equivalent to setting a time scale such that the

spacetime is asymptotically flat with solution (3.2.39). To integrate the stellar structure equations it is necessary that the value of α at the origin is known, for this we will take advantage of the fact that the differential equation (3.4.11) is linear in α, i.e., we can add a constant to α and the resulting function satisfies exactly the same equation (3.4.11). Thus, we can write

$$\alpha(x) = \alpha_{\text{num}}(x) + \alpha_{\text{c}}, \tag{3.4.19}$$

where $\alpha_{\text{num}}(0) = 0$ and the constant α_{c} is found by imposing the boundary condition (3.2.49):

$$\alpha_{\text{c}} = \ln\left(1 - \frac{2m}{x_1}\right) - \alpha_{\text{num}}(x_1). \tag{3.4.20}$$

Therefore, instead of numerically integrating $\alpha(x)$, we will integrate $\alpha_{\text{num}}(x)$, which verifies the equation (3.4.11).

3.4.1 Numerical method and graphs

The system consisting of the equations (3.4.11)-(3.4.13) is solved numerically using the fourth-order Runge Kutta method for values of central density between $\rho_{\text{c}} = 2 \times 10^{14}$ g/cm^3 and $\rho_{\text{c}} = 5 \times 10^{17}$ g/cm^3. The complete code can be found in this repository and the integration scheme is detailed as follows:

- Given a central density, we found the value of the central pressure using the EOS from chapter 2.
- We integrate numerically using a equispaced interval of the x domain with 10^6 points and the function `solve_ivp` from the library `scipy.integrate` of `Python`. This function is useful because it can stop the integration given a certain condition, in our case, that the pressure at the surface of the star is zero.
- Once the integration is finished, we store and save the dimensionless radius and mass of the star (the last element of the arrays of x and m, respectively) in `NumPy` arrays.
- We calculate the constant (3.4.20) and save the arrays of: x (from zero to x_1), the metric functions α and β, the pressure, the energy density and the adiabatic index (it will be used later), all of them as a function of x. The

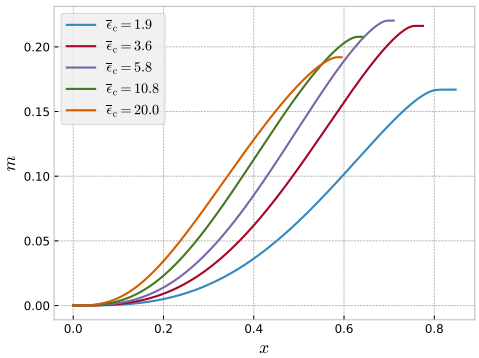

(a) Dimensionless mass function m versus the dimensionless radial coordinate x.

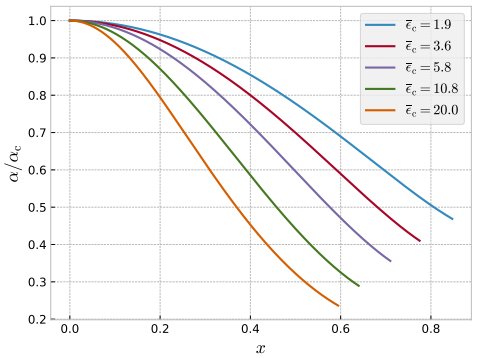

(b) Metric function α (normalized respect to its value at the origin) versus the dimensionless radial coordinate x.

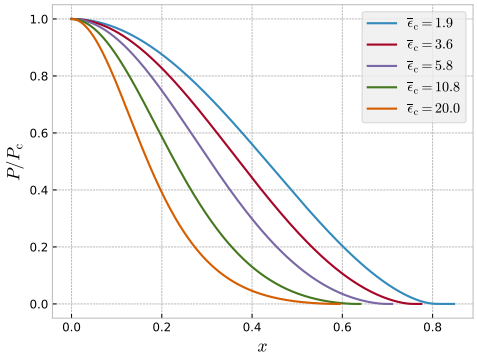

(c) Pressure P (normalized respect to its value at the origin) versus the dimensionless radial coordinate x.

Figure 3.4.1: Solutions of the T.O.V. equation for different values of the dimensionless central energy density $\bar{\epsilon}_c$.

files are saved in HDF5 format using the package `h5py`, which is a "Pythonic" interface to save binary data, allowing us to store huge amounts of numerical data, and easily manipulate that data with `NumPy`.

- We proceed similarly for each central density value.

Figure 3.4.1 shows the plots of the functions that were integrated (m, α and P) using the SLy EOS for different values of central density. First, we can note the different values of the coordinate x for which the pressure is zero, corresponding to different radii for different central densities. A characteristic that immediately attracts attention in the graph (3.4.1a) is that the function $m(x)$ increases with ρ_c up to a certain maximum value, after which it decreases. Physically, this means

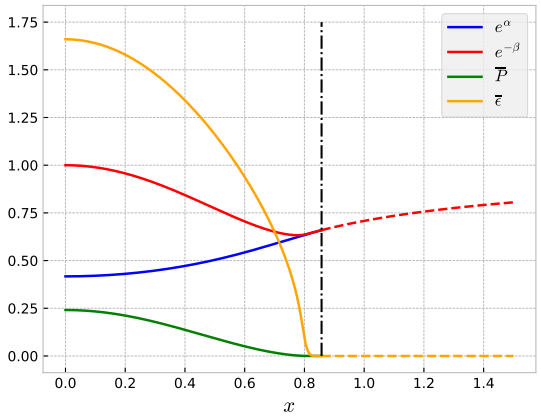

Figure 3.4.2: Solution for a central density $\rho_c = 9.5 \times 10^{17}$ g/cm^3, using the SLy EOS. The plot shows the metric functions $e^{\alpha(x)}$ and $e^{-\beta(x)}$, as well as the dimensionless pressure $\overline{P}(x)$ and energy density $\overline{\epsilon}(x)$. The vertical line indicates the position of the surface of the star. The numerical solution (left side of the vertical line) smoothly matches with the exterior exact solution (right side of the vertical line).

that there is a maximum value of the mass with respect to the central density of the neutron star, see figure 3.4.3b. In addition, the continuity of the interior solution with the exterior solution is evident in the figure 3.4.2.

Continuing with the SLy EOS, integrating for various values of central density, we found different equilibrium configurations that a neutron star (modeled with this EOS) can have in General Relativity, represented in figure 3.4.3.

Similarly for the other EOSs, we can represent the mass-radius relation resulting from the T.O.V. equation, see figure 3.4.4. The maximum masses for each EOS are shown in table 3.4.1. We observe that the causality condition cuts the curves so that the speed of sound is smaller than the speed of light (the solid curves for SLy, BSk19 and BSk22 EOSs). In principle, this condition could change the maximum mass in each curve that are physical, but it is not the case in our results. In particular, for the SLy and BSk19 EOSs, the maximum mass coincides with the last point where $v_s = c$, but the BSk22 EOS admits more solutions on the left branch of the maximum mass. The last turn of the curve for the SLy EOS satisfies the causality condition again. Cutting the curves at the point where the causality condition is not satisfied (or just marking the solution) has been done, for example, in Refs. [50, 53, 67]. Nevertheless, if the EOS is non-relativistic, we should only consider the solutions where $v_s \ll c$, such as when the speed

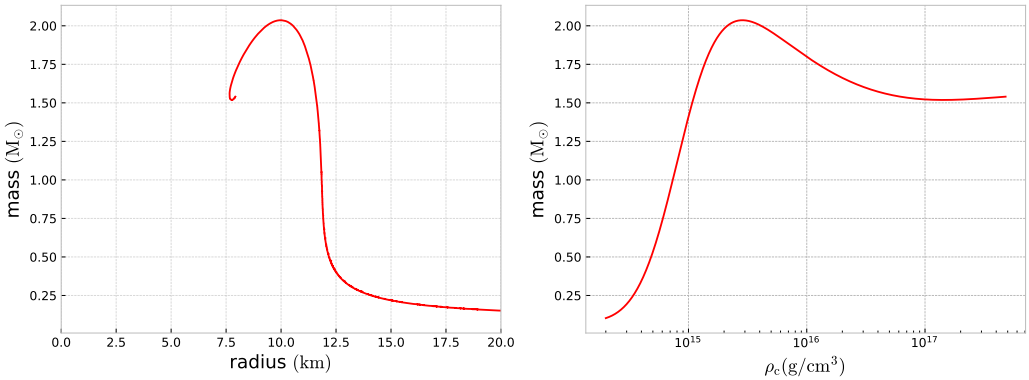

(a) Mass-radius relation.

(b) Mass-central density relation.

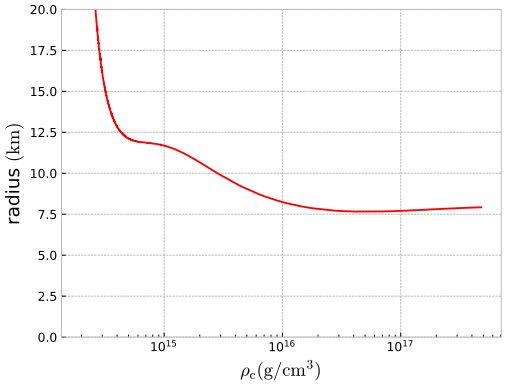

(c) Radius-central density relation.

Figure 3.4.3: Profiles for neutron star solutions using SLy EOS in GR.

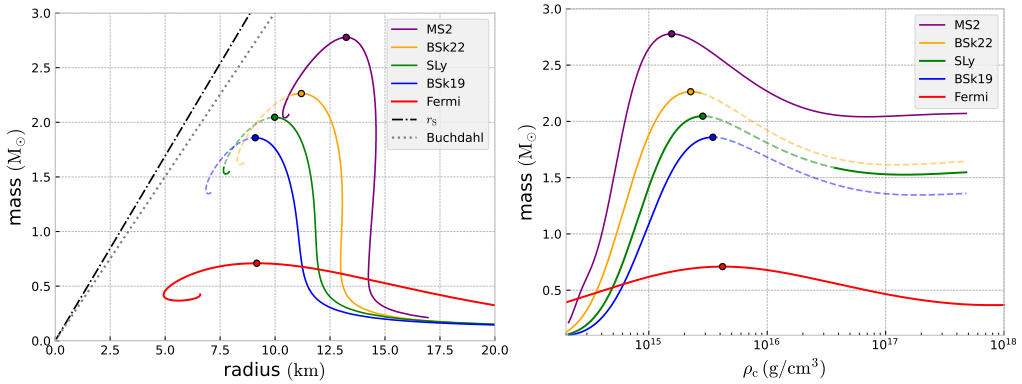

(a) Mass-radius relation.

(b) Mass-central density relation.

Figure 3.4.4: Profiles for neutron star solutions using SLy, BSk19, BSk22, MS2 and Fermi EOSs in GR. The circles mark the maximum mass. The dashed lines of the curves are the solutions whose the speed of sound is greater than the speed of light.

of sound is, for instance, 10% the speed of light. Therefore, as shown in figure 2.4.4, the plots should be truncated at $\rho_c \sim 10^{14}$ g/cm^3, corresponding to masses significantly smaller than 0.1 $M_\odot$. Thus, since the pressure/density profiles are similar for these EOSs, we can overlook this fact. We note that the equilibrium configurations are below the curve given by the Schwarzchild radius r_S and the Buchdahl's bound, but that does not mean that such mass-radius configurations can occur in nature, as we shall see in the next section.

EOS	$M_{\max}$ ($M_\odot$)	R (km)
Fermi	0.71	9.17
SLy	2.05	9.98
BSk19	1.86	9.10
BSk22	2.26	11.20
MS2	2.78	13.24

Table 3.4.1: Maximum masses with their respective radii for SLy, BSk19, BSk22, MS2 and Fermi EOSs.

3.5 Stability of relativistic stars

Equilibrium configurations of neutron stars are obtained by integrating the T.O.V. equation. In what follows, we will study if that equilibrium is stable under adiabatic radial oscillations. The calculations presented here were first developed in 1964 by Chandrasekhar [37].

Consider a perfect fluid sphere oscillating radially with a small amplitude. The non-perturbed metric is given by

$$ds^2 = -e^{\alpha_0}(cdt)^2 + e^{\beta_0}dr^2 + r^2[d\theta^2 + \sin^2\theta d\varphi^2], \tag{3.5.1}$$

where we have used the subscript 0 to denote the fields of the equilibrium configuration. Rewriting the equilibrium equations (3.2.40)-(3.2.42) for the fields α_0, β_0 and P_0, we have

$$\frac{d\alpha_0}{dr} = -\frac{1}{r}\left(1 - e^{\beta_0}\right) + \frac{8\pi G}{c^4}P_0 r e^{\beta_0}, \tag{3.5.2}$$

$$\frac{d\beta_0}{dr} = \frac{1}{r}\left(1 - e^{\beta_0}\right) + \frac{8\pi G}{c^4}\epsilon_0 r e^{\beta_0}, \tag{3.5.3}$$

$$\frac{dP_0}{dr} = -\frac{1}{2}(\epsilon_0 + P_0)\frac{d\alpha_0}{dr}. \tag{3.5.4}$$

The perturbations are assumed to be radial, then the spacetime preserves its spherical symmetry. For any spacetime with this characteristics, independent if is static or dynamic, one can always introduce Schwarzschild coordinates such that

$$ds^2 = -e^{\alpha}(dx^0)^2 + e^{\beta}dr^2 + r^2[d\theta^2 + \sin^2\theta d\varphi^2], \tag{3.5.5}$$

where $x^0 = ct$, $\alpha = \alpha(x^0, r)$ and $\beta = \beta(x^0, r)$ are the new functions of the metric, now perturbed. Therefore, we can write

$$\alpha(x^0, r) = \alpha_0(r) + \delta\alpha(x^0, r), \tag{3.5.6}$$

$$\beta(x^0, r) = \beta_0(r) + \delta\beta(x^0, r), \tag{3.5.7}$$

and similarly for the pressure P, the energy density ϵ and the baryon number density n. In addition, another perturbation is necessary to describe the oscillations: the radial displacement δr of the fluid from its equilibrium position. Thus, a fluid element located at the radial coordinate r in the equilibrium configuration is displaced to the radial coordinate $r + \delta r(x^0, r)$ at coordinate time t in the equilibrium configuration.

To perform the analysis of the oscillation, all equations will be linearized in the perturbation functions δr, $\delta\alpha$, $\delta\beta$, δP, $\delta\epsilon$ y δn.

3.5.1 Equations governing radial perturbations

Eulerian and Lagrangian perturbations

The evolution of these perturbations will be governed by: the Einstein field equations, the conservation of the energy-momentum tensor and the laws of Thermodynamics. However, before deriving these equations, we introduce two concepts. Similarly in the context of fluid mechanics, we define the **Eulerian perturbations**, denoted by δP and $\delta\epsilon$, as changes measured by a fixed observer at event of coordinates $(x^0, r, \theta, \varphi)$. On the other hand, we have the **Lagrangian perturbations**, denoted by ΔP and $\Delta\epsilon$, that are changes measured by an observer located at r in the equilibrium configuration, but located at $r + \delta r(x^0, r)$ in the perturbed configuration. Eulerian and Lagrangian perturbations can be related

by

$$\Delta P(x^0, r) = P[x^0, r + \delta r(x^0, r)] - P_0(r) \approx \delta P + P_0' \delta r, \tag{3.5.8}$$

$$\Delta \epsilon(x^0, r) = \epsilon[x^0, r + \delta r(x^0, r)] - \epsilon_0(r) \approx \delta \epsilon + \epsilon_0' \delta r, \tag{3.5.9}$$

$$\Delta n(x^0, r) = n[x^0, r + \delta r(x^0, r)] - n_0(r) \approx \delta n + n_0' \delta r. \tag{3.5.10}$$

Baryon conservation

Baryon conservation law (2.1.4) governs the evolution of the perturbations δn and Δn. The equation (2.1.4) can be written as

$$\frac{dn}{d\tau} = -n \nabla_\mu u^\mu. \tag{3.5.11}$$

By introducing small radial perturbations in the star, the u^0 and u^r components are the only non-zero ones. The 4-velocity components are related by the following expressions:

$$\frac{u^r}{u^0} = \frac{dr/d\tau}{d(ct)/d\tau} = \frac{1}{c}\frac{dr}{dt} = \frac{1}{c}\frac{\partial \delta r}{\partial t} \equiv \frac{1}{c}\dot{\delta r}, \tag{3.5.12}$$

and

$$-(u^0)^2 e^\alpha + (u^r)^2 e^\beta = -c^2. \tag{3.5.13}$$

From equation (3.5.12), we have $u^r = u^0 \dot{\delta r}/c$. Replacing this in equation (3.5.13), we obtain

$$-(u^0)^2 e^\alpha + \left(\dot{\delta r}\right)^2 (u^0)^2 e^\beta = -c^2, \tag{3.5.14}$$

$$u^0 = c e^{-\alpha/2} \approx c e^{-\alpha_0/2} \left(1 - \frac{1}{2}\delta\alpha\right). \tag{3.5.15}$$

Therefore, the result at first order in δr, $\delta\alpha$ and $\delta\beta$ is

$$u^0 = c e^{-\alpha_0/2} \left(1 - \frac{1}{2}\delta\alpha\right), \tag{3.5.16}$$

$$u^r = \dot{\delta r} e^{-\alpha_0/2}. \tag{3.5.17}$$

Note that the u^r component is of first order in the perturbation, unlike u^0 which has terms of zeroth and first order.

Now, for any perturbed field $\psi = \psi(x^0, r)$, i.e.,

$$\psi(x^0, r) = \psi_0(r) + \delta\psi(x^0, r) = \psi_0(r) + \Delta\psi(x^0, r) - \psi_0'(r)\delta r(x^0, r), \tag{3.5.18}$$

with $\Delta\psi = \delta\psi + \psi_0'\delta r$, we can write

$$\begin{aligned}
\frac{d\psi}{d\tau} &= \frac{u^0}{c}\frac{\partial}{\partial t}[\psi_0 + \Delta\psi - \psi_0'\delta r] + u^r\frac{\partial}{\partial r}[\psi_0 + \Delta\psi - \psi_0'\delta r] \\
&\approx \frac{u^0}{c}\frac{\partial\Delta\psi}{\partial t} - \frac{u^0}{c}\psi_0'\dot{\delta r} + u^r\psi_0' + u^r\frac{\partial\Delta\psi}{\partial r} \\
&\approx \left(\frac{u^0}{c}\frac{\partial\Delta\psi}{\partial t} + u^r\frac{\partial\Delta\psi}{\partial r}\right) - e^{-\alpha_0/2}\psi_0'\dot{\delta r} + e^{-\alpha_0/2}\psi_0'\dot{\delta r} \\
&= \frac{d\Delta\psi}{d\tau},
\end{aligned} \tag{3.5.19}$$

where in the penultimate line the components (3.5.16) and (3.5.17) for the 4-velocity were used. Thus, equation (3.5.11) can be written as

$$\frac{d\Delta n}{d\tau} = -n\nabla_\mu u^\mu. \tag{3.5.20}$$

Recall the identity [38]

$$\nabla_\mu u^\mu \equiv \frac{1}{\sqrt{-g}}\partial_\mu\left(\sqrt{-g}u^\mu\right), \tag{3.5.21}$$

where g is the metric determinant. In our case, we have

$$\sqrt{-g} = e^{\alpha/2}e^{\beta/2}r^2\sin\theta \approx e^{\alpha_0/2}e^{\beta_0/2}\left(1 + \frac{1}{2}\delta\alpha + \frac{1}{2}\delta\beta\right)r^2\sin\theta. \tag{3.5.22}$$

Using the identity (3.5.22) in the equation (3.5.20), we can write

$$u^\mu\frac{\partial\Delta n}{\partial x^\mu} = -\frac{n}{\sqrt{-g}}\partial_\mu(\sqrt{-g}u^\mu), \tag{3.5.23}$$

$$\begin{aligned}
\frac{u^0}{c}\frac{\partial\Delta n}{\partial t} + u^r\frac{\partial\Delta n}{\partial r} = &-\frac{n_0 + \delta n}{e^{\alpha_0/2+\beta_0/2}\left(1 + \frac{1}{2}\delta\alpha + \frac{1}{2}\delta\beta\right)r^2\sin\theta} \\
&\left[\frac{1}{c}\frac{\partial}{\partial t}\left(e^{\alpha_0/2+\beta_0/2}\left(1 + \frac{1}{2}\delta\alpha + \frac{1}{2}\delta\beta\right)r^2\sin\theta u^0\right)\right. \\
&\left.+\frac{\partial}{\partial r}\left(e^{\alpha_0/2+\beta_0/2}\left(1 + \frac{1}{2}\delta\alpha + \frac{1}{2}\delta\beta\right)r^2\sin\theta u^r\right)\right],
\end{aligned} \tag{3.5.24}$$

$$\frac{u^0}{c}\frac{\partial \Delta n}{\partial t} = -\frac{n_0+\delta n}{e^{\alpha_0/2+\beta_0/2}r^2\left(1+\frac{1}{2}\delta\alpha+\frac{1}{2}\delta\beta\right)}\left[\frac{1}{c}\frac{\partial}{\partial t}\left(e^{\alpha_0/2+\beta_0/2}r^2\left(1+\frac{1}{2}\delta\alpha+\frac{1}{2}\delta\beta\right)u^0\right)\right.$$
$$\left.+\frac{\partial}{\partial r}\left(e^{\alpha_0/2+\beta_0/2}r^2u^r\right)\right]. \tag{3.5.25}$$

Replacing the 4-velocity components (3.5.16) and (3.5.17) in equation (3.5.25), we obtain

$$e^{-\alpha_0/2}\frac{\partial \Delta n}{\partial t} = -\frac{n_0+\delta n}{e^{\alpha_0/2+\beta_0/2}r^2\left(1+\frac{1}{2}\delta\alpha+\frac{1}{2}\delta\beta\right)}$$
$$\left[\frac{\partial}{\partial t}\left(r^2e^{\beta_0/2}\left(1+\frac{1}{2}\delta\alpha+\frac{1}{2}\delta\beta\right)\left(1-\frac{1}{2}\delta\alpha\right)\right)+\frac{\partial}{\partial r}\left(e^{\beta_0/2}r^2\dot{\delta r}\right)\right], \tag{3.5.26}$$

$$\begin{aligned}\frac{\partial \Delta n}{\partial t} &= -\frac{n_0+\delta n}{e^{\beta_0/2}r^2\left(1+\frac{1}{2}\delta\alpha+\frac{1}{2}\delta\beta\right)}\left[\frac{1}{2}r^2e^{\beta_0/2}\frac{\partial\delta\beta}{\partial t}+\frac{\partial}{\partial r}\left(e^{\beta_0/2}r^2\dot{\delta r}\right)\right]\\ &= -\frac{n_0+\delta n}{e^{\beta_0/2}r^2}\left(1-\frac{1}{2}\delta\alpha-\frac{1}{2}\delta\beta\right)\left[\frac{1}{2}r^2e^{\beta_0/2}\frac{\partial\delta\beta}{\partial t}+\frac{\partial}{\partial r}\left(e^{\beta_0/2}r^2\dot{\delta r}\right)\right] \qquad (3.5.27)\\ &= -n_0\left[\frac{1}{2}\frac{\partial\delta\beta}{\partial t}+r^{-2}e^{-\beta_0/2}\frac{\partial}{\partial r}\left(e^{\beta_0/2}r^2\dot{\delta r}\right)\right].\end{aligned}$$

Integrating with respect to the time coordinate t and using the equation (3.5.10), we obtain the equation that governs the evolution of the perturbation δn:

$$\delta n = -n_0\left[r^{-2}e^{-\beta_0/2}(r^2e^{\beta_0/2}\delta r)'+\frac{1}{2}\delta\beta\right]-n_0'\delta r. \tag{3.5.28}$$

Note that the integration constant is zero, since when we "turn off" the perturbations ($\delta r = \delta\beta = 0$), we impose $\delta n = 0$.

Adiabaticity

For adiabatic oscillations, the Lagrangian changes in number density and pressure are related by the adiabatic index (2.1.12), then

$$\Gamma = \frac{n}{P}\left(\frac{\partial P}{\partial n}\right)_s = \frac{n}{p}\frac{\Delta P}{\Delta n}. \tag{3.5.29}$$

Combining this relation with (3.5.28), and equation (3.5.8) for δP in terms of

ΔP, we found that

$$\Gamma = \frac{(n_0 + \delta n)(\delta P + P_0' \delta r)}{-n_0(P_0 + \delta P)\left[r^{-2}e^{-\beta_0/2}(r^2 e^{\beta_0/2}\delta r)' + \frac{1}{2}\delta\beta\right]}, \tag{3.5.30}$$

$$-\Gamma n_0 P_0 \left[r^{-2}e^{-\beta_0/2}(r^2 e^{\beta_0/2}\delta r)' + \frac{1}{2}\delta\beta\right] = n_0\delta P + n_0 P_0'\delta r. \tag{3.5.31}$$

Simplifying, we obtain the equation that governs the evolution of the perturbation δP:

$$\delta P = -\Gamma P_0 \left[r^{-2}e^{-\beta_0/2}(r^2 e^{\beta_0/2}\delta r)' + \frac{1}{2}\delta\beta\right] - P_0'\delta r. \tag{3.5.32}$$

Energy conservation

Recall the first law of thermodynamics (2.1.7). Since we are studying adiabatic radial oscillations, the entropy of the fluid remains constant. Thus, applying the first law along a flow line, plus the assumption that the entropy per baryon is conserved along the flow line, we find the law of (local) conservation of energy:

$$\frac{d\epsilon}{d\tau} = \frac{\epsilon + P}{n}\frac{dn}{d\tau}. \tag{3.5.33}$$

Rewriting in terms of Lagrangian perturbations, we obtain

$$\frac{d\Delta\epsilon}{d\tau} = \frac{\epsilon + P}{n}\frac{d\Delta n}{d\tau}. \tag{3.5.34}$$

Expanding the equation (3.5.34) to first order, we have

$$\begin{aligned}\frac{d\Delta\epsilon}{d\tau} &= \frac{(\epsilon_0 + P_0 + \delta\epsilon + \delta P)}{(n_0 + \delta n)}\frac{d\Delta n}{d\tau} \\ &= \frac{\epsilon_0 + P_0}{n_0}\frac{d\Delta n}{d\tau}.\end{aligned} \tag{3.5.35}$$

Integrating with respect to the proper time τ and setting the integration constant to zero (since $\Delta\epsilon = 0$ when $\delta n = 0$), we find a relation between the Lagrangian perturbations of ϵ and n given by

$$\Delta\epsilon = \frac{\epsilon_0 + P_0}{n_0}\Delta n. \tag{3.5.36}$$

Combining (3.5.36) with equation (3.5.28) for Δn and equation (3.5.9) for $\delta\epsilon$ in terms of $\Delta\epsilon$, we obtain the equation for the evolution of $\delta\epsilon$:

$$\delta\epsilon = -(\epsilon_0 + P_0)\left[r^{-2}e^{-\beta_0/2}(r^2 e^{\beta_0/2}\delta r)' + \frac{1}{2}\delta\beta\right] - \epsilon_0'\delta r. \tag{3.5.37}$$

Einstein field equations

Two of the Einstein field equations, when linearized, reduce to the equations governing the evolution of the perturbations $\delta\alpha$ and $\delta\beta$. The complete calculation can be found in appendix B, the main results will be summarized here. The relevant components of the Einstein tensor, when we evaluate in the metric (3.5.5), are:

$$G_{0r} = \frac{1}{cr}\frac{\partial\beta}{\partial t}(x^0, r), \tag{3.5.38}$$

$$G_{rr} = -\frac{1}{r^2}\left[e^{\beta(x^0,r)} - r\frac{\partial\alpha}{\partial r}(x^0, r) - 1\right]. \tag{3.5.39}$$

At first order, we can write these components as follows

$$G_{0r} = \frac{1}{rc}\frac{\partial\delta\beta}{\partial t}, \tag{3.5.40}$$

$$G_{rr} = (G_{rr})_0 - \frac{1}{r^2}e^{\beta_0}\delta\beta + \frac{1}{r}\frac{\partial\delta\alpha}{\partial r}, \tag{3.5.41}$$

where

$$(G_{rr})_0 = -\frac{1}{r^2}\left[e^{\beta_0} - r\frac{\partial\alpha_0}{\partial r} - 1\right] \tag{3.5.42}$$

is the (rr) component of the unperturbed Einstein tensor.

The components of the energy-momentum tensor (3.2.7) of interest, are:

$$T_{0r} = -\frac{1}{c}(\epsilon_0 + P_0)e^{\beta_0}\dot{\delta r}, \tag{3.5.43}$$

$$T_{rr} = P_0 e^{\beta_0} + P_0 e^{\beta_0}\delta\beta + \delta P e^{\beta_0}. \tag{3.5.44}$$

Consequently, the $(0r)$ component of field equation reduces to equation (B.16), that is,

$$\delta\beta = -\frac{8\pi G}{c^4}(\epsilon_0 + P_0)re^{\beta_0}\delta r = -\left(\frac{d\alpha_0}{dr} + \frac{d\beta_0}{dr}\right)\delta r. \tag{3.5.45}$$

Using the above equation in equations (3.5.28), (3.5.32) and (3.5.37), we can write them as follows:

$$\delta n = -n_0 r^{-2}(r^2 \delta r e^{-\alpha_0/2})' e^{\alpha_0/2} - n_0' \delta r, \tag{3.5.46}$$

$$\delta P = -\Gamma P_0 r^{-2}(r^2 \delta r e^{-\alpha_0/2})' e^{\alpha_0/2} - P_0' \delta r, \tag{3.5.47}$$

$$\delta \epsilon = -(\epsilon_0 + P_0) r^{-2}(r^2 \delta r e^{-\alpha_0/2})' e^{\alpha_0/2} - \epsilon_0' \delta r. \tag{3.5.48}$$

On the other hand, linearizing the (rr) component of field equation, we obtain the equation for the evolution of the perturbation $\delta\alpha$ (see (B.27)):

$$\frac{\partial \delta\alpha}{\partial r} = -\frac{8\pi G}{c^4}\Gamma P_0 r^{-1} e^{\alpha_0/2+\beta_0}(r^2 e^{-\alpha_0/2}\delta r)' + \frac{8\pi G}{c^4}\left[P_0' r - \epsilon_0 - P_0\right] e^{\beta_0}\delta r. \tag{3.5.49}$$

Momentum conservation

Consider the conservation law of the energy-momentum tensor (3.2.25). Using the form of this tensor for a perfect fluid (3.2.7), we find that

$$\partial_\nu(\epsilon + P)u^\mu u^\nu + (\epsilon + P)a^\mu + (\epsilon + P)u^\mu \nabla_\nu u^\nu + c^2 g^{\mu\nu}\partial_\nu P = 0, \tag{3.5.50}$$

where $a^\mu = u^\nu \nabla_\nu u^\mu$ is the 4-acceleration of the fluid. Taking the r component of this equation, the first and third terms vanish, since u^r is of first order in the perturbation and both $\partial_\nu(\epsilon + P)u^\nu$ and $\nabla_\nu u^\nu$ are also of first order because they are zero in the equilibrium configuration. Thus, equation (3.5.50) reduces to

$$(\epsilon + P)a^r + c^2 e^{-\beta} P' = 0. \tag{3.5.51}$$

Let us determine the a^r component of the 4-acceleration, to first order:

$$\begin{aligned} a^r &= u^0 \nabla_0 u^r + u^r \nabla_r u^r \\ &\approx u^0 \left(\frac{1}{c}\frac{\partial u^r}{\partial t} + \Gamma^r{}_{0\lambda} u^\lambda\right) \\ &\approx e^{-\alpha_0}\ddot{\delta r} + \frac{c^2}{2} e^{-\beta_0}(1 - \delta\beta)\alpha_0' + \frac{c^2}{2} e^{-\beta_0}\delta\alpha'. \end{aligned} \tag{3.5.52}$$

Thus, equation (3.5.51) can be written to first order as follows:

$$\begin{aligned}&(\epsilon_0+P_0)\left[e^{-\alpha_0}\ddot{\delta r}+\frac{c^2}{2}e^{-\beta_0}(1-\delta\beta)\alpha_0'+\frac{c^2}{2}e^{-\beta_0}\delta\alpha'\right]\\&+\frac{c^2}{2}(\delta\epsilon+\delta P)e^{-\beta_0}\alpha_0'+c^2e^{-\beta_0}(1-\delta\beta)(P_0'+\delta P')=0.\end{aligned}\tag{3.5.53}$$

If we write this equation only in terms of the functions in the equilibrium configuration, then we obtain an equation for the evolution of δr:

$$\begin{aligned}&\frac{1}{c^2}(\epsilon_0+P_0)e^{\beta_0-\alpha_0}\ddot{\delta r}\\&=\frac{4\pi G}{c^4}(\epsilon_0+P_0)\left[\Gamma P_0 r^{-1}e^{\alpha_0/2+\beta_0}(r^2e^{-\alpha_0/2}\delta r)'-(P_0'r-\epsilon_0-P_0)\,e^{\beta_0}\delta r\right]\\&\quad+\frac{1}{2}\left[(\epsilon_0+P_0)r^{-2}(r^2\delta re^{-\alpha_0/2})'e^{\alpha_0/2}+\Gamma P_0r^{-2}(r^2\delta re^{-\alpha_0/2})'e^{\alpha_0/2}\right.\\&\quad\left.+\epsilon_0'\delta r+P_0'\delta r\right]\alpha_0'+\left[\Gamma P_0r^{-2}(r^2\delta re^{-\alpha_0/2})'e^{\alpha_0/2}+P_0'\delta r\right]'.\end{aligned}\tag{3.5.54}$$

If we define the **normalized displacement function**

$$\sigma:=r^2e^{-\alpha_0/2}\delta r,\tag{3.5.55}$$

we can write equation (3.5.54) as follows

$$\begin{aligned}&\frac{1}{c^2}(\epsilon_0+P_0)r^{-2}e^{\beta_0-\alpha_0/2}\ddot{\sigma}\\&=\frac{4\pi G}{c^4}(\epsilon_0+P_0)\left[\Gamma P_0r^{-1}e^{\alpha_0/2+\beta_0}\sigma'-(P_0'r-\epsilon_0-P_0)\,r^{-2}e^{\alpha_0/2+\beta_0}\sigma\right]\\&\quad+\frac{1}{2}\left[(\epsilon_0+P_0)r^{-2}\sigma'e^{\alpha_0/2}+\Gamma P_0r^{-2}\sigma'e^{\alpha_0/2}+(\epsilon_0'+P_0')r^{-2}e^{\alpha_0/2}\sigma\right]\alpha_0'\\&\quad+\left[\Gamma P_0r^{-2}\sigma'e^{\alpha_0/2}+P_0'r^{-2}e^{\alpha_0/2}\sigma\right]'.\end{aligned}\tag{3.5.56}$$

Multiplying both sides by $e^{\alpha_0+\beta_0/2}$, followed by an extensive calculation, equation (3.5.56) reduces to [38]

$$W\ddot{\sigma}=(Q\sigma')'+R\sigma,\tag{3.5.57}$$

where the coefficients are given by

$$W=\frac{1}{c^2}(\epsilon_0+P_0)r^{-2}e^{\alpha_0/2+3\beta_0/2},\tag{3.5.58}$$

$$Q=\Gamma P_0r^{-2}e^{3\alpha_0/2+\beta_0/2},\tag{3.5.59}$$

$$R = e^{3\alpha_0/2+\beta_0/2}\left[\frac{(P_0')^2}{\epsilon_0+P_0}r^{-2} - 4P_0'r^{-3} - \frac{8\pi G}{c^4}(\epsilon_0+P_0)P_0 r^{-2}e^{\beta_0}\right]. \tag{3.5.60}$$

There are infinite ways to write (3.5.57), but this form is preferred because it leads us to a Sturm-Liouville problem for the radial perturbations.

Boundary conditions

Not all solutions of equation (3.5.57) are physically acceptable. In order to be so, the displacement function δr must produce finite density and pressure perturbations at the center of the star, which means

$$\lim_{r\to 0^+}\frac{\delta r}{r} = \text{finite}. \tag{3.5.61}$$

In fact, if we expand equations (3.5.47) and (3.5.48), we have

$$\delta P = -2\Gamma P_0 r^{-1}\delta r - \Gamma P_0\delta r' + \frac{1}{2}\Gamma P_0\delta r\alpha_0' - P_0'\delta r, \tag{3.5.62}$$

$$\delta\epsilon = -2(\epsilon_0+P_0)r^{-1}\delta r - (\epsilon_0+P_0)\delta r' + \frac{1}{2}(\epsilon_0+P_0)\delta r\alpha_0' - \epsilon_0'\delta r. \tag{3.5.63}$$

Taking the limit $r\to 0$, the expressions are finite if the equation (3.5.61) is verified, since it implies that $\delta r(x^0,0)=0$ and

$$\delta r'(x^0,0) = \lim_{r\to 0}\frac{\delta r(x^0,r)-\delta r(x^0,0)}{r} = \lim_{r\to 0}\frac{\delta r}{r} = \text{finite}. \tag{3.5.64}$$

In terms of the function σ, this boundary condition translates to

$$\lim_{r\to 0^+}\frac{\sigma}{r^3} = \text{finite}. \tag{3.5.65}$$

In addition, the displacement function must also leave the pressure equal to zero at the surface of the star. Thus, from equations (3.5.47) and (3.5.8), we must have

$$\lim_{r\to R}\Delta P = \lim_{r\to R}[\Gamma P_0 r^{-2}e^{\alpha_0/2}\sigma'] = 0. \tag{3.5.66}$$

3.5.2 Stability and normal modes

Assume that the normalized displacement function (3.5.55) has a harmonic time dependence, that is [2],

$$\sigma(x^0, r) = u(r)e^{-i\omega t}. \tag{3.5.67}$$

Thus, the dynamic equation (3.5.57) and the boundary conditions (3.5.61)-(3.5.66) reduce to a Sturm-Liouville problem with Dirichlet-Neumann boundary conditions for the squared frequency ω^2 (eigenvalue) and the amplitude $u(r)$ (eigenfunction):

$$(Qu')' + Ru + \omega^2 Wu = 0, \tag{3.5.68}$$

where the boundary conditions are:

$$\lim_{r\to 0} \frac{u(r)}{r^3} = \text{finite}, \tag{3.5.69}$$

$$\lim_{r\to R}[\Gamma P_0 r^{-2} e^{\Phi_0} u'(r)] = 0. \tag{3.5.70}$$

Since we obtained a Sturm-Liouville problem, we have the following results [5]:

1. The eigenvalues ω^2 are all real.
2. The eigenvalues form an infinite discrete sequence

$$\omega_0^2 < \omega_1^2 < \omega_2^2 < \cdots . \tag{3.5.71}$$

3. The eigenfunction u_0 corresponding to ω_0^2 has no nodes in the interval $0 < r < R$. Generally, u_n has n nodes in this interval.
4. The functions u_n are orthogonal with weight W:

$$\int_0^R u_n(r)u_m(r)W(r)\,dr = 0, \qquad m \neq n. \tag{3.5.72}$$

5. The functions u_n are **normal modes** and form a complete set for the expansion of any function satisfying the boundary conditions (3.5.69) and (3.5.70).

[2] Since the differential equation is linear, this is equivalent to take the Fourier transform.

Consequently, under radial perturbations we say that

- the star is **unstable**, if any of the eigenvalues ω_n^2 is negative, since we would have purely imaginary frequencies and the amplitude of the perturbation of the star would grow exponentially as $e^{|\omega_n|t}$.
- the star is **stable**, if all of the eigenvalues ω_n^2 are positive, since the frequency is real and any perturbation of the star will oscillate as $e^{i\omega t}$.

Lastly, one important consequence of the property 2. is that if the fundamental radial mode of a star is stable ($\omega_0^2 > 0$), then all radial modes are stable. In contrast, if the star is radially unstable, the fastest growing instability will occur through the fundamental mode (ω_0^2 is "more negative" than the other ω_n^2's).

In what follows, we will relate this type of stability analysis to more general properties of stars, for example, how can we relate the eigenfrequencies to the mass and central density of the star?

3.5.3 Sufficient and necessary conditions for stability

A solution of the T.O.V. equation that satisfies the appropriated boundary conditions describes a stellar configuration in hydrostatic equilibrium. This equilibrium can be stable or unstable. Consider a sequence of equilibrium configurations obtained by integrating the T.O.V. equations, with different values of central density ρ_c. The mass of the star will be a function of the central density, $M = M(\rho_c)$. The star will pass from stability to instability with respect to any radial mode of oscillation only if at a value of central density the following condition is satisfied:

$$\frac{dM(\rho_c)}{d\rho_c} = 0. \tag{3.5.73}$$

This result applies to EOSs without discontinuities at zero temperature. We will now give a heuristic proof of this result found in [36] [3].

The $M(\rho_c)$ profile is represented in figure 3.5.1, where each point on this curve defines an equilibrium configuration of the star. Given a star in the equilibrium configuration A, if a small radial perturbation reduces its central density, the new (non-equilibrium) configuration will be represented by the point A_1. This point is

[3] For a more rigorous proof, see chapter 7 of [68].

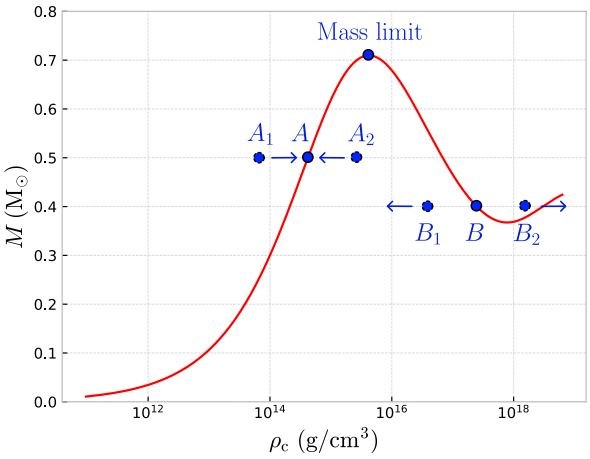

Figure 3.5.1: Mass-central density relation for NS using the Fermi EOS in GR.

above the curve, then the perturbed star has a mass greater than the mass of the corresponding equilibrium configuration for that central density. Consequently, the star is out of equilibrium because gravity exceeds pressure, and the star will contract, increasing its central density, thus returning to the equilibrium configuration A.

Similarly, if the radial perturbation increases its central density, the new configuration is represented by the point A_2 located under the curve. The star in the point A_2 has a mass smaller than the one corresponding to the equilibrium configuration for that central density. In this case, gravity is weaker than pressure, and the star will expand to return to the equilibrium configuration. Thus, we say that the equilibrium in A is stable. In conclusion, if A is a stable equilibrium configuration, then

$$\frac{dM}{d\rho_c} > 0, \tag{3.5.74}$$

at the point A. In contrast, for the point B where

$$\frac{dM}{d\rho_c} < 0, \tag{3.5.75}$$

a displacement to the configuration B_1, gravity is weaker that the pressure inside the star, so it will expand reducing its central density. Similarly, a displacement to the configuration B_2, gravity exceeds pressure, so the star will contract increasing its central density. Thus, the equilibrium configuration B is unstable.

In figure 3.5.1, the branch to the left of the maximum mass corresponds to

stable equilibrium configurations, while the right branch corresponds to unstable equilibrium configurations [36].

Is the condition $dM/d\rho_c > 0$ sufficient to say that the star is stable?

Harrison, Thorne, Wakano and Wheeler [68] proved that an equilibrium configuration has a zero-frequency mode of oscillation if condition (3.5.73) is verified. Thus, as a consequence of the eigenfrequency ordering and the fact that an oscillation mode changes stability at a stationary point (3.5.73), we can infer the following: if the fundamental mode becomes unstable at the maximum mass, then the next mininum in the sequence the stability is restored to the fundamental mode or the next oscillation mode (overtone) becomes unstable, and so on.

For instance, in the branch to the left of the maximum mass in figure 3.5.1 all the modes have $\omega_n^2 > 0$ and the right branch has one or more modes with $\omega_n^2 < 0$, in particular, the fundamental mode becomes unstable [36]. However, upon reaching the other critical (or stationary) point of the plot (a minimum), the fundamental mode remains unstable, while the first overtone (mode with $n = 1$) becomes unstable, even though $dM/d\rho_c > 0$. In conclusion:

> The statement $dM/d\rho_c > 0$ is a necessary condition for stellar stability but not sufficient.

3.5.4 Numerical solution

The problem of radial perturbations is not new; several methods have been used to estimate the frequencies of the radial modes for a variety of EOSs. A common analytical method to understand the stability of a star is to use a variational principle, in particular, the **Rayleigh-Ritz variational technique** [69]. This technique tells us that the eigenfunctions that satisfy equation (3.5.68) are those that minimize the functional

$$I[u] = \frac{\int_0^R (Qu'^2 - Ru^2)\, dr}{\int_0^R Wu^2\, dr}, \tag{3.5.76}$$

and the minimum value that it takes is ω_0^2. If it is positive, the star is stable and if it is negative, the star is unstable under adiabatic radial perturbations. Since

the denominator of equation (3.5.76) is positive definite, we have stability if and only if

$$\int_0^R (Qu'^2 - Ru^2)\, dr > 0, \tag{3.5.77}$$

for all the functions u that satisfy the boundary conditions (3.5.69) and (3.5.70).

Using this method, one can prove that Newtonian stars are stable if the pressure-averaged adiabatic index

$$\bar{\Gamma} := \frac{\int_0^R \Gamma P_0 4\pi r^2\, dr}{\int_0^R P_0 4\pi r^2\, dr}, \tag{3.5.78}$$

is greater that $4/3$; unstable if $\bar{\Gamma} < 4/3$, and marginally unstable if $\bar{\Gamma} = 4/3$ [5]. In the last case, the fundamental frequency is equal to zero. For relativistic stars, the criterion is no longer valid as a test for stability.

The method described above is difficult to implement in the context of relativistic stars. For this reason, numerical methods have been used to analyze the stability of stars solving equation (3.5.68) with boundary conditions (3.5.69) and (3.5.70). The most used method is the **shooting method** [70]. In simple words, this method consists of starting with a trial value of ω^2, integrating toward its surface and searching for the value of ω_n^2 such that the boundary condition at the surface is satisfied and the solution has n nodes.

Defining $v := Qu'$, the second order differential equation (3.5.68) can be written as the following system of first order differential equations for u and v:

$$\frac{du}{dr} = \frac{v}{Q}, \tag{3.5.79}$$

$$\frac{dv}{dr} = -(R + \omega^2 W)u. \tag{3.5.80}$$

If we assume that each function is regular close to the origin, then we can expand

$$f(r) = f_0 + f_1 r + f_2 r^2 + \cdots, \quad r \to 0, \tag{3.5.81}$$

with $f = \{u, v, \alpha_0, \beta_0, \Gamma, P_0, \epsilon_0\}$. Using the boundary condition (3.5.69), we find $u_0 = u_1 = u_2 = 0$. Thus, replacing these expansions in equations (3.5.79) and (3.5.80), we found that

$$v(r) = 3u_3 \Gamma(0) P_0(0) e^{3\alpha_0(0)/2 + \beta_0(0)/2} + \mathcal{O}(r). \tag{3.5.82}$$

Choosing $u_3 = 1/(3\Gamma(0)P_0(0)e^{3\alpha_0(0)/2+\beta_0(0)/2})$, the initial values for the integration are $u(0) = 0$ and $v(0) = 1$. With this choice we do not lose generality because the differential equations are linear, and it is equivalent to divide the equations by $3u_3\Gamma(0)P_0(0)e^{3\alpha_0(0)/2+\beta_0(0)/2}$ and define new variables $\tilde{u} := u/(3\Gamma(0)P_0(0)e^{3\alpha_0(0)/2+\beta_0(0)/2})$ and $\tilde{v} := v/(3\Gamma(0)P_0(0)e^{3\alpha_0(0)/2+\beta_0(0)/2})$. At the surface of the star, the condition (3.5.70) translates to $v(R) = 0$.

Performing a dimensional analysis, we found that u has units of length cube and v has units of pressure. Therefore, we propose to rewrite these functions in terms of normalized functions in the following way:

$$u(r) =: a^3\overline{u}(r), \qquad v(r) =: K\overline{v}(r), \tag{3.5.83}$$

where the constants a and K are defined in (3.4.10) and (2.3.11), respectively.

Following the same approach made in the static case, we express the radial coordinate, the pressure and the energy density as

$$r = ax, \qquad P_0 = K\overline{P}_0, \qquad \epsilon_0 = K\overline{\epsilon}_0. \tag{3.5.84}$$

Therefore, we can write the normalized form of the system of differential equations (3.5.79) and (3.5.80) as follows

$$\frac{d\overline{u}}{dx} = A(x)\overline{v}, \tag{3.5.85}$$

$$\frac{d\overline{v}}{dx} = -[B(x) + \Omega^2 C(x)]\overline{u}, \tag{3.5.86}$$

where $\Omega^2 := a^2\omega^2/c^2$ is the normalized squared frequency and the coefficients are given by

$$A(x) = \frac{x^2}{\Gamma\overline{P}_0 e^{3\alpha_0/2+\beta_0/2}}, \tag{3.5.87}$$

$$B(x) = \frac{e^{3\alpha_0/2+\beta_0/2}}{x^3}\left[\frac{x}{(\overline{\epsilon}_0+\overline{P}_0)}\left(\frac{d\overline{P}_0}{dx}\right)^2 - 4\frac{d\overline{P}_0}{dx} - 4x(\overline{\epsilon_0}+\overline{P}_0)\overline{P}_0 e^{2\beta_0}\right], \tag{3.5.88}$$

$$C(x) = \frac{(\overline{\epsilon}_0+\overline{P}_0)}{x^2}e^{\alpha_0/2+3\Lambda_0/2}. \tag{3.5.89}$$

The boundary conditions at the origin are $\overline{u}(0) = 0$ and $\overline{v}(0) = 1$, and at the

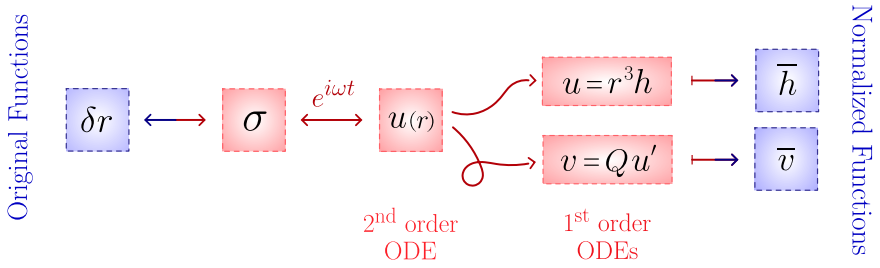

Figure 3.5.2: Changes of variable for radial perturbations.

surface of the star ($R = ax_1$), $\overline{v}(x_1) = 0$.

The system of differential equations for the functions $\overline{u}$ and $\overline{v}$ cannot be integrated numerically in a proper manner, since we have a divergence at the origin due to the division by power of x, see the coefficients in (3.5.87)-(3.5.89). To solve this problem, a change of variable is proposed for $\overline{u}$:

$$\overline{u}(x) = \overline{h}(x)x^3 \tag{3.5.90}$$

such that $\overline{h}(0) = 1/(3\Gamma(0)P_0(0)e^{3\alpha_0(0)/2+\beta_0(0)/2})$. A summary of all the changes of variable made in this section is found in figure 3.5.2.

Thus, the system of differential equations that is numerically integrated is

$$\frac{d\overline{h}}{dx} = \tilde{A}\overline{v} - \frac{3\overline{h}}{x}, \tag{3.5.91}$$

$$\frac{d\overline{v}}{dx} = -[\tilde{B} + \Omega^2\tilde{C}]\overline{h}, \tag{3.5.92}$$

where the coefficients are given by

$$\tilde{A}(x) = \frac{1}{x\Gamma\overline{P}_0 e^{3\alpha_0/2+\beta_0/2}}, \tag{3.5.93}$$

$$\tilde{B}(x) = e^{3\alpha_0/2+\beta_0/2}\left[\frac{x}{(\overline{\epsilon}_0+\overline{P}_0)}\left(\frac{d\overline{P}_0}{dx}\right)^2 - 4\frac{d\overline{P}_0}{dx} - 4x(\overline{\epsilon}_0+\overline{P}_0)\overline{P}_0 e^{\beta_0}\right], \tag{3.5.94}$$

$$\tilde{C}(x) = x(\overline{\epsilon}_0+\overline{P}_0)e^{\alpha_0/2+3\beta_0/2}. \tag{3.5.95}$$

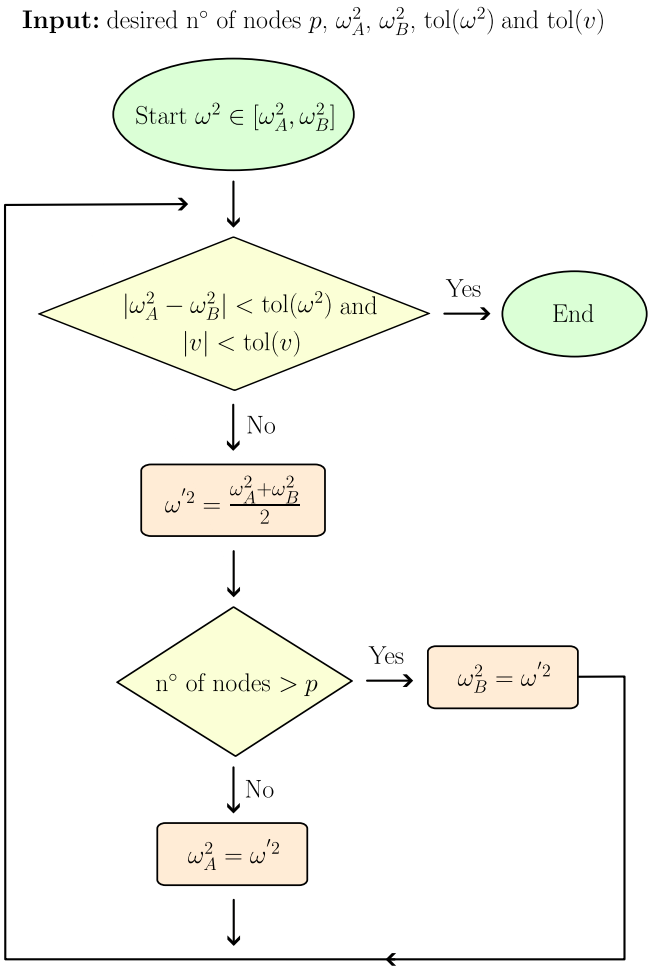

Figure 3.5.3: Numerical scheme of the shooting method.

Numerical scheme

In what follows, the implementation of the shooting method will be discussed. First, we define an initial interval for the value of the eigenfrequency, say $[\omega_A^2, \omega_B^2]$, with $\omega_A^2 < 0$. We divide the interval into two regions with the midpoint $\omega'^2 = (\omega_A^2 + \omega_B^2)/2$. If the solution of the function v for ω'^2 has a number of nodes greater than required, we change the upper limit of the interval from ω_B^2 to ω'^2. Otherwise, we change the lower limit from ω_A^2 to ω'^2. This procedure is repeated until $|\omega_A^2 - \omega'^2|$ (or $|\omega_B^2 - \omega'^2|$) is smaller than a given tolerance and $|\overline{v}|$ is close to zero, also given a tolerance value. In figure 3.5.3, the numerical scheme described is summarized. The advantage of implementing the shooting method in this way is that we can guarantee the convergence of the value obtained from the eigenfrequency for a given tolerance value.

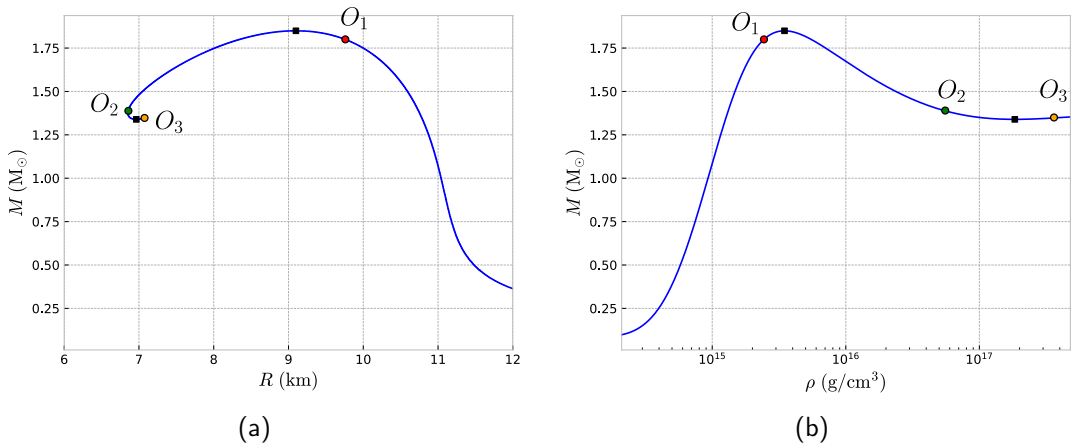

Figure 3.5.4: Mass versus radius and central density curves for neutron stars using the BSk19 EOS in GR. In the plots, the local maximum and local minimum are represented by squares.

The program is tested for NS solutions O_i, with $i = 1, 2, 3$, represented in figure 3.5.4. The masses, radii, central densities, and eigenfrequencies for the first three radial modes are registered in table 3.5.1. We observe that for the O_1 solution, for which $dM/d\rho_c > 0$, all of the squared eigenfrequencies are positive, then the solution is stable. Since the O_2 solution satisfies $dM/d\rho_c < 0$, the solution is unstable, which is verified by the fact that ω_0^2 is negative. However, the O_3 solution satisfies the condition $dM/d\rho_c > 0$ and $\omega_0^2, \omega_1^2 < 0$, then the NS is unstable, consistent with the fact that $dM/d\rho_c > 0$ is a necessary condition. The radial profiles of the radial displacement modes δr_n and the Lagrangian perturbation modes of the pressure ΔP_n for the fundamental mode ($n = 0$) and the n-overtones ($n = 1, 2, 5, 10$) were computed for these NS solutions, see figure 3.5.5. We can observe that the amplitude of the radial displacement grows as the radial coordinate increases, whereas ΔP oscillates with a decaying amplitude and finally vanishes at the surface of the star (satisfying the boundary conditions). Nevertheless, all the functions are smooth with respect to changes of the radial coordinate. For higher-order modes, some of the nodes move across the core-crust transition and lie in the crust ($0.9R \lesssim r \leq R$ [5]), where the radial displacement changes signs rapidly with a large amplitude, but ΔP_n has a small amplitude in the crust. This behavior for the higher-order modes is attenuated in solutions O_2 and O_3, i.e., as we move along the mass-radius curve (increasing the central density). The fundamental mode for the Lagrangian perturbation increases its

amplitude in the core of the NS. We discover that the apparent divergence of the radial displacement at the surface of the star is due to numerical error, since as the number of points increases and the tolerances of the eigenfrequencies are smaller, this growth is still present but with a smaller amplitude. Similar results are obtained for the SLy, BSk22 and MS2 EOSs.

	$M_{\max}$ ($M_\odot$)	R (km)	ρ_c (g/cm^3)	ω_0^2 (10^8s^{-2})	ω_1^2 (10^8s^{-2})	ω_2^2 (10^8s^{-2})
O_1	1.8	9.76	2.44×10^{15}	1.50	20.92	48.26
O_2	1.39	6.86	5.55×10^{16}	- 7.41	6.79	23.56
O_3	1.35	7.07	3.62×10^{17}	-10.40	-1.55	7.11

Table 3.5.1: Mass, radius, central density, and eigenfrequencies for the first three radial modes for NS solutions O_i, with $i = 1, 2, 3$, represented in figure 3.5.4.

As discussed in section 3.5.3, the change of neutron star stability occurs in the solution with the highest mass. We verify this statement by determining the eigenfrequencies of the first three radial modes for the SLy, BSk19, BSk22 and MS2 EOSs, see figure 3.5.6. We observe that ω_0^2 becomes negative at the maximum mass, independent of the EOS. In addition, the eigenfrequency ω_1^2 is negative just after the local minimum, confirming the theorem stated by Harrison, Thorne, Wakano and Wheeler [68] and discussed in the section 3.5.3, i.e., the solutions that verify $dM/d\rho_c = 0$ have a zero-frequency radial mode. Moreover, the fundamental mode becomes unstable at the maximum mass, and stability is not restored at the next minimum of the sequence since the next radial mode also becomes unstable.

Thus, the NS solutions on the left branch of the maximum mass are stable and the causality condition holds, proving once again that the condition $dM/\rho_c > 0$ and the causality condition are necessary (but not sufficient) conditions for stellar stability. Therefore, the study of radial perturbations is important for testing the stability of neutron star solutions.

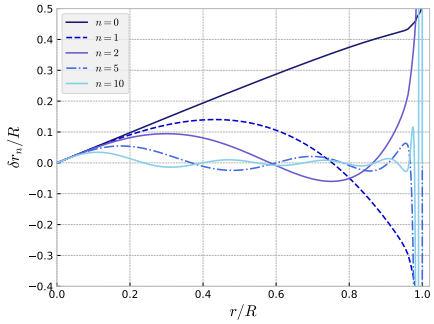

(a) Radial displacement, O_1 solution

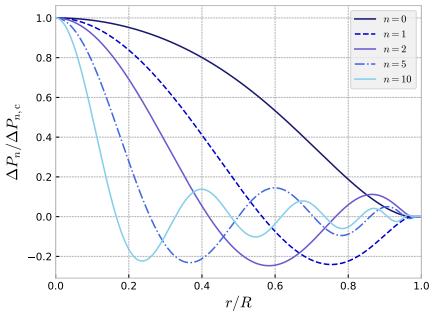

(b) Lagrangian perturbation of the pressure, O_1 solution

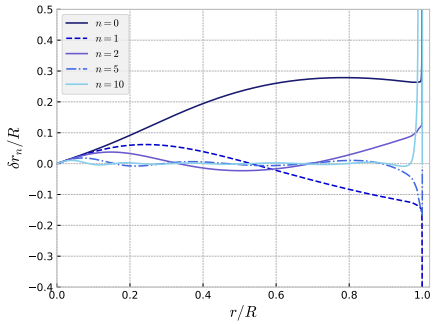

(c) Radial displacement, O_2 solution

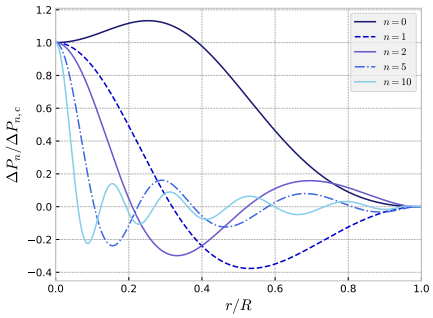

(d) Lagrangian perturbation of the pressure, O_2 solution

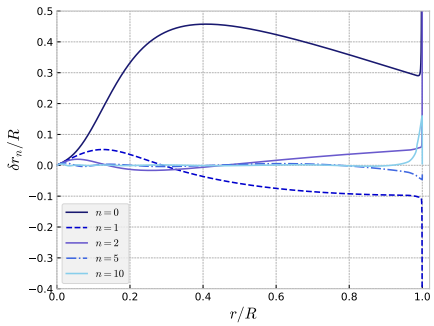

(e) Radial displacement, O_3 solution

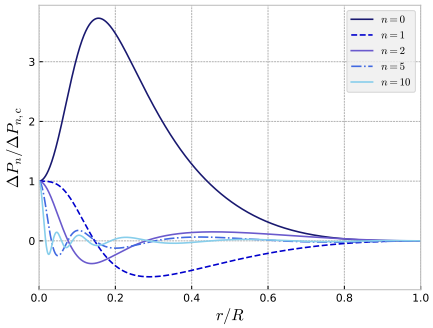

(f) Lagrangian perturbation of the pressure, O_3 solution

Figure 3.5.5: Plots of the radial displacement modes δr_n and the Lagrangian perturbation modes of the pressure ΔP_n versus the normalized radial coordinate r/R for the fundamental mode ($n = 0$) and the n-overtones ($n = 1, 2, 5, 10$) in NS solutions O_i, with $i = 1, 2, 3$, using the BSk19 EOS, shown in figure 3.5.4.

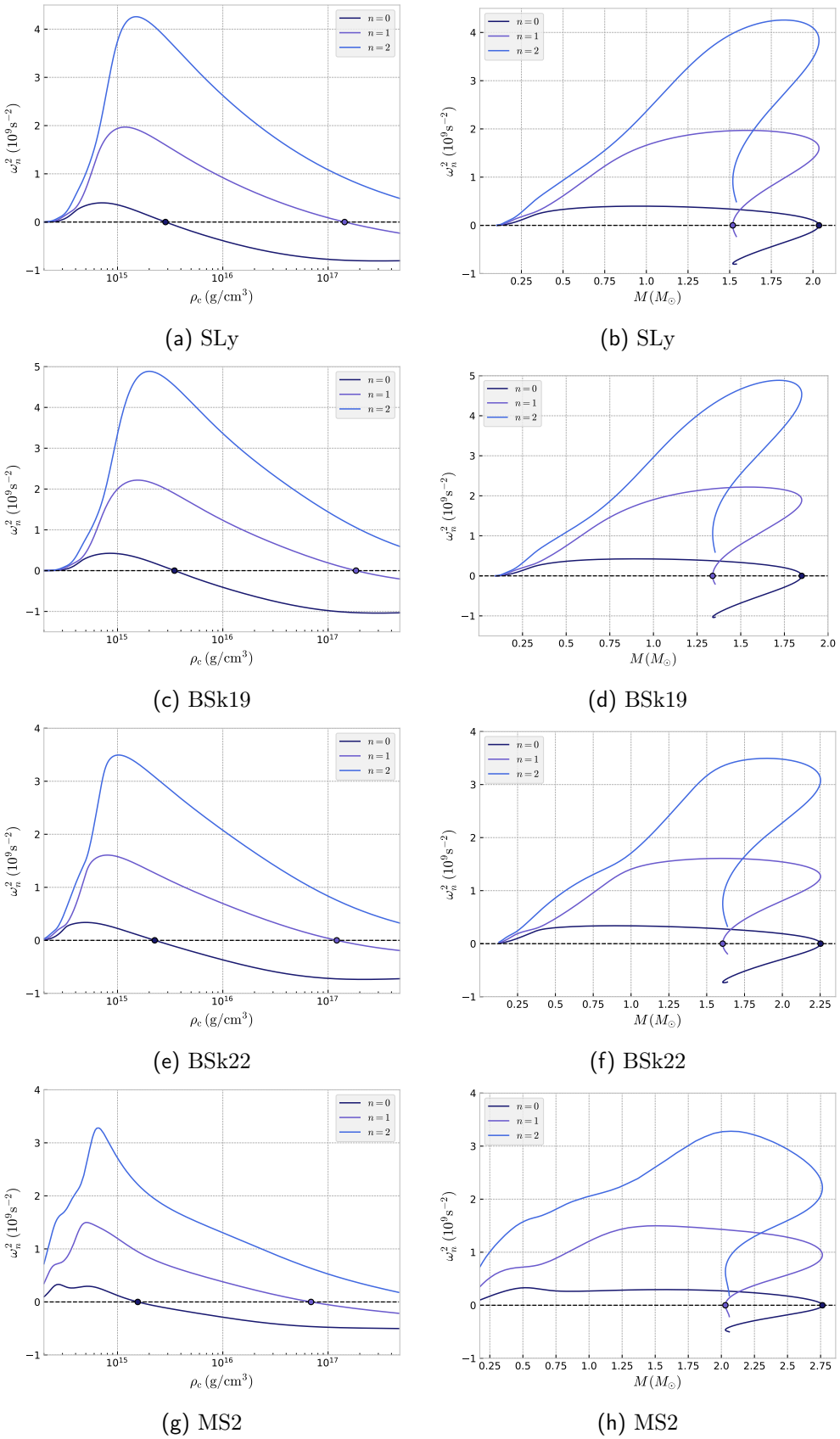

(a) SLy (b) SLy

(c) BSk19 (d) BSk19

(e) BSk22 (f) BSk22

(g) MS2 (h) MS2

Figure 3.5.6: Squared frequency versus central density and mass curves for the first three radial modes using the SLy, BSk19, BSk22 and MS2 EOSs. The circles indicate where the squared frequencies become negative.

Chapter 4

Star Models in 4D Einstein-Gauss-Bonnet Gravity

4.1 Towards a 4-dimensional Gauss-Bonnet gravity

David Lovelock in his paper "The Einstein Tensor and Its Generalizations" [16] solved the following problem: to seek all tensors A^{ij} with the properties:

(a) A^{ij} is symmetric, i.e., $A^{ij} = A^{ji}$.

(b) A^{ij} is a function of the metric tensor g_{ab} and its two derivatives, i.e., $A^{ij} = A^{ij}(g_{ab}, \partial_c g_{ab}, \partial_{cd} g_{ab})$.

(c) A^{ij} is divergence-free, i.e., $\nabla_j A^{ij} = 0$.

(d) A^{ij} is linear in the second derivatives of g_{ab}.

He showed that in a four dimensional spacetime, such tensor must take the form:

$$A^{ij} = aG^{ij} + bg^{ij}, \tag{4.1.1}$$

where a and b are constants. The resulting field equations would then be the Einstein equations with cosmological constant. Thus, if we want to modify General Relativity in 4 dimensions, then it is necessary to either add other fields besides the metric tensor, or relax one of the above conditions on A^{ij}, for example, allowing higher order derivatives of the metric.

If the spacetime has dimension $D \geq 5$, the action of the theory has higher order

terms in the curvature. The first of these higher terms is the Gauss Bonnet action term which is quadratic in the curvature:

$$S_{\mathrm{D}}^{\mathrm{GB}} = \alpha \int d^D x \sqrt{-g} \mathcal{G}, \tag{4.1.2}$$

where α is a coupling constant, and $\mathcal{G} = R^{\mu\nu\rho\tau} R_{\mu\nu\rho\tau} - 4R^{\mu\nu} + R^2$ is the Gauss-Bonnet term. In $D = 4$, $\mathcal{G}$ is a total derivative, thus not contributing to the system's dynamics

In early 2020, Glavan and Lin [17] consider the D-dimensional Einstein-Gauss-Bonnet action

$$S_{\mathrm{D}}^{\mathrm{EGB}} = \int d^D x \sqrt{-g} \left[\frac{1}{2\kappa}(R - 2\Lambda) + \alpha \mathcal{G} \right], \tag{4.1.3}$$

of which the field equations are [28]

$$\frac{1}{2\kappa} \left(R_{\mu\nu} - \frac{1}{2} g_{\mu\nu} R + \Lambda g_{\mu\nu} \right) + \alpha \mathcal{H}_{\mu\nu} = 0, \tag{4.1.4}$$

where the "Gauss-Bonnet tensor" is given by

$$\mathcal{H}_{\mu\nu} = 2R_{\mu\rho\sigma\lambda} R_{\nu}{}^{\rho\sigma\lambda} - 4R_{\mu\rho} R_{\nu}{}^{\rho} - 4R_{\mu\rho\nu\sigma} R^{\rho\sigma} + 2RR_{\mu\nu} - \frac{1}{2} \mathcal{G} g_{\mu\nu}. \tag{4.1.5}$$

They showed that the GB contribution to solutions to the D-dimensional field equations can be non-trivial for $D \to 4$ under the following rescaling of the GB coupling constant:

$$\alpha \to \frac{\alpha}{D-4}. \tag{4.1.6}$$

Despite this apparent violation of the Lovelock theorem, a number of sensible 4-dimensional metrics can be obtained. This was done for spherical black holes [17–21], cosmological solutions [17, 22, 23], star-like solutions [24, 25], radiating solutions [26], collapsing solutions [27], etc. In reality the existence of such limiting solutions does not actually imply the existence of a well-defined 4D theory, and a number of articles [28–30] came out shortly after criticizing the method. For example, Gürses et al. [28] showed that there is a part of the tensor $\mathcal{H}_{\mu\nu}$ which is always higher dimensional even though one part of the tensor can be made finite with the procedure of dividing by $1/(D-4)$ and then formally assuming that the remaining indices are four dimensional. The important point here is that if

one drops the extra dimensional part, then the Bianchi identity is not satisfied for the remaining four dimensional theory, then one cannot couple the theory to conserved matter fields.

Two independent groups [31, 32] derived consistent versions of what has come to be known as 4D Einstein-Gauss-Bonnet (4DEGB) gravity, making use of the same rescaling (4.1.6). In both cases, a scalar field is introduced into the action making 4DEGB gravity a Horndeski theory of gravity. In the former this is done via a conformal rescaling trick (in analogy to an earlier procedure where in the $D \to 2$ limit of GR was obtained [71]), and in the latter a Kaluza-Klein dimensional reduction technique [72]. These two approaches yield identical theories, with the exception that the latter method yields additional terms in the metric equations of motion that depend on the curvature of the maximally symmetric $(D-4)$-dimensional space. Taking these terms to vanish yields the 4DEGB action term is given by [31, 32]

$$S_4^{GB} = \alpha \int d^4x\sqrt{-g}\left[\phi\mathcal{G} + 4G_{\mu\nu}\nabla^\mu\phi\nabla^\nu\phi - 4(\nabla\phi)^2\Box\phi + 2(\nabla\phi)^4\right], \tag{4.1.7}$$

where ϕ is a new scalar field.

4.2 $4D$ Einstein-Gauss-Bonnet gravity

The Einstein-Gauss-Bonnet theory of gravity in $D = 4$ dimensions is defined by adding (4.1.7) to the Einstein-Hilbert action term [31]:

$$S_{\text{EGB}} = \frac{1}{2\kappa}\int d^4x\sqrt{-g}\left[R - 2\Lambda + \alpha\left(\phi\mathcal{G} + 4G_{\mu\nu}\nabla^\mu\phi\nabla^\nu\phi - 4(\nabla\phi)^2\Box\phi + 2((\nabla\phi)^2)^2\right)\right] + S_{\text{m}}, \tag{4.2.1}$$

where $\kappa = 8\pi G c^{-4}$, α is the 4DEGB coupling constant (with units of length squared), ϕ is the (dimensionless) scalar field and S_{m} is the matter action.

The field equation for the scalar field is given by [31]

$$\mathcal{G} - 8G_{\mu\nu}\nabla^\mu\nabla^\nu\phi - 8R_{\mu\nu}\nabla^\mu\phi\nabla^\nu\phi + 8(\Box\phi)^2 - 8\nabla_\mu\nabla_\nu\phi\nabla^\mu\nabla^\nu\phi - 16\nabla_\mu\nabla_\nu\phi\nabla^\nu\phi\nabla^\mu\phi - 8(\nabla\phi)^2\Box\phi = 0, \tag{4.2.2}$$

while the variation with respect to the metric leads to the following field equations:

$$\begin{aligned}
&G_{\mu\nu}+\Lambda g_{\mu\nu}+\alpha\Big[\phi\mathcal{H}_{\mu\nu}-2R[\nabla_\mu\nabla_\nu\phi+(\nabla_\mu\phi)(\nabla_\nu\phi)]+8R^{\rho}{}_{(\mu}\nabla_{\nu)}\nabla_\rho\phi\\
&\quad+8R^{\rho}{}_{(\mu}\nabla_{\nu)}\phi\nabla_\rho\phi-2G_{\mu\nu}[(\nabla\phi)^2+2\Box\phi]-4[\nabla_\mu\nabla_\nu\phi+(\nabla_\mu\phi)(\nabla_\nu\phi)]\Box\phi\\
&\quad-[g_{\mu\nu}(\nabla\phi)^2-4(\nabla_\mu\phi)(\nabla_\nu\phi)](\nabla\phi)^2+8\nabla_\rho\nabla_{(\mu}\phi(\nabla_{\nu)}\phi)\nabla^\rho\phi\\
&\quad-4g_{\mu\nu}R^{\rho\sigma}[\nabla_\sigma\nabla_\rho\phi+(\nabla_\sigma\phi)(\nabla_\rho\phi)]+2g_{\mu\nu}(\Box\phi)^2-2g_{\mu\nu}(\nabla_\rho\nabla_\sigma\phi)(\nabla^\rho\nabla^\sigma\phi)\\
&\quad-4g_{\mu\nu}(\nabla_\rho\nabla_\sigma\phi)(\nabla^\rho\phi)(\nabla^\sigma\phi)+4(\nabla_\mu\nabla_\rho\phi)(\nabla_\nu\nabla^\rho\phi)\\
&\quad+4R_{\mu\rho\nu\sigma}[\nabla^\rho\nabla^\sigma\phi+(\nabla^\rho\phi)(\nabla^\sigma\phi)]\Big]\\
&=\frac{8\pi G}{c^4}T_{\mu\nu},
\end{aligned}\tag{4.2.3}$$

where

$$T_{\mu\nu}:=-\frac{2}{\sqrt{-g}}\frac{\delta S_{\rm m}}{\delta g^{\mu\nu}},\tag{4.2.4}$$

and $\mathcal{H}_{\mu\nu}$ is given by equation (4.1.5), which identically vanishes in four dimensions and less. In what follows, we will work with cosmological constant equal to zero.

One important property of the action (4.2.1) is its shift symmetry in the scalar field, i.e., it remains invariant under the transformation

$$\phi\to\phi+\mathcal{C},\tag{4.2.5}$$

for any constant $\mathcal{C}$.

4.2.1 Black Hole solution

This theory possesses an exact vacuum solution, with line element

$$ds^2=-f(r)(cdt)^2+\frac{dr^2}{f(r)}+r^2(d\theta^2+\sin^2\theta d\varphi^2),\tag{4.2.6}$$

where the metric function $f(r)$ and the (derivative of the) scalar field ϕ are given by [31]

$$f(r)=1+\frac{r^2}{2\alpha}\left(1-\sqrt{1+\frac{8\alpha GM}{c^2r^3}}\right),\tag{4.2.7}$$

$$\frac{d\phi}{dr}=\frac{\sqrt{f}-1}{r\sqrt{f}},\tag{4.2.8}$$

and M is an integration constant. This solution is asymptotically flat, and we can interpret M as the mass of a non-rotating black hole. There are two horizons for $\alpha < 0$, as well as for $M > c^2\sqrt{\alpha}/G = M_{\rm min}$ if $\alpha > 0$. The outer event horizon [25] is located at

$$r_{\rm h} = \frac{GM}{c^2} + \sqrt{\frac{G^2M^2}{c^4} - \alpha}. \tag{4.2.9}$$

There are other branches of spherically symmetric solutions in this theory, but this one is the only asymptotically flat spherically symmetric solution which is free of naked singularities [73]. For this reason, the spacetime outside a spherically symmetric neutron star will be given by the line element (4.2.6) with metric function (4.2.7).

Writing $f(r) = 1 + 2\varphi(r)/c^2$, we can compute the gravitational force per unit of mass in 4DEGB due to a spherical body [74]

$$\vec{f} = -\frac{d\varphi}{dr}\hat{r} = -\frac{c^2 r}{2\alpha}\left(1 - \frac{c^2r^3 + 2\alpha GM}{c^2r^3 + 8\alpha GM}\sqrt{1 + \frac{8\alpha GM}{c^2r^3}}\right)\hat{r}, \tag{4.2.10}$$

which is smaller in magnitude than its Newtonian $\alpha = 0$ counterpart ($\vec{f}_{\rm N} = -GM\hat{r}/r^2$) for $\alpha > 0$. The expression in (4.2.10) vanishes at $r = (\alpha GM/c^2)^{1/3}$, but this is always at a smaller value of r than the outer horizon $r_{\rm h}$ of the corresponding black hole. Hence the gravitational force outside of any spherical body, while weaker than in GR, is always attractive provided $\alpha > 0$. If $\alpha < 0$ then the corresponding gravitational force is more attractive than in GR. However, the requirement that atomic nuclei should not be shielded by a horizon yields the empirical constraint [25]

$$\alpha \gtrsim -10^{-30}\ \mathrm{m}^2, \tag{4.2.11}$$

making the associated gravitational effects totally undetectable. For practical purposes we can exclude negative α from our analysis.

An upper bound for the coupling constant

$$0 < \alpha \lesssim 10^{10}\ \mathrm{m}^2 \tag{4.2.12}$$

has been found using LAGEOS satellites [75]. Inclusion of preliminary calculations

on recent GW data suggests that these constraints could be even tighter [75],

$$0 < \alpha \lesssim 10^7 \text{ m}^2 \tag{4.2.13}$$

though a proper calculation remains to be carried out.

4.3 Stellar structure equations

Following the same approach as in GR, we consider a neutron star configuration as a static, spherically symmetric perfect fluid in hydrostatic equilibrium. The spacetime can be described by the line element

$$ds^2 = -e^{\chi(r)} f(r)(cdt)^2 + \frac{dr^2}{f(r)} + r^2(d\theta^2 + \sin^2\theta d\varphi^2), \tag{4.3.1}$$

where $f(r)$ and $\chi(r)$ are metric functions. The matter inside the star will be described in terms of the energy-momentum tensor of a perfect fluid (3.2.7).

Since we are considering the static case, the only non-vanishing component of the 4-velocity is u_0 so that $u_\mu = (u_0, 0, 0, 0)$. Using the identity $g_{\mu\nu}u^\mu u^\nu \equiv -c^2$, we can obtain

$$u_0 = -c\sqrt{f}e^{\chi/2}. \tag{4.3.2}$$

The energy-momentum tensor is then given by

$$T_{\mu\nu} = \text{diag}(\epsilon e^{\chi} f, P/f, Pr^2, Pr^2\sin^2\theta). \tag{4.3.3}$$

Replacing the metric (4.3.1) and the components of the energy-momentum tensor (4.3.3) in the field equations (4.2.3), the non-redundant equations are the components (00) and (rr) given, respectively, by

$$\begin{aligned}\frac{8\pi G}{c^4} r^2 f\epsilon = {} & r^2 f^3 \phi'^4 \alpha + 2r^2 f^2 \phi'^3 f' \alpha + 4r^2 f^3 \phi'^2 \phi'' \alpha - 6r f^2 \phi'^2 f' \alpha - 8r f^3 \phi' \phi'' \alpha \\ & - 2f^3 \phi'^2 \alpha - 2f^2 \phi'^2 \alpha + 6f^2 \phi' f' \alpha + 4f^3 \phi'' \alpha - 2f \phi' f' \alpha - 4f^2 \phi'' \alpha \\ & - rff' - f^2 + f,\end{aligned} \tag{4.3.4}$$

$$\frac{8\pi G}{c^4}r^2P = 1 - 6f\phi' f'\alpha + 6f^2\phi'^2\alpha + 2\phi' f'\alpha - 6f^2\phi'\chi'\alpha + 2f\phi'\chi'\alpha - 2f^2r^2\phi'^3\chi'\alpha + 6f^2r\phi'^2\chi'\alpha - 2fr^2\phi'^3 f'\alpha + 6fr\phi'^2 f'\alpha - 8f^2r\phi'^3\alpha + 3f^2r^2\phi'^4\alpha - 2f\phi'^2\alpha + f\chi' r + f + f' r. \tag{4.3.5}$$

Since the action is invariant under the transformation (4.2.5), it can be shown that the equation (4.2.2) for the scalar field in the spacetime given by (4.3.1) can be recast as [76]

$$\frac{dj^r}{dr} = 0, \tag{4.3.6}$$

with

$$j^r = \frac{4\alpha}{r^2}[(r\phi' - 1)^2 f - 1][2\phi' f - \chi' f - f']. \tag{4.3.7}$$

If we want the spacetime to be asymptotically flat and match the exterior solution, we need

$$(r\phi' - 1)^2 f - 1 = 0. \tag{4.3.8}$$

Solving for ϕ' leads us back to equation (4.2.8), which also holds for the interior of the neutron star.

Replacing the expression (4.2.8) for the scalar field in equations (4.3.4) and (4.3.5), and solving for the derivative of f and χ, we obtain

$$\frac{df}{dr} = -\frac{(8\pi G/c^4)\epsilon r^4 + \alpha f^2 + (r^2 - 2\alpha)f - r^2 + \alpha}{r\left(r^2 - 2\alpha f + 2\alpha\right)}, \tag{4.3.9}$$

$$\frac{d\chi}{dr} = \frac{8\pi G}{c^4}\frac{r^3\left(\epsilon + P\right)}{f\left(r^2 - 2\alpha f + 2\alpha\right)}. \tag{4.3.10}$$

On the other hand, the r-component of the conservation equation for the energy-momentum tensor, i.e. $\nabla_\mu T^{\mu r} = 0$, leads to

$$\frac{dP}{dr} = -\frac{1}{2}(\epsilon + P)\left(\chi' + \frac{f'}{f}\right). \tag{4.3.11}$$

Replacing the equations (4.3.9) and (4.3.10) in (4.3.11), we find

$$\frac{dP}{dr} = -\frac{\left(\epsilon + P\right)\left[-\alpha f^2 - \left(r^2 - 2\alpha\right)f + (8\pi G/c^4)r^4 P + r^2 - \alpha\right]}{2rf\left(r^2 - 2\alpha f + 2\alpha\right)}, \tag{4.3.12}$$

which defines the modified T.O.V. equation for this theory in terms of the metric function f, the pressure and the energy density.

Boundary conditions

We determine the boundary conditions at the origin by assuming that each function is regular close to the origin, that is,

$$h(r) = h_0 + h_1 r + h_2 r^2 + \cdots, \quad r \to 0, \tag{4.3.13}$$

with $h = \{f, \chi, \phi, \epsilon, P\}$. Replacing this expansion in equations (4.2.8), (4.3.9), (4.3.10) and (4.3.12), solving order by order, and requiring that the scalar field is regular at the origin implies

$$f(r) = 1 + \frac{1}{2\alpha}\left(1 - \sqrt{1 + \frac{32\pi G}{3c^4}\alpha\epsilon_c}\right) r^2 + \mathcal{O}(r^3), \tag{4.3.14}$$

$$\chi(r) = \chi_c + \frac{4\pi G}{c^4}\frac{\epsilon_c + P_c}{\sqrt{1 + (32\pi G/3c^4)\alpha\epsilon_c}} r^2 + \mathcal{O}(r^3), \tag{4.3.15}$$

$$P(r) = P_c + \mathcal{O}(r^2), \tag{4.3.16}$$

where P_c is the central pressure, ϵ_c the central energy density and χ_c an arbitrary constant that is fixed by matching the interior and exterior solutions. We integrate the coupled system of equations (4.3.9), (4.3.10) and (4.3.12) from $r = 0$ until the pressure vanishes. The point at which the pressure reaches zero is the radius of the star.

4.4 Uniform density and Buchdahl limit

In this section, we discuss an analytical solution to the field equations (4.3.9), (4.3.10) and (4.3.12) for a relativistic star with uniform energy density. Although this model of the star is not realistic, in General Relativity predicts the existence of an upper bound for the stellar compactness, the Buchdahl limit.

As we mentioned, we consider a star with uniform energy density:

$$\epsilon(r) = \begin{cases} \epsilon_c = \text{const}, & r < R \\ 0, & r > R \end{cases}. \tag{4.4.1}$$

In this case, the equation for f is separated from the other equations. In order to solve this equation it is convenient to introduce a new function $\mu(r)$ defined by [24]

$$\mu = \frac{1-f}{r^2}. \tag{4.4.2}$$

In terms of μ, the equation (4.3.9) takes the form

$$\frac{d}{dr}\left[r^3(\mu + \alpha\mu^2)\right] = \frac{8\pi G}{c^4}\epsilon_c r^2. \tag{4.4.3}$$

Integrating this equation and asking that the solution is regular at the origin (the integration constant is zero), we obtain

$$\mu + \alpha\mu^2 = \frac{8\pi G}{3c^4}\epsilon_c. \tag{4.4.4}$$

Solving the quadratic equation for μ and imposing an asymptotically flat exterior solution, we obtain

$$\mu = -\frac{1}{2\alpha}\left(1 - \sqrt{1 + \frac{32\pi G}{3c^4}\alpha\epsilon_c}\right). \tag{4.4.5}$$

In other words, we have

$$f(r) = 1 + \frac{r^2}{2\alpha}\left(1 - \sqrt{1 + \frac{32\pi G}{3c^4}\alpha\epsilon_c}\right), \quad r \leq R. \tag{4.4.6}$$

The matching condition gives the relation among the mass, the radius and the energy density of the star, namely

$$M = \frac{4\pi}{3c^2}\epsilon_c R^3. \tag{4.4.7}$$

Now, with the explicit form of f we can obtain the pressure P. Replacing $f = 1 - \mu r^2$ and ϵ_c in terms of μ, in equation (4.3.12), we find

$$\frac{dP}{dr} = \frac{3r(\alpha\mu^2 - \mu - \kappa P)\left(\alpha\mu^2 + \mu + \kappa P/3\right)}{2\kappa(2\alpha\mu + 1)(1 - \mu r^2)}. \tag{4.4.8}$$

Using the separation of variables method, we obtain

$$\int \frac{dP}{(\alpha\mu^2-\mu-\kappa P)(\alpha\mu^2+\mu+\kappa P/3)} = \int \frac{3r\,dr}{2\kappa(2\alpha\mu+1)(1-\mu r^2)}, \tag{4.4.9}$$

$$\ln\left[\frac{\kappa P+3(\alpha\mu^2+\mu)}{\kappa P-(\alpha\mu^2+\mu)}\right] = -\ln(\sqrt{1-\mu r^2})+\mathcal{C}, \tag{4.4.10}$$

$$\frac{\kappa P+3(\alpha\mu^2+\mu)}{\kappa P-(\alpha\mu^2+\mu)} = \frac{e^{\mathcal{C}}}{\sqrt{1-\mu r^2}}. \tag{4.4.11}$$

The integration constant $\mathcal{C}$ can be found by considering the pressure to be zero at the surface of the star, $P(R)=0$. Therefore,

$$e^{\mathcal{C}} = -\frac{3(\alpha\mu^2+\mu)\sqrt{1-\mu R^2}}{\alpha\mu^2+\mu}. \tag{4.4.12}$$

Replacing the value of $e^{\mathcal{C}}$ in (4.4.11) and solving for $P(r)$, we have

$$\begin{aligned} P &= \frac{\frac{3(\alpha\mu^2+\mu)\sqrt{1-\mu R^2}}{\sqrt{1-\mu r^2}}-3(\alpha\mu^2+\mu)}{\kappa\left(1+\frac{3(\alpha\mu^2+\mu)\sqrt{1-\mu R^2}}{(\alpha\mu^2-\mu)\sqrt{1-\mu r^2}}\right)} \\ &= \frac{3}{\kappa}(\alpha\mu^2+\mu)\frac{\sqrt{1-\mu R^2}-\sqrt{1-\mu r^2}}{\sqrt{1-\mu r^2}+3\frac{\alpha\mu^2+\mu}{\alpha h^2-\mu}\sqrt{1-\mu R^2}} \\ &= \frac{3}{\kappa}(\alpha\mu^2+\mu)\frac{\sqrt{1-\mu r^2}-\sqrt{1-\mu R^2}}{3\frac{1+\alpha\mu}{1-\alpha\mu}\sqrt{1-\mu R^2}-\sqrt{1-\mu r^2}}. \end{aligned} \tag{4.4.13}$$

Using equation (4.4.4), we finally obtain an exact solution for the pressure in terms of the radial coordinate r given by

$$P(r) = \epsilon\frac{\sqrt{1-\mu r^2}-\sqrt{1-\mu R^2}}{3\frac{1+\alpha\mu}{1-\alpha\mu}\sqrt{1-\mu R^2}-\sqrt{1-\mu r^2}}, \quad r\leq R. \tag{4.4.14}$$

This expression is valid for all $\alpha>0$ and for $\alpha<0$ such that $1+4\kappa\alpha\epsilon_{\rm c}/3\geq 0$. If we take the limit $\alpha\to 0$ (General Relativity), the function μ goes to $\kappa\epsilon/3$ and we recover the solution (3.3.13) using (4.4.7) and the definition of the Schwarzschild radius.

The solution for the derivative of the scalar field is obtained by evaluating (4.4.6) in equation (4.2.8). On the other hand, to determine the function χ, we introduce

a new function $Q(r) := e^{\chi} f$ and take the derivative:

$$\frac{dQ}{dr} = Q\left(\chi' + \frac{f'}{f}\right). \tag{4.4.15}$$

Using equation (4.3.11), we obtain an equation for Q:

$$\frac{dQ}{dr} = -\frac{2Q}{\epsilon_c + P}\frac{dP}{dr}. \tag{4.4.16}$$

Solving for Q, we have

$$Q = \frac{A}{(\epsilon_c + P)^2}, \tag{4.4.17}$$

where A is an integration constant. Evaluating at $r = R$, we find that $A = \epsilon_c^2(1 - \mu R^2)$. Thus,

$$Q = \epsilon_c^2 \frac{(1 - \mu R^2)}{(\epsilon_c + P)^2}. \tag{4.4.18}$$

Replacing the expression (4.4.14) for P in (4.4.18), we obtain an expression for χ:

$$e^{\chi} = -\frac{1}{4}\left(\frac{1 - \alpha\mu}{1 + 2\alpha\mu}\right)^2 \left[1 - 3\frac{1 + \alpha\mu}{1 - \alpha\mu}\sqrt{\frac{1 - \mu R^2}{1 - r^2\mu}}\right]^2, \quad r \leq R. \tag{4.4.19}$$

The profiles of the pressure, metric functions, and the derivative of the scalar field inside a star with uniform density are represented in figure 4.4.1. We observe for $\alpha = 0.1R^2$ and $\mu = 9.6/R^2$ that the pressure is divergent close to the origin because it is the limit where the Buchdahl bound is violated. These expressions for P and χ coincide with the ones found by Doneva and Yazadjiev in Ref. [24] for the ill-defined 4D Einstein-Gauss-Bonnet gravity by Glavan and Lin.

Buchdahl bound

The pressure is always maximum at the center of the star, and in the uniform density case assumes the value

$$P(0) = \epsilon_c \frac{1 - \sqrt{1 - \mu R^2}}{3\frac{1+\alpha\mu}{1-\alpha\mu}\sqrt{1 - \mu R^2} - 1}. \tag{4.4.20}$$

The central pressure must be finite and positive to sustain equilibrium, so we need

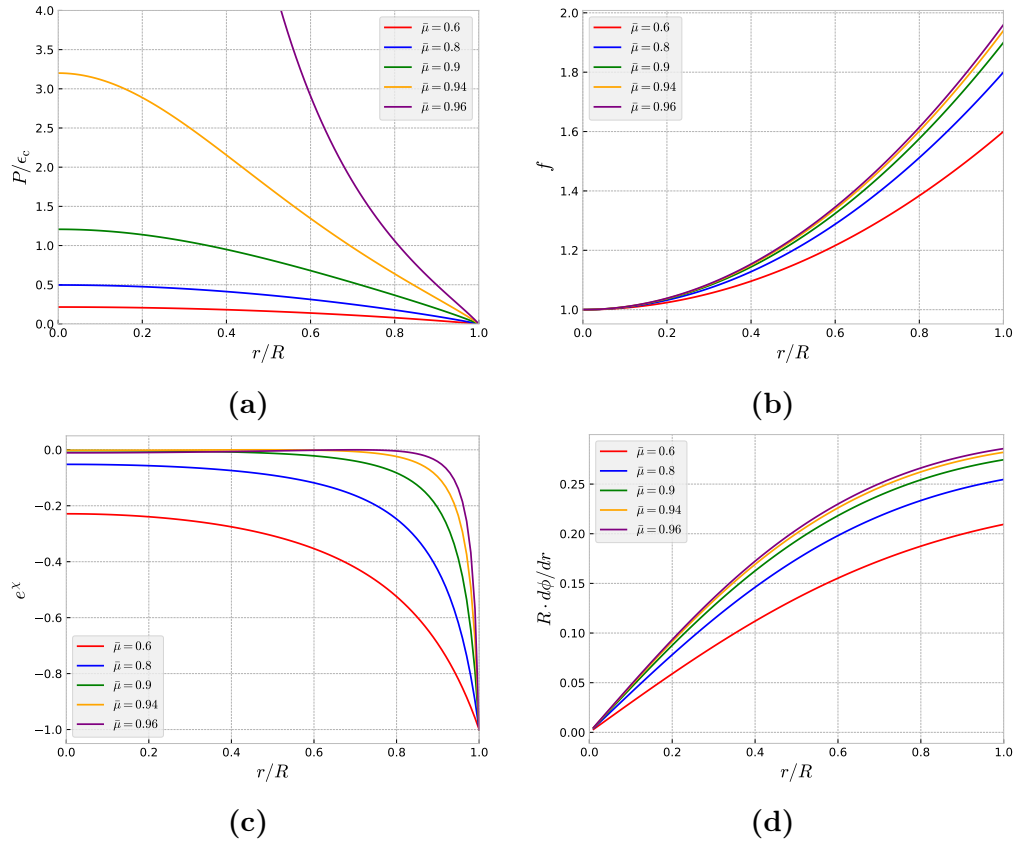

Figure 4.4.1: Profiles of the pressure, metric functions f and e^{χ}, and the derivative of the scalar field for a star with uniform density in 4DEGB gravity for $\alpha = 0.1R^2$ and different values of $\bar{\mu} := \mu R^2$, with R the radius of the star.

that

$$3\frac{1+\alpha\mu}{1-\alpha\mu}\sqrt{1-\mu R^2} > 1. \tag{4.4.21}$$

Expressing μ in terms of the mass and radius of the star, the inequality

$$\sqrt{1-\mu R^2}(1+\alpha\mu) > \frac{1}{3}(1-\alpha\mu), \tag{4.4.22}$$

where

$$\mu := \frac{1}{2\alpha}\left(\sqrt{1+\frac{8\alpha GM}{c^2R^3}}-1\right), \tag{4.4.23}$$

defines the modified Buchdahl bound of the theory. Sumanta and Dadhich [77] generalized this result to any EOS which the energy density and the pressure are positive and monotonically decreasing. Moreover, the Buchdahl bound intersects the black hole horizon (4.2.9) at the minimum black hole mass allowed by this theory, $M_{\rm int} = c^2\sqrt{\alpha}/G$, which was first discussed in Ref. [74].

4.5 Numerical solutions

In this section, numerical solutions to the relativistic stellar structure equations in the context of 4DEGB for neutron stars will be determined using the EOSs described in chapter 2. For this purpose, we will normalize the equations (4.3.9), (4.3.10) and (4.3.12) in the same way as in GR. We write the normalized radial coordinate x, pressure $\overline{P}$ and the energy density $\bar{\epsilon}$ as follows

$$r = ax, \quad P = K\overline{P}, \quad \epsilon = K\bar{\epsilon}, \tag{4.5.1}$$

where the constants a and K are defined in (3.4.10) and (2.3.11), respectively. Replacing equations (4.3.9), (4.3.10) and (4.3.12), we have

$$\frac{df}{dx} = -\frac{2\bar{\epsilon}x^4 + (\alpha/a^2)f^2 + (x^2 - 2\alpha/a^2)f - x^2 + \alpha/a^2}{x\left(x^2 - 2(\alpha/a^2)f + 2\alpha/a^2\right)}, \tag{4.5.2}$$

$$\frac{d\chi}{dx} = \frac{2x^3\left(\bar{\epsilon} + \overline{P}\right)}{f\left(x^2 - 2(\alpha/a^2)f + 2\alpha/a^2\right)}, \tag{4.5.3}$$

$$\frac{d\overline{P}}{dx} = -\frac{\left(\bar{\epsilon} + \overline{P}\right)\left[-(\alpha/a^2)f^2 - \left(x^2 - 2\alpha/a^2\right)f + 2x^4\overline{P} + x^2 - \alpha/a^2\right]}{2xf\left(x^2 - 2(\alpha/a^2)f + 2\alpha/a^2\right)}. \tag{4.5.4}$$

Here we see that it is convenient to normalize the coupling constant α defining $\gamma := \alpha/a^2$. Thus, we have reduced the coupled equations (4.3.9), (4.3.10) and (4.3.12) to the following normalized equations:

$$\frac{df}{dx} = -\frac{2\bar{\epsilon}x^4 + \gamma f^2 + (x^2 - 2\gamma)f - x^2 + \gamma}{x\left(x^2 - 2\gamma f + 2\gamma\right)}, \tag{4.5.5}$$

$$\frac{d\chi}{dx} = \frac{2x^3\left(\bar{\epsilon} + \overline{P}\right)}{f\left(x^2 - 2\gamma f + 2\gamma\right)}, \tag{4.5.6}$$

$$\frac{d\overline{P}}{dx} = -\frac{\left(\bar{\epsilon} + \overline{P}\right)\left[-\gamma f^2 - \left(x^2 - 2\gamma\right)f + 2x^4\overline{P} + x^2 - \gamma\right]}{2xf\left(x^2 - 2\gamma f + 2\gamma\right)}, \tag{4.5.7}$$

where the boundary conditions are: $f(0) = 1$, $\chi(0) = \chi_c$ and $\overline{P}(0) = \overline{P}_c$.

To numerically integrate this system of differential equations it is necessary that the value of χ at the origin is known, and for this we will take advantage of the fact that the differential equation (4.3.10) is linear in χ. We write

$$\chi(x) = \chi_{\text{num}}(x) + \chi_c, \tag{4.5.8}$$

where $\chi_{\rm num}$ is the function that will be integrated with $\chi_{\rm num}(0) = 0$ and the constant $\chi_{\rm c}$ is found by imposing $\chi(x_1) = 0$.

Since the pressure is monotonically decreasing from its maximum value at the center of the star, there will be a point $x = x_1$ such that $\overline{P}(x_1) = 0$, and this will be the normalized radius of the star. The radius of the star will be then given by (3.4.17), just as in GR. However, the mass of the star is obtained by matching the interior and exterior solutions, solving the following equation for M:

$$f_{\rm num}(R) = 1 + \frac{R^2}{2\alpha}\left(1 - \sqrt{1 + \frac{8\alpha GM}{c^2 R^3}}\right). \tag{4.5.9}$$

The system of differential equations for the functions f, χ and $\overline{P}$ cannot be integrated numerically in a proper manner, since we have a divergence at the origin due to the division by powers of x, see equations (4.5.5)-(4.5.7). To solve this problem, a change of variable is proposed for f:

$$f(x) = 1 + x^2 g(x). \tag{4.5.10}$$

Using the expansion (4.3.14), we have

$$g(0) = \frac{1}{2\alpha}\left(1 - \sqrt{1 + \frac{32\pi G}{3c^4}\alpha\epsilon_{\rm c}}\right). \tag{4.5.11}$$

Finally, the system of differential equations that is numerically integrated is

$$\frac{dg}{dx} = \frac{3\gamma g^2 - 3g - 2\overline{\epsilon}}{x(1 - 2\gamma g)}, \tag{4.5.12}$$

$$\frac{d\chi}{dx} = \frac{2x\left(\overline{\epsilon} + \overline{P}\right)}{(1 + x^2 g)(1 - 2\gamma g)}, \tag{4.5.13}$$

$$\frac{d\overline{P}}{dx} = \frac{x\left(\overline{\epsilon} + \overline{P}\right)\left[\gamma g^2 + g - 2\overline{P}\right]}{2(1 + x^2 g)\left(1 - 2\gamma g\right)}. \tag{4.5.14}$$

Numerical scheme

The system consisting of the equations (4.3.9), (4.3.10) and (4.3.12) is solved numerically using the fourth-order Runge Kutta method for values of central

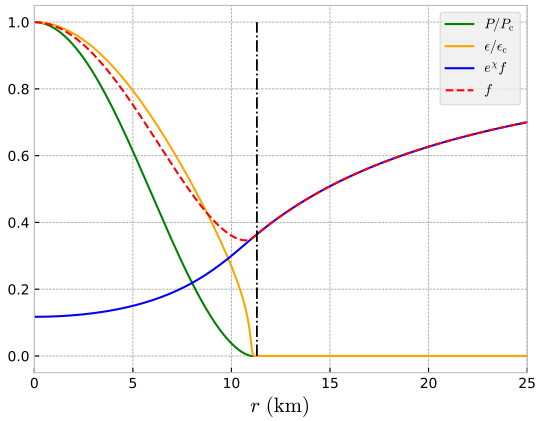

Figure 4.5.1: Solution for a central density $\rho_c = 2 \times 10^{15}\text{g/cm}^3$, using the SLy EOS in 4DEGB for $\alpha = 10$ km^2. The plot shows the metric components $e^{\chi(r)}f(r)$ and $f(r)$, as well as the pressure and the energy density, normalized with respect to their values at the origin. The vertical line represents the position of the surface of the star. The numerical solution (left side of the vertical line) smoothly matches the exterior exact solution (right side of the vertical line).

density between $\rho_c = 2 \times 10^{14}$ g/cm^3 and $\rho_c = 5 \times 10^{19}$ g/cm^3. The complete code can be found in this repository and the integration scheme is the same as in GR. However, not all densities in this interval are allowed in all cases. For $\alpha < 0$ there is, according to (4.3.14), a maximum critical value ρ_c such that $1 + (32\pi G\alpha\rho_c)/(3c^2) \leq 0$. On the other hand, for $\alpha > 0$, we increase ρ_c up to the point when the function f approaches zero, that is, the solution approaches a black hole.

Figure 4.5.1 shows the plots of the metric functions, the pressure and the energy density using the SLy EOS for $\alpha = 10$ km^2, we can see the matching between the interior and the exterior solution. Integrating for various values of central density, we found different equilibrium configurations that neutron star (modeled with this EOS) can have in 4DEGB for the same value of the coupling constant, represented in figure 4.5.2.

In figure 4.5.3a we show the mass-radius relation of stars for the SLy EOS, reproducing the same result reported in Ref. [25], and in figures 4.5.3c and 4.5.3e for the BSk19-22 EOSs, using different values of the coupling constant α. First, we see that positive values of α increase the mass of the NS for any given value of radius with respect to GR due to the weaker gravity described by a positive α. The BSk19 EOS predicts smaller and lighter neutron stars, while BSk22 predicts

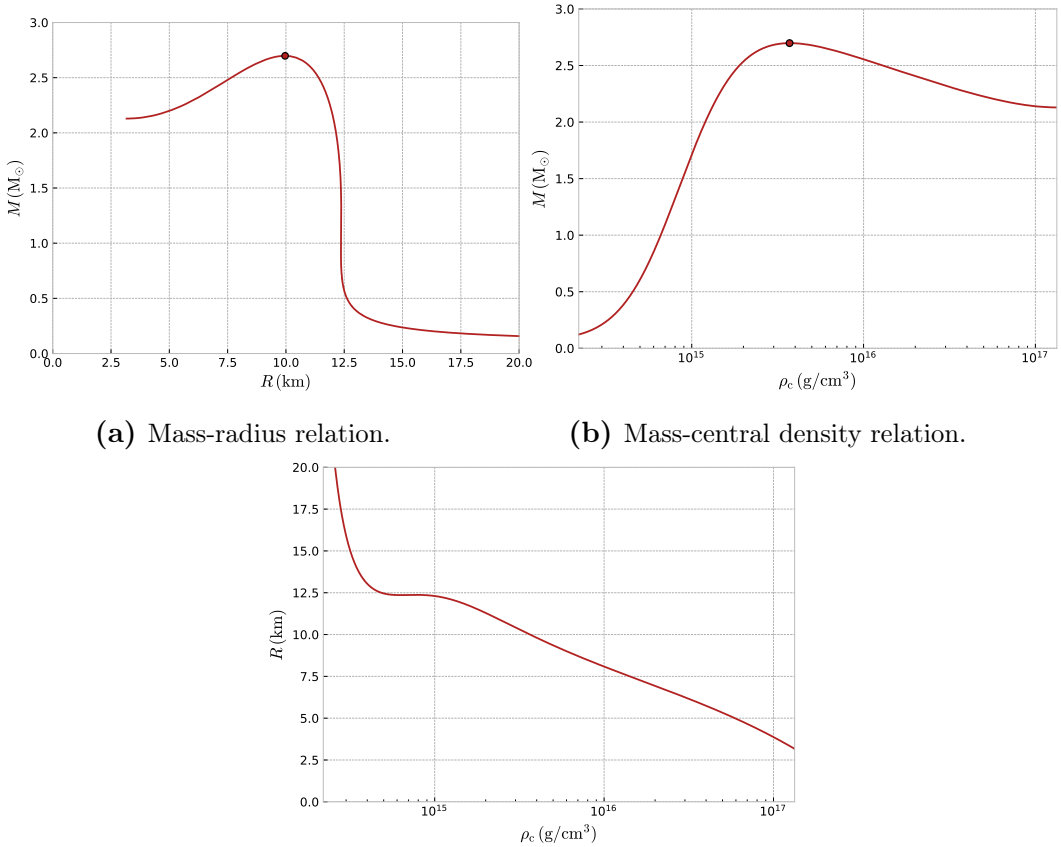

(a) Mass-radius relation.

(b) Mass-central density relation.

(c) Radius-central density relation.

Figure 4.5.2: Profiles for neutron star solutions using SLy EOS in 4D Einstein-Gauss-Bonnet gravity for $\alpha = 10$ km^2.

larger, more massive neutron stars (see figure 4.5.5 for a clear comparison using $\alpha = 10$ km^2). This is due to the stiffness of the EOS increasing from BSk19 to BSk22. Therefore, even though the SLy EOS provides a unified model of matter, the BSk models are more flexible and offer a broader range of possible neutron star configurations due to their different versions. Finally, in figure 4.5.4*a* the same results are shown for the MS2 EOS, which are strikingly similar to those shown for the non-relativistic equations of state. We note that when the large α solutions have a maximum mass near the black hole horizon with the non-relativistic EOSs, this maximum mass point is relatively further from this intersection in MS2.

In figures 4.5.3b, 4.5.3d and 4.5.3f the mass versus central density curves are plotted for the SLy, BSk19 and BSk22 EOSs. The vertical dashed lines demarcate the central density where the speed of sound is equal to the speed of light. In figure 4.5.3b the solutions between the two vertical lines do not satisfy the condition

of maximum speed of sound. Similarly, in figures 4.5.3d and 4.5.3f the solutions lying to the right of the vertical line are also excluded. This condition defines maximum masses for which the solution is reliable. For example, in figure 4.5.3b, the maximum mass point is located to the right of the first vertical line for $\alpha \gtrsim 3$ km^2, but to the left for smaller α (for instance, $\alpha = 1$ km^2). In other words, as we increase the value of the coupling α the maximum mass points of the $M - \rho_c$ curves move to the left, toward the vertical causality line. Therefore, there must be a value of α such that all neutron star solutions satisfy the causality condition, which is the case for $\alpha = 300$ km^2. Cutting the curves at the point where the causality condition is not satisfied (or simply marking the solution) was discussed in the previous chapter in the context of General Relativity. Finally in figure 4.5.4*b* the same data is plotted for the relativistic MS2 equation of state - in this case the causality line is absent as this EOS always respects causality.

Charmousis et. al. [25] pointed out that at high densities, the neutron star equilibrium configurations approach the black hole limit asymptotically, and we have numerically confirmed that these two sequences (NS and BH configurations) become arbitrarily close near the minimum mass black hole of the theory. This result is compatible with the modified Buchdahl bound of this theory given by (4.4.22). This compatibility is due to the fact that the Buchdahl bound intersects the black hole horizon (4.2.9) at the minimum black hole mass allowed by this theory, $M_{\rm int} = c^2\sqrt{\alpha}/G$. These results imply that compact objects in 4DEGB can have radii smaller than those of the GR Buchdahl bound $R \geq 9GM/4c^2$ or even that of the Schwarzschild radius $r_s = 2GM/c^2$.

In short, we find that the neutron star solutions in 4DEGB gravity are qualitatively similar for each of these EOSs. We explore the effects of different possible values of the 4DEGB coupling constant α and find that larger values of α tend to inflate the mass-radius profiles. In table 4.5.1, we show the maximum masses and the corresponding radii for $\alpha = 0$ (GR), $\alpha = 10$ km^2 and $\alpha = 100$ km^2 and for the different EOSs. We see that the maximum masses increase with increasing α, whereas the radii stay essentially unaltered. In addition, difference amongst the maximum masses for different EOSs are suppressed for higher values of α. For $\alpha = 300$ km^2, $M_{\rm max} = 11.66$ M$_\odot$ and $R = 17.33$ km for all realistic EOSs considered in this work, these values approach the mass and radius of lightest associated 4DEGB black hole.

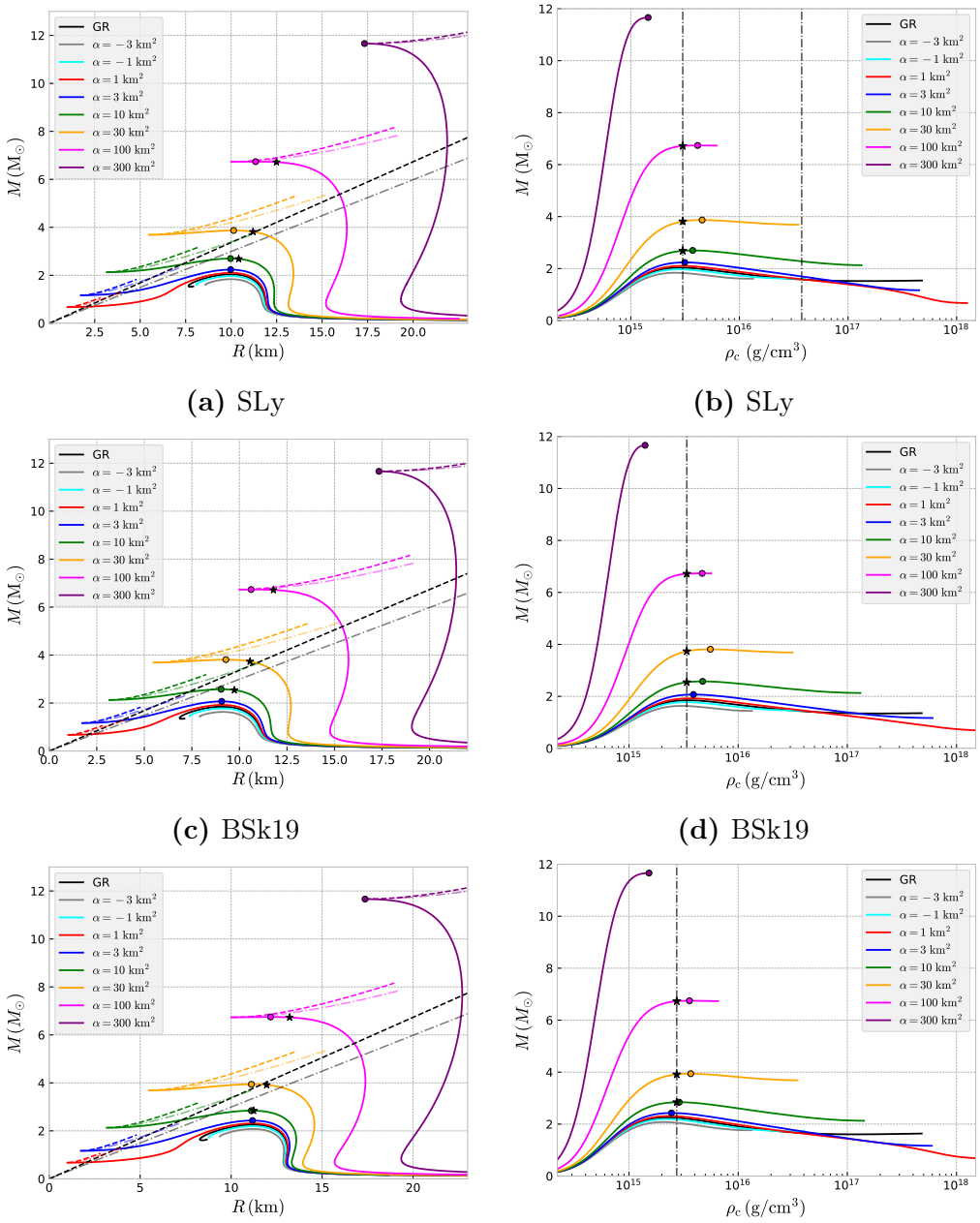

(a) SLy **(b)** SLy

(c) BSk19 **(d)** BSk19

(e) BSk22 **(f)** BSk22

Figure 4.5.3: Mass versus radius and central density curves for neutron stars using the SLy, BSK19 and BSk22 EOSs in GR (black solid line) and in 4DEGB gravity for different values of α (colorful solid lines). The starred points mark the last NS configuration where the speed of sound is equal to the speed of light. In the plots (a), (c) and (e), the dashed lines represent the mass-radius curves for the relevant black holes, and the dashed-dotted lines correspond to the Buchdahl limits in these two theories of gravity. In the plots (b), (d) and (f), the vertical lines mark the central density where the speed of sound is equal to the speed of light.

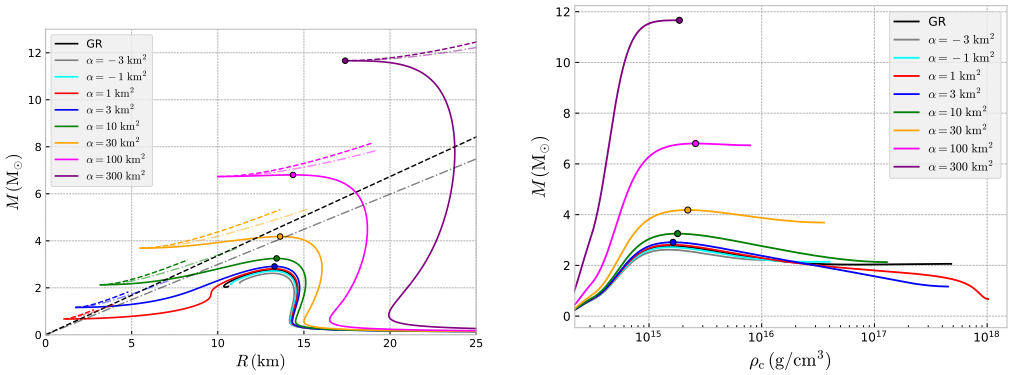

(a) MS2 **(b)** MS2

Figure 4.5.4: Mass versus radius and central density curves for neutron stars using the MS2 EOS in GR (black solid line) and in 4DEGB gravity for different values of α (colorful solid lines). In the plot (a), the dashed lines represent the mass-radius curves for the relevant black holes, and the dashed-dotted lines correspond to the Buchdahl limits in these two theories of gravity. In plot (b) we note the lack of a vertical line marking the transition from subluminal to superluminal sound speeds as this EOS always respects causality.

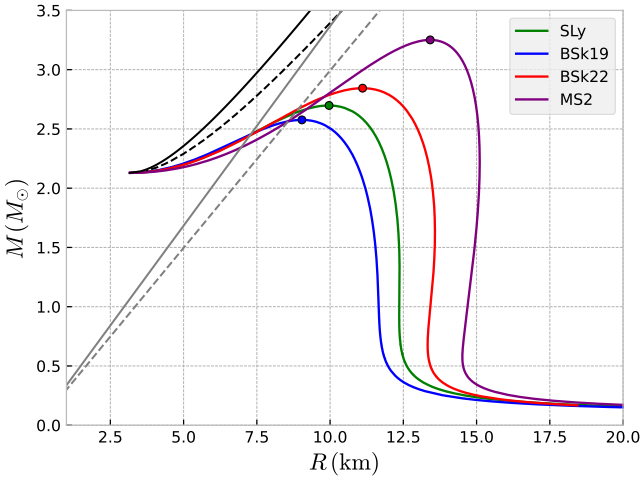

Figure 4.5.5: Mass-radius relation for neutron stars using the SLy, BSk19-22 and MS2 EOSs in 4DEGB gravity for $\alpha = 10$ km^2. The black solid line corresponds to the mass-radius relation for the black holes, and the dashed line represents the 4DEGB Buchdahl limit for that particular value of α. In contrast, the grey solid and dashed lines show the mass-radius relation for the black holes and the Buchdahl limit, respectively, in General Relativity. The coloured dots mark the maximal mass point of a given curve.

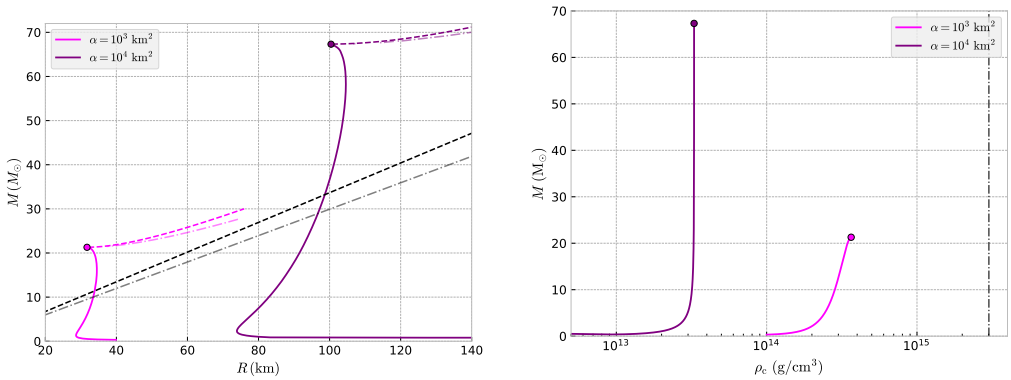

(a) **(b)**

Figure 4.5.6: Mass versus radius and central density curves for NS using the SLy EOS in 4DEGB gravity for $\alpha = 10^3$ km^2 and $\alpha = 10^4$ km^2. In plot (a) the dashed lines represent the black hole horizons, and the dashed-dotted lines correspond to the Buchdahl limits in these two theories. The maximum mass solutions effectively overlap with the minimum mass black hole horizon/Buchdahl bound intersection point. In plot (b) the vertical line marks the central density where the speed of sound is equal to the speed of light.

	$\alpha = 0$		$\alpha = 10$ km^2		$\alpha = 100$ km^2	
EOS	$M_{\max}$ ($\mathrm{M}_\odot$)	R (km)	$M_{\max}$ ($\mathrm{M}_\odot$)	R (km)	$M_{\max}$ ($\mathrm{M}_\odot$)	R (km)
BSk19	1.86	9.10	2.58	9.04	6.73	10.61
SLy	2.05	9.98	2.70	9.97	6.74	11.34
BSk22	2.26	11.20	2.84	11.11	6.75	12.17
MS2	2.78	13.24	3.25	13.42	6.80	14.37

Table 4.5.1: Maximum masses with their respective radii for SLy, BSk19, BSk22, MS2 EOSs in GR and 4DEGB for $\alpha = 0$ (GR) and $\alpha = 10$ km^2.

4.6 Radial perturbations

Equilibrium configurations of a compact star are obtained by integrating the equations (4.3.9)-(4.3.12). In what follows, we will study whether that equilibrium is stable under adiabatic radial oscillations following the approach of section 3.5. In GR, a necessary but insufficient condition for the stability of compact stars is $dM/d\rho_c < 0$, corresponding to the parts of the solution curves before the maximum mass point. There is no similar theorem in 4DEGB, so we will investigate if this holds in spite of the modifications to gravity.

Consider a perfect fluid sphere oscillating radially with a small amplitude and radial displacement δr . Since the oscillations are radial, the spacetime preserves

its spherical symmetry. Thus, we can express the line element as follows

$$ds^2 = -e^{\chi} f (dx^0)^2 + \frac{dr^2}{f} + r^2(d\theta^2 + \sin^2\theta d\varphi^2), \tag{4.6.1}$$

where $x^0 = ct$, $\chi = \chi(x^0, r)$ and $f = f(x^0, r)$ are the new metric functions, which have now been perturbed. With this we can write

$$\chi(x^0, r) = \chi_0(r) + \delta\chi(x^0, r), \tag{4.6.2}$$

$$f(x^0, r) = f_0(r) + \delta f(x^0, r), \tag{4.6.3}$$

where we have used the subscript 0 to denote the field in the equilibrium configuration (non-perturbed). Similar expressions are constructed for the scalar field, the pressure and the energy density.

The expression obtained for the Eulerian perturbations of the pressure and the energy density in section 3.5 are independent of the gravitational theory. Thus, with the substitutions

$$e^{\alpha} \to e^{\chi} f, \quad e^{\beta} \to \frac{1}{f}, \tag{4.6.4}$$

we can write equations (3.5.32) and (3.5.37) as

$$\delta P = \Gamma P_0 \left[\frac{\delta f}{2 f_0} - \sqrt{f_0} r^{-2} \frac{\partial}{\partial r} \left(\frac{r^2 \delta r}{\sqrt{f_0}} \right) \right] - P_0' \delta r, \tag{4.6.5}$$

$$\delta\epsilon = (\epsilon_0 + P_0) \left[\frac{\delta f}{2 f_0} - \sqrt{f_0} r^{-2} \frac{\partial}{\partial r} \left(\frac{r^2 \delta r}{\sqrt{f_0}} \right) \right] - \epsilon_0' \delta r. \tag{4.6.6}$$

Field equations

The relevant components of the (linearlized) energy-momentum tensor (4.3.3) are:

$$T_{0r} = -\frac{(\epsilon_0 + P_0)}{c f_0} \frac{\partial \delta r}{\partial t}, \tag{4.6.7}$$

$$T_{rr} = \frac{1}{f_0} \left(P_0 + \delta P - P_0 \frac{\delta f}{f_0} \right). \tag{4.6.8}$$

The linearlized scalar field equation (4.2.2) is given by

$$
\begin{aligned}
&4r^2\left(\chi_0' f_0^{11/2} r - 2f_0^{11/2} + f_0^{9/2} f_0' r + 2f_0^5\right)\frac{\partial^2\delta\phi}{\partial r^2} + 2r^2\left(\chi_0'^2 f_0^{11/2} r + 2f_0^{11/2}\chi_0'' r\right.\\
&\left.+4\chi_0' f_0^{9/2} f_0' r + 2f_0^{9/2} f_0'' r - 4f_0^{9/2} f_0' + f_0^{7/2} f_0'^2 r + 2\chi_0' f_0^5 + 4f_0' f_0^4\right)\frac{\partial\delta\phi}{\partial r}\\
&- 2r f_0^3\left(2f_0^{1/2} + \chi_0' f_0 r + f_0' r - 2f_0\right)\frac{\partial\delta f}{\partial r} + \left(-2\chi_0' f_0^{7/2} r - \chi_0'^2 f_0^4 r^2 - \chi_0' f_0' f_0^3 r^2\right.\\
&\left.+4f_0^{7/2} + 2f_0^{5/2} f_0' r - 2f_0^4\chi_0'' r^2 + 2\chi_0' f_0^4 r + 2f_0'^2 f_0^2 r^2 - 2f_0^3 f_0'' r^2 - 4f_0^4\right)\delta f = 0.
\end{aligned}
\tag{4.6.9}
$$

On the other hand, the $(0r)$ and (rr) components of the linearized field equation (4.2.3) are given, respectively, by

$$
\frac{r^2 + 2\alpha(1-f_0)}{r^3 f_0}\frac{\partial\delta f}{\partial t} = \frac{8\pi G}{c^4}\frac{(\epsilon_0 + P_0)}{f_0}\frac{\partial\delta r}{\partial t},
\tag{4.6.10}
$$

$$
\begin{aligned}
&\frac{1}{r}\left(r^2 + 2\alpha(1-f_0)\right)\left(\frac{\partial\delta\chi}{\partial r} + \frac{1}{f_0}\frac{\partial\delta f}{\partial r}\right) + \frac{1}{r^2 f_0^{9/2}}\left(-2\alpha\chi_0' r f_0^{9/2} - f_0' r^3 f_0^{5/2}\right.\\
&+ \frac{8\pi G}{c^4} r^4 P_0 f_0^{5/2} + \alpha f_0^{9/2} - 2\alpha f_0' r f_0^{5/2} + 2\alpha\chi_0' r f_0^3 + r^2 f_0^{5/2} + 3\alpha f_0^{5/2}\\
&\left.+2\alpha f_0' r f_0^2 - 4\alpha f_0^3\right)\delta f - \frac{4\alpha}{r f_0^{3/2}}\left(r f_0^{3/2}\chi_0' + r f_0' f_0^{1/2} - 2f_0^{3/2}\right)\frac{\partial\delta\phi}{\partial r} = \frac{8\pi G}{c^4}\frac{r^2\delta P}{f_0},
\end{aligned}
\tag{4.6.11}
$$

the other components are fully satisfied. Solving the equation (4.6.10) for δf, we find that

$$
\delta f = \frac{8\pi G}{c^4}\frac{(\epsilon_0 + P_0) r^3\delta r}{r^2 - 2\alpha f_0 + 2\alpha} = f_0\chi_0'\delta r,
\tag{4.6.12}
$$

where we have used equation (4.3.10) for χ_0'.

Equation (4.6.12) allow us to write the perturbations δP and $\delta\epsilon$ in terms only of the fields in the equilibrium configuration and the radial displacement δr:

$$
\delta P = -\Gamma P_0 r^{-2}\sqrt{f_0} e^{\chi_0/2}\frac{\partial\sigma}{\partial r} - P_0'\delta r,
\tag{4.6.13}
$$

$$
\delta\epsilon = -(\epsilon_0 + P_0) r^{-2}\sqrt{f_0} e^{\chi_0/2}\frac{\partial\sigma}{\partial r} - \epsilon_0'\delta r,
\tag{4.6.14}
$$

where we have used the *normalized displacement function* (3.5.55) express in terms of f and χ:

$$
\sigma := \frac{r^2 e^{-\chi_0/2}}{\sqrt{f_0}}\delta r.
\tag{4.6.15}
$$

Replacing (4.6.12) and (4.6.13) in equation (4.6.11), we obtain an equation for $\partial\delta\chi/\partial r$ in terms of the $\delta\phi$ and δr:

$$\frac{\partial\delta\chi}{\partial r} = c_1\frac{\partial\delta\phi}{\partial r} + c_2\frac{\partial\delta r}{\partial r} + c_3\delta r, \tag{4.6.16}$$

where the coefficients are

$$c_1 = \frac{4\alpha\left(rf_0^{3/2}\chi_0' - 2f_0^{3/2} + rf_0^{1/2}f_0' + 2f_0\right)}{f_0^{3/2}(r^2 - 2\alpha f_0 + 2\alpha)}, \tag{4.6.17}$$

$$c_2 = -\frac{f_0^{1/2}e^{\chi_0/2}\chi_0'(\epsilon_0 + P_0 + \Gamma P_0)}{r^2(\epsilon_0 + P_0)}, \tag{4.6.18}$$

$$\begin{aligned} c_3 = -\frac{e^{\chi_0/2}}{2r^3f_0^{3/2}(r^2 - 2\alpha f_0 + 2\alpha)}\Big(&-6\alpha rf_0^3\chi_0'^2 + r^3f_0^2\chi_0'^2 + 4\alpha r\chi_0'^2f_0^{3/2} - 4\alpha rf_0^3\chi_0'' \\ &+ 2r^3f_0^2\chi_0'' + 2\alpha rf_0^2\chi_0'^2 - 6\alpha r\chi_0'f_0'f_0^2 + r^3f_0f_0'\chi_0' + \frac{16\pi G}{c^4}r^4P_0f_0\chi_0' + 10\alpha f_0^3\chi_0' \\ &+ 4\alpha rf_0^2\chi_0'' - 4r^2f_0^2\chi_0' + 2\alpha r\chi_0'f_0'f_0 - 8\alpha f_0^{3/2}\chi_0' + 4\alpha rf_0^{1/2}f_0'\chi_0' + \frac{16\pi G}{c^4}r^4f_0P_0' \\ &- 8\alpha f_0^2\chi_0' + 2r^2f_0\chi_0' + 6\alpha f_0\chi_0'\Big). \end{aligned} \tag{4.6.19}$$

Momentum conservation

Consider the r component of the conservation law of the energy-momentum tensor, if we linearized this equation, we have

$$\begin{aligned} &\frac{\epsilon_0 + P_0}{c^2f_0^2e^{\chi_0}}\frac{\partial^2\delta r}{\partial t^2} + \frac{\epsilon_0 + P_0}{2f_0}\frac{\partial\delta f}{\partial r} + \frac{1}{2}(\epsilon_0 + P_0)\frac{\partial\delta\chi}{\partial r} + \left(\frac{1}{2}\chi_0'(\epsilon_0 + P_0) + P_0'\right)\frac{\delta f}{f_0} \\ &\quad + \frac{\partial\delta P}{\partial r} + \frac{1}{2}\left(\chi_0' + \frac{f_0'}{f_0}\right)(\delta\epsilon + \delta P) = 0. \end{aligned} \tag{4.6.20}$$

Using the expressions for δf, $\delta\chi$, δP and $\delta\epsilon$ in (4.6.9) and (4.6.20), we obtain the dynamic equations for σ and $\delta\phi$, respectively,

$$A_1(r)\frac{\partial^2\sigma}{\partial t^2} + A_2(r)\frac{\partial^2\sigma}{\partial r^2} + A_3(r)\frac{\partial\sigma}{\partial r} + A_4(r)\sigma + A_5(r)\frac{\partial\delta\phi}{\partial r} = 0, \tag{4.6.21}$$

$$B_1(r)\frac{\partial^2\delta\phi}{\partial r^2} + B_2(r)\frac{\partial\delta\phi}{\partial r} + B_3(r)\frac{\partial\sigma}{\partial r} + B_4(r)\sigma = 0, \tag{4.6.22}$$

where the coefficients are given by

$$A_1 = \frac{(\epsilon_0 + P_0)e^{\chi_0/2}}{c^2 r^2 f_0}, \tag{4.6.23}$$

$$A_2 = -\Gamma P_0 r^{-2} f_0 e^{3\chi_0/2}, \tag{4.6.24}$$

$$A_3 = -\frac{d}{dr}\left[\Gamma P_0 r^{-2} f_0 e^{3\chi_0/2}\right], \tag{4.6.25}$$

$$\begin{aligned} A_4 = {} & \frac{(\epsilon_0 + P_0)e^{3\chi_0/2}}{4r^2}\left(2f_0\chi_0'' + 2f_0'' - \frac{f_0'^2}{f_0}\right) \\ & + \frac{(\epsilon_0 + P_0)e^{3\chi_0/2}}{4f_0 r^3(r^2 - 2\alpha f_0 + 2\alpha)}\Big[-4\alpha\chi_0'(r\chi_0' - 2)f_0^{3/2} - 4\alpha r\chi_0' f_0'\sqrt{f_0} \\ & + r f_0^2(r^2 + 2\alpha f_0 + 2\alpha)\chi_0'^2 - f_0\chi_0'\left(-2r(r^2 + 2\alpha)f_0' - 6f_0^2\alpha\right. \\ & \left. +4(r^2 + 2\alpha)f_0 - \frac{8\pi G}{c^4}\epsilon_0 r^4 + \frac{8\pi G}{c^4}P_0 r^4 + 2(r^2 + 3\alpha)\right) \\ & +f_0'\left(8f_0^2\alpha - 4(r^2 + 2\alpha)f_0 + \frac{8\pi G}{c^4}r^4(\epsilon_0 + P_0)\right)\Big], \end{aligned} \tag{4.6.26}$$

$$A_5 = \frac{2\alpha(\epsilon_0 + P_0)\left(r\sqrt{f_0}\chi_0' + \frac{rf_0'}{\sqrt{f_0}} - 2\sqrt{f_0} + 2\right)e^{\chi_0}}{r^2 - 2\alpha f_0 + 2\alpha}, \tag{4.6.27}$$

$$B_1 = 8r^4(r f_0^2\chi_0' + 2f_0^{3/2} + r f_0 f_0' - 2f_0^2), \tag{4.6.28}$$

$$\begin{aligned} B_2 = {} & 4r^4(r\chi_0'^2 f_0^2 + 2f_0^{3/2}\chi_0' + 4r f_0 f_0'\chi_0' + 2f_0^2 r\chi_0'' + 2r f_0 f_0'' + f_0'^2 r \\ & + 4f_0'\sqrt{f_0} - 4f_0 f_0'), \end{aligned} \tag{4.6.29}$$

$$B_3 = -4\chi_0' r(\chi_0' f_0^2 r + 2f_0^{3/2} + r f_0 f_0' - 2f_0^2)e^{\chi_0/2}, \tag{4.6.30}$$

$$\begin{aligned} B_4 = {} & -2\Big(2r^2\chi_0'^3 f_0^2 + 4\chi_0'^2 f_0^{3/2} r + 5\chi_0'^2 r^2 f_0 f_0' + 4r^2 f_0^2\chi_0''\chi_0' - 8r\chi_0'^2 f_0^2 \\ & + 2\chi_0' r^2 f_0'' f_0 + \chi_0' r^2 f_0'^2 + 4f_0^{3/2}\chi_0'' r + 2r^2 f_0\chi_0'' f_0' - 12f_0^{3/2}\chi_0' \\ & +4\chi_0'\sqrt{f_0}f_0' r - 10r f_0 f_0'\chi_0' - 4f_0^2 r\chi_0'' + 12f_0^2\chi_0'\Big)e^{\chi_0/2}. \end{aligned} \tag{4.6.31}$$

The solutions of equations (4.6.21) and (4.6.22) are physically acceptable if the displacement function δr does not produce infinite density and pressure perturbations at the center of the star and leave the pressure equal to zero at the surface of the star. Therefore, the boundary conditions (3.5.65) and (3.5.66) still hold for σ and ΔP, respectively.

4.6.1 Numerical analysis

Assuming that the normalized displacement function and the perturbation of the scalar field has a harmonic time dependence, we can write

$$\sigma(x^0, r) = u(r)e^{-i\omega t}, \tag{4.6.32}$$

$$\delta\phi(x^0, r) = \varphi(r)e^{-i\omega t}. \tag{4.6.33}$$

Therefore, the evolution equations (4.6.21) and (4.6.22) reduce to

$$A_2u'' + A_3u' + [A_4 - \omega^2 A_1]u + A_5\varphi' = 0, \tag{4.6.34}$$

$$B_1\varphi'' + B_2\varphi' + B_3u' + B_4u = 0. \tag{4.6.35}$$

Note that equation (4.6.34) can be written as

$$-\frac{d}{dr}\left(A_2u'\right) = [A_4 - \omega^2 A_1]u + A_5\varphi'. \tag{4.6.36}$$

On the other hand, if we multiply the equation (4.6.35) by some function η, and divide it by B_1, then we have

$$\eta\varphi'' + \frac{\eta B_2}{B_1}\varphi' + \frac{\eta B_3}{B_1}u' + \frac{\eta B_4}{B_1}u = 0. \tag{4.6.37}$$

If we want to complete the derivative for φ', we need that

$$\frac{d\eta}{dr} = \eta\frac{B_2}{B_1}. \tag{4.6.38}$$

Solving for η, we obtain the following integrating factor:

$$\eta(r) = \exp\left(\int \frac{B_2}{B_1}dr\right) = \sqrt{f_0}\left(rf_0\chi_0' + rf_0' + 2(\sqrt{f_0} - f_0)\right)e^{\chi_0/2}. \tag{4.6.39}$$

Thus, we can write equation (4.6.35) as follows

$$\frac{d}{dr}\left(\eta\varphi'\right) + \frac{B_3}{B_1}\eta u' + \frac{B_4}{B_1}\eta u = 0. \tag{4.6.40}$$

Defining $v := -A_2 u'$ and $\psi = \eta\varphi'$, the system of second order differential equations given by (4.6.36) and (4.6.40) can be written as the following system of first order differential equations for the functions u, v and ψ:

$$u' = d_1 v, \tag{4.6.41}$$

$$v' = [d_2 + \omega^2 d_3]u + d_4\psi, \tag{4.6.42}$$

$$\psi' = d_5 v + d_6 u, \tag{4.6.43}$$

where the coefficients are given by

$$d_1 = -\frac{1}{A_2}, \tag{4.6.44}$$

$$d_2 = A_4, \tag{4.6.45}$$

$$d_3 = -A_1, \tag{4.6.46}$$

$$d_4 = \frac{A_5}{\eta} = \frac{2\alpha(\epsilon_0 + P_0)e^{\chi_0/2}}{f_0(r^2 - 2\alpha f_0 + 2\alpha)}, \tag{4.6.47}$$

$$d_5 = \frac{B_3}{B_1 A_2}\eta = \frac{\left(r f_0\chi_0' + r f_0' + 2(\sqrt{f_0} - f_0)\right)\chi_0'}{2\Gamma P_0\sqrt{f_0}e^{\chi_0/2}r}, \tag{4.6.48}$$

$$d_6 = -\frac{B_4}{B_1}\eta = -\frac{B_4 e^{\chi_0/2}}{8r^4\sqrt{f_0}}. \tag{4.6.49}$$

Near the origin we expand the functions u, v, ψ, Γ, P_0, ϵ_0, f_0 and δr_0 as per equation (4.3.13). Using the boundary condition (3.5.65), we have $u_0 = u_1 = u_2 = 0$. In addition, we know from the non-perturbed case that $f_0(0) = 1$, $f_0'(0) = 0$ and $\chi_0'(0) = 0$. Therefore,

$$u(r) = u_3 r^3 + \mathcal{O}(r^4), \tag{4.6.50}$$

$$f_0(r) = 1 + f_{0,2}r^2 + f_{0,3}r^3 + \mathcal{O}(r^4), \tag{4.6.51}$$

$$\chi_0(r) = \chi_c + \chi_{0,2}r^2 + \chi_{0,3}r^3 + \mathcal{O}(r^4). \tag{4.6.52}$$

Replacing these expansions in equations (4.6.41)-(4.6.43), we obtain

$$v(r) = 3u_3\Gamma(0)P_c e^{3\chi_c/2} + \mathcal{O}(r), \tag{4.6.53}$$

$$\psi(r) = \psi_2 r^2 + \mathcal{O}(r^3). \tag{4.6.54}$$

Choosing $u_3 = 1/(3\Gamma(0)P_c e^{3\chi_c/2})$, the initial values for the integration are $u(0) = 0$,

$v(0) = 1$ and $\psi(0) = 0$. With this choice we do not lose generality because the differential equations are linear, and it is equivalent to divide the system of equations by $3u_3\Gamma(0)P_c e^{3\chi_c/2}$ and define new variables $\tilde{u} := u/(3u_3\Gamma(0)P_c e^{3\chi_c/2})$ and $\tilde{v} := u/(3u_3\Gamma(0)P_c e^{3\chi_c/2})$. At the surface of the star the condition (3.5.66) translates to $v(R) = 0$. Equation (4.6.36) with these boundary conditions would be a Sturm-Liouville problem if it were not for the differential equation (4.6.40) for the scalar field coupled to (4.6.36).

Perfoming a dimensional analysis, we find that u has units of length cube, v has units of pressure and ψ has units of one over length. Therefore, we propose to rewrite these functions in terms of normalized functions in the following way:

$$u(r) = a^3\overline{u}(r), \qquad v(r) = K\overline{v}(r), \qquad \psi(r) = \frac{\overline{\psi}(r)}{a}, \tag{4.6.55}$$

where the constants a and K are defined in (3.4.10) and (2.3.11), respectively.

Following the same approach as in the static case, we express the radial coordinate, the pressure and the energy density as

$$r = ax, \quad P_0 = K\overline{P}_0, \quad \epsilon_0 = K\bar{\epsilon}_0. \tag{4.6.56}$$

Thus, we can write the normalized form of the system of differential equations (4.6.41), (4.6.42) and (4.6.43) as follows

$$\frac{d\overline{u}}{dx} = \bar{d}_1\overline{v}, \tag{4.6.57}$$

$$\frac{d\overline{v}}{dx} = [\bar{d}_2 + \Omega^2\bar{d}_3]\overline{u} + \bar{d}_4\overline{\psi}, \tag{4.6.58}$$

$$\frac{d\overline{\psi}}{dx} = \bar{d}_5\overline{v} + \bar{d}_6\overline{u}, \tag{4.6.59}$$

where $\Omega^2 := a^2\omega^2/c^2$ is the normalized squared frequency and the coefficients are

given by

$$\bar{d}_1 = \frac{x^2}{\Gamma \overline{P}_0 f_0 e^{3\chi_0/2}}, \tag{4.6.60}$$

$$\begin{aligned}
\bar{d}_2 = {} & \frac{(\overline{\epsilon}_0 + \overline{P}_0)e^{3\chi_0/2}}{4x^2}\left[2f_0\frac{d^2\chi_0}{dx^2} + 2\frac{d^2 f_0}{dx^2} - \frac{1}{f_0}\left(\frac{df_0}{dx}\right)^2\right] \\
& + \frac{(\overline{\epsilon}_0 + \overline{P}_0)e^{3\chi_0/2}}{4f_0x^3(x^2 - 2\gamma f_0 + 2\gamma)}\left[-4\gamma\frac{d\chi_0}{dx}\left(x\frac{d\chi_0}{dx} - 2\right)f_0^{3/2}\right. \\
& - 4\gamma x\frac{d\chi_0}{dx}\frac{df_0}{dx}\sqrt{f_0} + xf_0^2(x^2 + 2\gamma f_0 + 2\gamma)\left(\frac{d\chi_0}{dx}\right)^2 \\
& - f_0\frac{d\chi_0}{dx}\left(-2x(x^2 + 2\gamma)\frac{df_0}{dx} - 6f_0^2\gamma + 4(x^2 + 2\gamma)f_0\right. \\
& \left. -2\overline{\epsilon}_0x^4 + 2\overline{P}_0x^4 + 2(x^2 + 3\gamma)\right) \\
& \left. + \frac{df_0}{dx}\left(8f_0^2\gamma - 4(x^2 + 2\gamma)f_0 + 2x^4(\overline{\epsilon}_0 + \overline{P}_0)\right)\right],
\end{aligned} \tag{4.6.61}$$

$$\bar{d}_3 = -\frac{(\overline{\epsilon}_0 + \overline{P}_0)e^{\chi_0/2}}{x^2 f_0}, \tag{4.6.62}$$

$$\bar{d}_4 = \frac{2\gamma(\overline{\epsilon}_0 + \overline{P}_0)e^{\chi_0/2}}{f_0(x^2 - 2\gamma f_0 + 2\gamma)}, \tag{4.6.63}$$

$$\bar{d}_5 = \frac{xf_0\frac{d\chi_0}{dx} + x\frac{df_0}{dx} + 2(\sqrt{f_0} - f_0)}{2\Gamma x\overline{P}_0\sqrt{f_0}e^{\chi_0/2}}\frac{d\chi_0}{dx}, \tag{4.6.64}$$

$$\begin{aligned}
\bar{d}_6 = {} & \frac{e^{\chi_0}}{4\sqrt{f_0}x^4}\left(2x^2\left(\frac{d\chi_0}{dx}\right)^3 f_0^2 + 4\left(\frac{d\chi_0}{dx}\right)^2 f_0^{3/2}x + 5\left(\frac{d\chi_0}{dx}\right)^2 x^2 f_0\frac{df_0}{dx}\right. \\
& + 4x^2 f_0^2\frac{d^2\chi_0}{dx^2}\frac{d\chi_0}{dx} - 8x\left(\frac{d\chi_0}{dx}\right)^2 f_0^2 + 2\frac{d\chi_0}{dx}x^2\frac{d^2 f_0}{dx^2}f_0 \\
& + \frac{d\chi_0}{dx}x^2\left(\frac{df_0}{dx}\right)^2 + 4f_0^{3/2}\frac{d^2\chi_0}{dx^2}x + 2x^2 f_0\frac{d^2\chi_0}{dx^2}\frac{df_0}{dx} - 12f_0^{3/2}\frac{d\chi_0}{dx} \\
& \left. + 4\frac{d\chi_0}{dx}\sqrt{f_0}\frac{df_0}{dx}x - 10xf_0\frac{df_0}{dx}\frac{d\chi_0}{dx} - 4f_0^2x\frac{d^2\chi_0}{dx^2} + 12f_0^2\frac{d\chi_0}{dx}\right).
\end{aligned} \tag{4.6.65}$$

The boundary conditions at the origin are: $\overline{u}(0) = 0$, $\overline{v}(0) = 1$ and $\overline{\psi}(0) = 0$, and at the surface of the star ($R = ax_1$), $\overline{v}(x_1) = 0$.

The system of differential equations for the functions $\overline{u}$, $\overline{v}$ and $\overline{\psi}$ cannot be integrated numerically in a proper manner, since we have a divergence at the origin due to the division by powers of x, see the coefficients in (4.6.60)-(4.6.65).

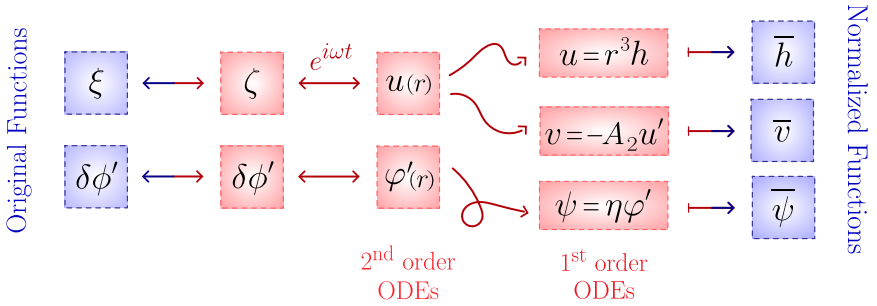

Figure 4.6.1: Changes of variable for radial perturbations.

To solve this problem, a change of variable is proposed for $\overline{u}$:

$$\overline{u}(x) = \overline{h}(x)x^3, \tag{4.6.66}$$

such that $\overline{h}(0) = 1/(3\Gamma(0)P_c e^{3\chi_c/2})$. A summary of all the changes of variable made in this section is found in figure 4.6.1.

Thus, the system of differential equations that is numerically integrated is

$$\frac{d\overline{h}}{dx} = \tilde{d}_1\overline{v} - \frac{3\overline{h}}{x}, \tag{4.6.67}$$

$$\frac{d\overline{v}}{dx} = [\tilde{d}_2 + \Omega^2\tilde{d}_3]\overline{h} + \tilde{d}_4\overline{\psi}, \tag{4.6.68}$$

$$\frac{d\overline{\psi}}{dx} = \tilde{d}_5\overline{v} + \tilde{d}_6\overline{h}, \tag{4.6.69}$$

where the coefficients are given by

$$\tilde{d}_1 = \frac{1}{x\Gamma P_0 f_0 e^{3\chi_0/2}}, \tag{4.6.70}$$

$$\tilde{d}_2 = x^3\bar{d}_2, \tag{4.6.71}$$

$$\tilde{d}_3 = -\frac{x(\bar{\epsilon}_0 + \overline{P}_0)e^{\chi_0/2}}{f_0}, \tag{4.6.72}$$

$$\tilde{d}_4 = \bar{d}_4, \tag{4.6.73}$$

$$\tilde{d}_5 = \bar{d}_5, \tag{4.6.74}$$

$$\tilde{d}_6 = x^3\bar{d}_6. \tag{4.6.75}$$

To find the appropriate numerical method to integrate the system of equations (4.6.67)-(4.6.69), we assume that there is an ordered set of frequencies $\omega_0^2 < \omega_1^2 <$

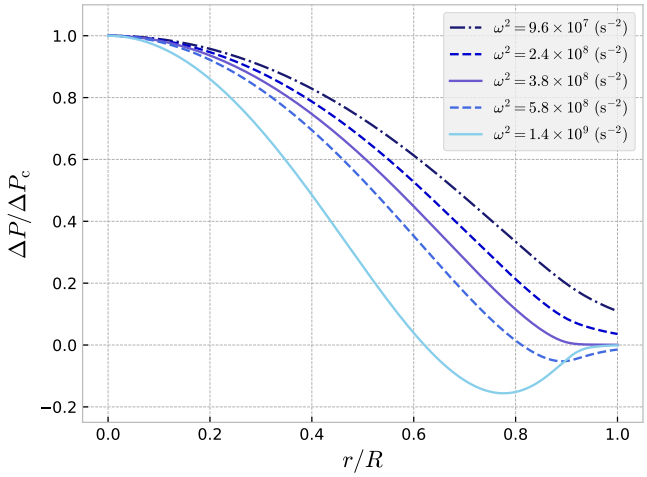

Figure 4.6.2: Normalized Lagrangian perturbation of the pressure inside the star for several test values of ω^2 with central density $\rho_c = 7.47 \times 10^{14}$ g/cm^3.

$\omega_2^2 < \cdots$ such that the n-th frequency corresponds to an eigenfunction with n nodes that satisfies the boundary conditions of the problem. We can observe this behavior in figure 4.6.2, which shows solutions for the Lagrangian perturbation of the pressure for some values of ω^2. This property is typical of a Sturm-Liouville problem, and so we use the same shooting method discussed in subsection 3.5.4.

As a demonstration, we have computed the radial profiles of the radial displacement modes δr_n, the Lagrangian perturbation modes of the pressure ΔP_n, and the derivative of the perturbation of the scalar field modes $d\varphi_n/dr$ for the fundamental mode ($n = 0$) and the n-overtones ($n = 1, 2, 10, 15$) for a NS of mass 1.08 $M_\odot$ and radius $R = 12$ km using the SLy EOS for $\alpha = 10$ km^2 (see figure 4.6.3). We observe that the amplitude of the radial displacement grows as the radial coordinate increases, whereas ΔP and $d\varphi/dr$ oscillate with a decaying amplitude before vanishing at the surface of the star. Nevertheless, all the functions are smooth respect to the radial coordinate. For higher-order modes, some of the nodes move across the core-crust transition and lie in the crust, where the radial displacement changes signs rapidly with a large amplitude, but ΔP_n possesses a small amplitude in the crust. This behavior were observed in GR (see figure 3.5.5). We discovered that the apparent divergence of the radial displacement at the surface of the star is due to numerical error. This, however, does not affect the values of eigenfrequencies.

In figure 4.6.4, we show the eigenfrequencies of the first three oscillation modes

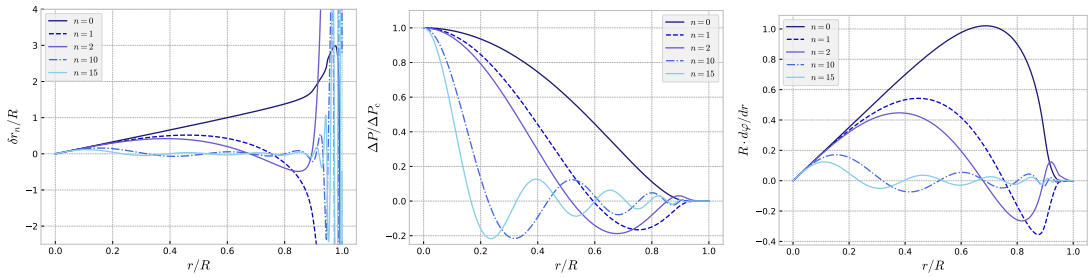

(a) Radial displacement **(b)** Lagrangian perturbation of the pressure **(c)** Derivative of the perturbation of the scalar field

Figure 4.6.3: Plots of the radial displacement modes δr_n, the Lagrangian perturbation modes of the pressure ΔP_n and the derivative of the perturbation of the scalar field modes $d\varphi_n/dr$ with respect to the normalized radial coordinate r/R for the fundamental mode ($n = 0$) and the n-overtones ($n = 1, 2, 10, 15$) in a NS of mass 1.08 $M_\odot$ and radius $R = 12$ km using the SLy EOS for $\alpha = 10$ km^2.

as a function of central density for the SLy EOS with a value of $\alpha = 10$ km^2. We observe that the squared frequencies of the overtones remain positive for all central densities, but for the fundamental mode there is a value of ρ_c for which ω_0^2 becomes negative (and remains so). The point where ω_0 is zero coincides with the maximum value of the mass, namely 2.70 $M_\odot$. Consequently, all NS solutions with central density greater than this critical value are unstable. This result is similar to GR where the change of stability also occurs at the maximum mass solution. If we vary the value of the coupling constant α, we obtain the same result, see figure 4.6.5a.

In figures 4.6.5 and 4.6.6, the results of the fundamental eigenfrequency are shown for the BSk19, BSk22 and MS2 EOSs for different values of α. In figure 4.6.7, we compare the fundamental frequencies of the SLy, BSk and MS2 EOSs. Based on these results we can say that the change of stability for NS in 4DEGB gravity also occurs at the maximum mass solution (independent of the EOS or whether it is relativistic). Interestingly, in the fundamental eigenfrequency versus central density plots we notice the curves start to approach a positive value again near the BH horizon of the theory. We can interpret this as if the NS solutions were trying to return to stability near the maximum central density, unlike in Einstein's theory, where they remain wholly unstable. We find that higher values of the 4DEGB coupling α tend to increase the mass of neutron stars of the same radius until the maximum mass point is at the end of the mass-radius curve. These

interesting parts of the solution space show possible extreme compact objects, too dense to exist in GR. For instance, if $\alpha = 100$ km^2, we obtain stable NS solutions (under radial perturbations) that satisfy the causality condition with masses greater than a black hole in GR for the same radius (see figure 4.5.3 and 4.5.4).

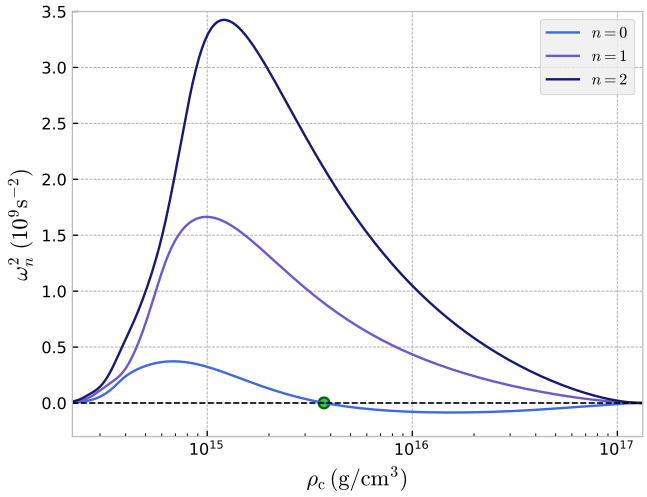

Figure 4.6.4: Eigenfrequencies of the first three oscillations modes for $\alpha = 10$ km^2 using the SLy EOS. The green point indicates where ω_0^2 becomes negative, which coincides with the maximum value of the mass 2.70 $M_\odot$.

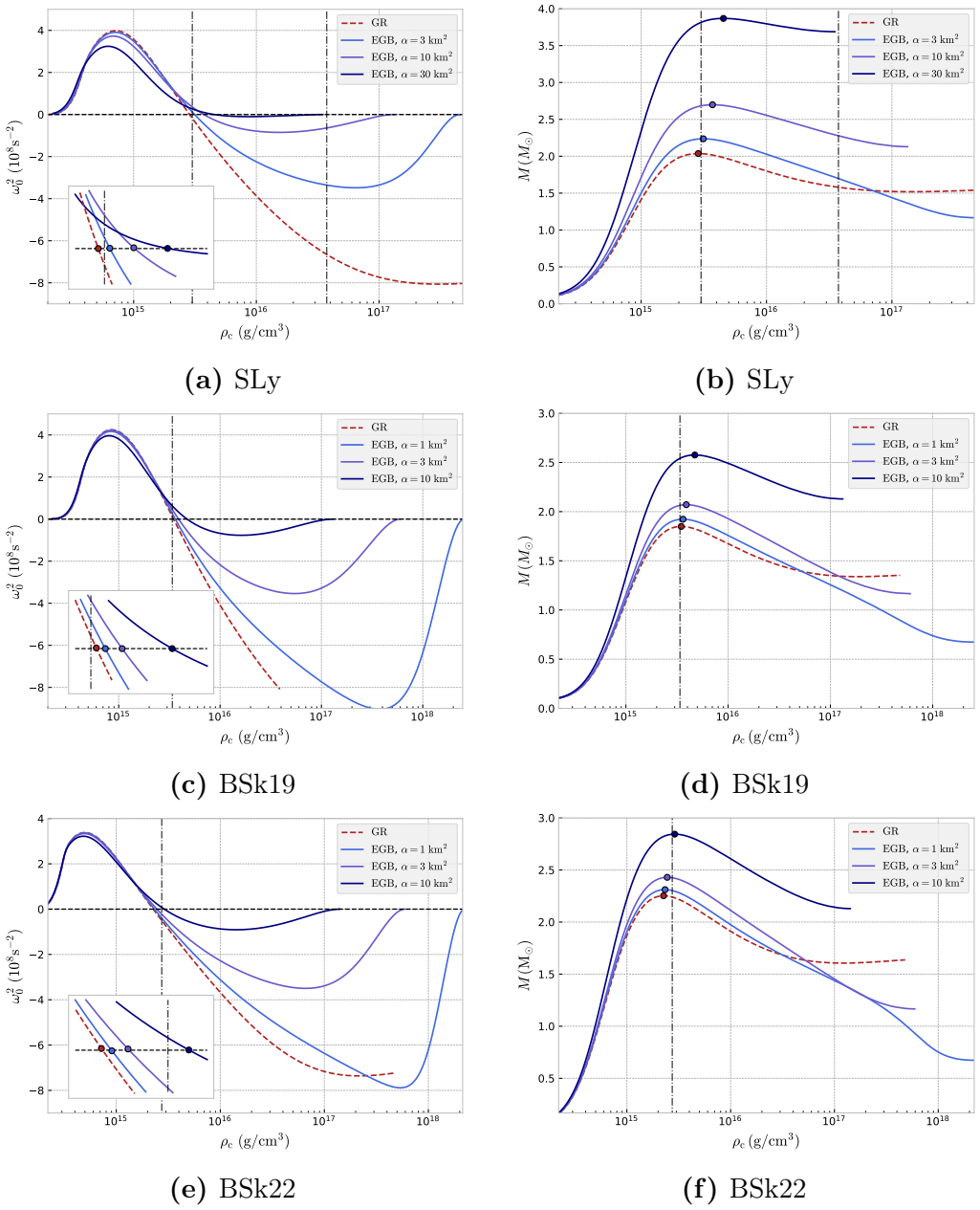

Figure 4.6.5: Fundamental eigenfrecuency and mass versus central density curves for neutron stars using the SLy, BSk19 and BSk22 EOSs in GR (red dashed line) and in 4DEGB for different values of α (blue lines). In the plots (a), (c) and (e), the colored circles mark the spot where the fundamental eigenfrecuency is zero, while in the plots (b), (d) and (f) they mark the maximum mass. In the plots the vertical lines mark the central density at which the speed of sound is equal to the speed of light. Beyond this value of density the speed of sound will be greater than the speed of light, breaking causality. In plots (a) and (b) the second vertical line marks the central density at which the speed of sound is again subluminal.

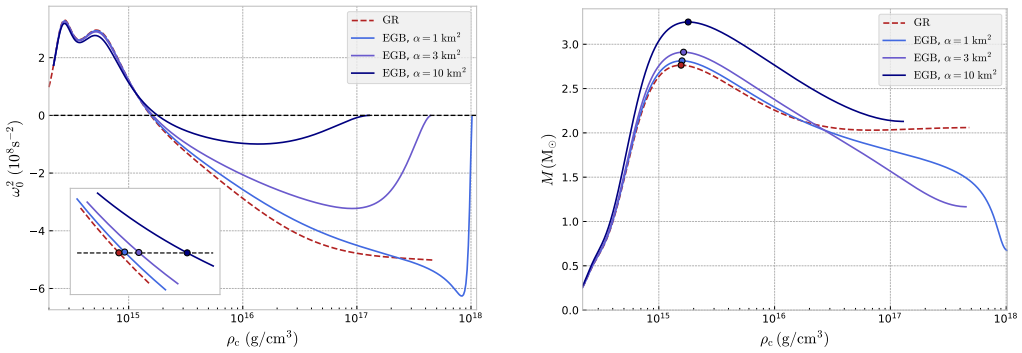

(a) MS2 **(b)** MS2

Figure 4.6.6: Fundamental eigenfrecuency and mass versus central density curves for neutron stars using the MS2 EOS in GR (red dashed line) and in 4DEGB for different values of α (blue lines). In the plot (a) the colored circles mark the spot where the fundamental eigenfrecuency is zero, while in the plot (b) they mark the maximum mass. We note the lack of vertical lines marking the transition from a subluminal to superluminal sound speed in these plots, as the MS2 EOS does not have problems with causality.

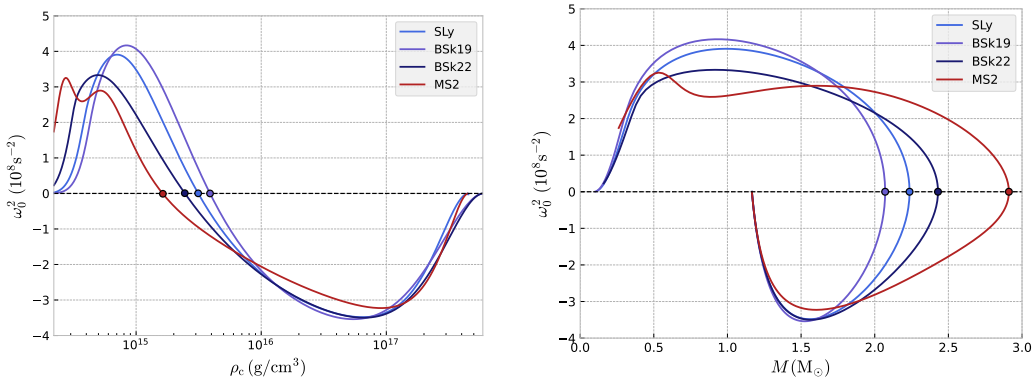

(a) **(b)**

Figure 4.6.7: Fundamental eigenfrecuency versus central density and mass curves for neutron stars using the SLy, BSk19-22 and MS2 EOSs in 4DEGB gravity for $\alpha = 3$ km^2.

Chapter 5

Conclusion

The objectives set out at the beginning of this work have been fulfilled and we have verified our hypothesis, since neutron star solutions were studied and analyzed in this new theory of gravity known as 4D Einstein-Gauss-Bonnet. In short, we have investigated the stability of neutron stars using the SLy, BSk and MS2 EOSs, the latter being the only relativistic. We found that the neutron star solutions in 4DEGB are qualitatively similar for each of these EOSs, with a larger α increasing the mass of the neutron star. Our numerical results indicate that the coincidence of the maximum mass points with the transition to instability still holds in this modified theory of gravity. Surprisingly, we have found solutions for which the fundamental eigenfrequency ω_0^2 returns to zero for large values of central density. This happens, for instance, when $\rho_c \sim 10^{17}$ g/cm^3 for the MS2 EOS and $\alpha = 10$ km^2, exhibited in figure 4.6.6a. Such results hint at possible strange black hole-sized stable objects that are not present in GR.

For some EOSs and some values of α we found that the maximum mass points are not reached before causality-violating pressures are required, however maximal solutions do exist that respect causality. For example, for the BSk19 EOS the maximum mass solution is not physical for $\alpha \lesssim 100$ km^2, however the maximal solution for $\alpha = 300$ km^2 does respect causality (see figure 4.5.3d). For large enough coupling to the higher curvature gravity terms a maximum mass is not attained until the solution curve merges with the black hole horizon. This means that there is a whole range of stable 4DEGB objects that are disallowed in GR, many of which are smaller than the GR Schwarzschild radius. Observation of an

extreme compact object with these characteristics could be interpreted as evidence for these higher curvature contributions to gravity having an important role to play in real gravitational dynamics.

Nevertheless, it is important to highlight potential improvements to this work. For instance, exploring other relativistic EOSs. One could also try to better understand the behavior of the radial displacement at the surface of the neutron star, which we have shown to be numerical in nature and does not affect the eigenfrequency values. On other remaining question could be to understand why the static NS solutions approach the black hole limit asymptotically.

As with all research work, this study does not end here; different new lines of future research can be explored to expand and deepen the obtained results. For instance,

- The study of other (hypothetical) compact objects, candidates for objects more massive than neutron stars but less massive than a black hole, whose equations of state differ significantly from those used for neutron stars, such as quark stars or hybrid stars. In the literature, equilibrium solutions of quark stars in 4DEGB have already been documented in Ref. [74], but it remains to be done the analysis of the fundamental radial oscillation modes.

- The analysis of the stability of charged stars, because in General Relativity the presence of charge can increase the stability or new instabilities can appear [78]. In principle, it is possible for charged stars to exist, but the observed stars are globally neutral due to the neutralization. However, in extreme conditions such as quark or strange stars, the presence of residual charge may be relevant to their stability.

- Another interesting direction is to explore other modified theories of gravity, both purely metric theories and theories with additional degrees of freedom (e.g., a scalar field). The remarkable thing about this work is that despite not defining a Sturm-Liouville problem, the equations can be solved with the same numerical methods used in GR, thus providing a procedure to address the problem of radial oscillations in stars in scalar-tensor theories of gravity.

References

[1] S. Chandrasekhar, *An Introduction to the Study of Stellar Structure* (The University of Chicago Press, 1939) Chap. 10-11.

[2] S. Chandrasekhar and E. Milne, "The Highly Collapsed Configurations of a Stellar Mass", Monthly Notices of the Royal Astronomical Society **91**, 456–466 (1931).

[3] R. Fowler, "On dense matter", Monthly Notices of the Royal Astronomical Society **87**, 114–122 (1926).

[4] P. Chavanis, "Statistical mechanics of self-gravitating systems in general relativity: I. The quantum Fermi gas", Eur. Phys. J. Plus **135**, 1–79 (2020).

[5] S. L. Shapiro and S. A. Teukolsky, *Black Holes, White Dwarfs, and Neutron Stars: The Physics of Compact Objetcs* (John Wiley and Sons, 1983).

[6] J. R. Oppenheimer and G. M. Volkoff, "On Massive Neutron Cores", Physical Review **55**, 377 (1939).

[7] G. J. Olmo, D. Rubiera-Garcia, and A. Wojnar, "Stellar structure models in modified theories of gravity: Lessons and challenges", Physics Reports **876**, 1–75 (2020).

[8] F. Özel and P. Freire, "Masses, Radii, and the Equation of State of Neutron Stars", Annual Review of Astronomy and Astrophysics **54**, 401–440 (2016).

[9] B. P. Abbott, R. Abbott, T. D. Abbott, et al. (LIGO Scientific Collaboration and Virgo Collaboration), "GW170817: Observation of Gravitational Waves from a Binary Neutron Star Inspiral", Phys. Rev. Lett. **119**, 161101 (2017).

[10] B. P. Abbott, R. Abbott, T. D. Abbott, et al., "GW170817: Measurements of Neutron Star Radii and Equation of State", Phys. Rev. Lett. **121**, 161101 (2018).

[11] B. P. Abbott, R. Abbott, T. D. Abbott, et al., "Properties of the Binary Neutron Star Merger GW170817", Phys. Rev. X **9**, 011001 (2019).

[12] T. Padmanabhan, "Cosmological constant—the weight of the vacuum", Physics Reports **380**, 235–320 (2003).

[13] H. Lu and C. N. Pope, "Critical Gravity in Four Dimensions", Phys. Rev. Lett. **106**, 181302 (2011).

[14] P. Bueno and P. A. Cano, "Einsteinian cubic gravity", Phys. Rev. D **94**, 104005 (2016).

[15] T. Kobayashi, "Horndeski theory and beyond: a review", Reports on Progress in Physics **82**, 086901 (2019).

[16] D. Lovelock, "The Einstein tensor and its generalizations", J. Math. Phys. **12**, 498–501 (1971).
[17] Dražen Glavan and Chunshan Lin, "Einstein-Gauss-Bonnet Gravity in Four-Dimensional Spacetime", Phys. Rev. Lett. **124**, 081301 (2020).
[18] A. Kumar, R. K. Walia, and S. G. Ghosh, "Bardeen Black Holes in the Regularized 4D Einstein Gauss Bonnet Gravity", Universe **8**, 232 (2022).
[19] P. G. Fernandes, "Charged black holes in AdS spaces in 4D Einstein Gauss-Bonnet gravity", Physics Letters B **805**, 135468 (2020).
[20] R. Kumar and S. G. Ghosh, "Rotating black holes in 4D Einstein-Gauss-Bonnet gravity and its shadow", Journal of Cosmology and Astroparticle Physics **2020**, 053–053 (2020).
[21] A. Kumar, D. Baboolal, and S. G. Ghosh, "Nonsingular Black Holes in 4D Einstein-Gauss-Bonnet Gravity", Universe **8**, 244 (2022).
[22] S.-L. Li, P. Wu, and H. Yu, *Stability of the Einstein Static Universe in 4D Gauss-Bonnet Gravity*, arXiv:2004.02080, 2020.
[23] T. Kobayashi, "Effective scalar-tensor description of regularized Lovelock gravity in four dimensions", Journal of Cosmology and Astroparticle Physics **2020**, 013–013 (2020).
[24] D. D. Doneva and S. S. Yazadjiev, "Relativistic stars in 4D Einstein-Gauss-Bonnet gravity", Journal of Cosmology and Astroparticle Physics **2021**, 024 (2021).
[25] C. Charmousis, A. Lehébel, E. Smyrniotis, et al., "Astrophysical constraints on compact objects in 4D Einstein-Gauss-Bonnet gravity", J. Cosmol. Astropart. Phys. **2022**, 033 (2022).
[26] S. G. Ghosh and S. D. Maharaj, "Radiating black holes in the novel 4D Einstein-Gauss-Bonnet gravity", Physics of the Dark Universe **30**, 100687 (2020).
[27] D. Malafarina, B. Toshmatov, and N. Dadhich, "Dust collapse in 4D Einstein-Gauss-Bonnet gravity", Physics of the Dark Universe **30**, 100598 (2020).
[28] M. Gürses, T. Ç. Şişman, and B. Tekin, "Is there a novel Einstein-Gauss-Bonnet theory in four dimensions?", The European Physical Journal C **80**, 10.1140/epjc/s10052-020-8200-7 (2020).
[29] W.-Y. Ai, "A note on the novel 4D Einstein-Gauss-Bonnet gravity", Communications in Theoretical Physics **72**, 095402 (2020).
[30] F.-W. Shu, "Vacua in novel 4D Einstein-Gauss-Bonnet gravity: Pathology and instability?", Physics Letters B **811**, 135907 (2020).
[31] R. A. Hennigar, D. Kubiznák, R. B. Mann, et al., "On taking the $D \to 4$ limit of Gauss-Bonnet gravity: theory and solutions", Journal of High Energy Physics **2020**, 27 (2020).
[32] P. G. S. Fernandes, P. Carrilho, T. Clifton, et al., "Derivation of Regularized Field Equations for the Einstein-Gauss-Bonnet Theory in Four Dimensions", Phys. Rev. D **102**, 024025 (2020).
[33] T. Clifton, P. Carrilho, P. G. S. Fernandes, et al., "Observational Constraints on the Regularized 4D Einstein-Gauss-Bonnet Theory of Gravity", Phys. Rev. D **102**, 084005 (2020).

[34] C. M. A. Zanoletti, B. R. Hull, C. D. Leonard, et al., "Cosmological constraints on 4-dimensional Einstein-Gauss-Bonnet gravity", JCAP **01**, 043 (2024).
[35] R. Abbott et al., "GW190814: Gravitational Waves from the Coalescence of a 23 Solar Mass Black Hole with a 2.6 Solar Mass Compact Object", The Astrophysical Journal Letters **896**, L44 (2020).
[36] N. K. Glendenning, *Compact stars: Nuclear physics, particle physics, and general relativity*, 2nd ed. (Springer, 2000) Chap. 3, pp. 129–134.
[37] S. Chandrasekhar, "Dynamical Instability of Gaseous Masses Approaching the Schwarzschild Limit in General Relativity", Phys. Rev. Lett. **12**, 114–116 (1964).
[38] C. W. Misner, K. S. Thorne, and J. A. Wheeler, *Gravitation* (W. H. Freeman, 1973) Chap. 26.
[39] P. S. Epstein, *A Textbook of Thermodynamics* (John Wiley and Sons, 1937) Chap. 13.
[40] M. Camenzind, *Compact Objects in Astroplhysics* (Springer, 2007) Chap. 5-6.
[41] N. Straumann, *General Relativity with Applications to Astrophysics* (Springer, 2004) Chap. 6.
[42] Y. B. Zel'dovich and I. D. Novikov, *Stars and Relativity* (Dover Publications, 1971) Chap. 6.
[43] W. Greiner, L. Neise, and H. Stocker, *Thermodynamics and Statistical Mechanics* (Springer, 1995) Chap. 14.
[44] T. Hamada and E. Salpeter, "Models for Zero-Temperature Stars", Astrophysical Journal **134**, 683 (1961).
[45] G. Baym, C. Pethick, and P. Sutherland, "The Ground State of Matter at High Densities: Equation of State and Stellar Models", Astrophysical Journal **170**, 299 (1971).
[46] S. Balberg and S. L. Shapiro, "The Properties of Matter in White Dwarfs and Neutron Stars", arXiv:astro-ph/0004317.
[47] Bartolini, Lorenzo, Gudnason, Sven Bjarke, Leutgeb, Josef, et al., "Neutron stars and phase diagram from a double hard-wall", EPJ Web Conf. **274**, 07007 (2022).
[48] A. Akmal and V. R. Pandharipande, "Spin-isospin structure and pion condensation in nucleon matter", Phys. Rev. C **56**, 2261–2279 (1997).
[49] J. M. Lattimer and M. Prakash, "Neutron Star Structure and the Equation of State", The Astrophysical Journal **550**, 426–442 (2001).
[50] F. Douchin and P. Haensel, "A unified equation of state of dense matter and neutron star structure", Astronomy and Astrophysics **380**, 151–167 (2001).
[51] V. R. Pandharipande and D. G. Ravenhall, "Hot Nuclear Matter", in *Nuclear matter and heavy ion collisions: proceedings of a nato advanced research workshop on nuclear matter and heavy ion collisions, held february 7–16, 1989, in les houches, france*, edited by M. Soyeur, H. Flocard, B. Tamain, et al. (Springer US, Boston, MA, 1989), pp. 103–132.

[52] A. Y. Potekhin, A. F. Fantina, N. Chamel, et al., "Analytical representations of unified equations of state for neutron-star matter", Astronomy and Astrophysics **560**, A48 (2013).
[53] J. M. Pearson, N. Chamel, A. Y. Potekhin, et al., "Unified equations of state for cold non-accreting neutron stars with Brussels–Montreal functionals – I. Role of symmetry energy", Monthly Notices of the Royal Astronomical Society **481**, 2994–3026 (2018).
[54] H. Müller and B. D. Serot, "Relativistic mean-field theory and the high-density nuclear equation of state", Nuclear Physics A **606**, 508–537 (1996).
[55] P. Haensel and A. Y. Potekhin, "Analytical representations of unified equations of state of neutron-star matter", Astronomy and Astrophysics **428**, 191–197 (2004).
[56] P. Haensel and B. Pichon, "Experimental nuclear masses and the ground state of cold dense matter", Astronomy and Astrophysics **283**, 313–318 (1994).
[57] C. Gungor and K. Y. Eksi, "Analytical Representation for Equations of State of Dense Matter", arXiv:1108.2166 (2011).
[58] J. W. Negele and D. Vautherin, "Neutron star matter at sub-nuclear densities", Nuclear Physics A **207**, 298–320 (1973).
[59] A. Einstein, "Die Feldgleichungen der Gravitation", Sitzungsberichte der Königlich Preußischen Akademie der Wissenschaften, 844–847 (1915).
[60] A. Einstein, "Kosmologische Betrachtungen zur allgemeinen Relativitätstheorie", Sitzung der physikalisch mathematischen Klasse, 142–152 (1917).
[61] D. Hilbert, "Die Grundlagen der Physik", Nachrichten von der Gesellschaft der Wissenschaften zu Göttingen – Mathematisch-Physikalische Klasse **3**, 395–407 (1915).
[62] K. Schwarzschild, "On the Gravitational Field of a Mass Point according to Einstein's Theory", Sitzungsber. Preuss. Akad. Wiss. Berlin. (Math. Phy.), 189–196 (1916).
[63] A. S. Eddington, "A Comparison of Whitehead's and Einstein's Formula", Nature **113**, 192 (1924).
[64] D. Finkelstein, "Past-Future Asymmetry of the Gravitational Field of a Point Particle", Phys. Rev. **110**, 965–967 (1958).
[65] G. D. Birkhoff and R. E. Langer, *Relativity and modern physics* (Harvard University Press, 1923).
[66] H. A. Buchdahl, "General Relativistic Fluid Spheres", Phys. Rev. **116**, 1027–1034 (1959).
[67] R.-H. Lin, X.-N. Chen, and X.-H. Zhai, "Realistic neutron star models in $f(T)$ gravity", The European Physical Journal C **82**, 308 (2022).
[68] B. K. Harrison, K. S. Thorne, M. Wakano, et al., *Gravitation Theory and Gravitational Collapse* (The University of Chigago Press, 1965) Chap. 7.
[69] G. Arfken and H. Weber, *Mathematical methods for physicists*, 6th ed. (Elsevier Academic Press, 2005) Chap. 17, p. 1072.

[70] K. D. Kokkotas and J. Ruoff, "Radial oscillations of relativistic stars", Astron. Astrophys. **366**, 565 (2001).
[71] R. B. Mann and S. F. Ross, "The $D \to 2$ limit of general relativity", Class. Quant. Grav. **10**, 1405–1408 (1993).
[72] H. Lu and Y. Pang, "Horndeski gravity as $D \to 4$ limit of Gauss-Bonnet", Phys. Lett. B **809**, 135717 (2020).
[73] P. G. S. Fernandes, P. Carrilho, T. Clifton, et al., "Black holes in the scalar-tensor formulation of 4D Einstein-Gauss-Bonnet gravity: Uniqueness of solutions, and a new candidate for dark matter", Phys. Rev. D **104**, 044029 (2021).
[74] M. Gammon, S. Rourke, and R. B. Mann, "Quark stars with a unified interacting equation of state in regularized 4D Einstein-Gauss-Bonnet gravity", Phys. Rev. D **109**, 024026 (2024).
[75] P. G. S. Fernandes, P. Carrilho, T. Clifton, et al., "The 4D Einstein–Gauss–Bonnet theory of gravity: a review", Classical and Quantum Gravity **39**, 063001 (2022).
[76] M. Saravani and T. P. Sotiriou, "Classification of shift-symmetric Horndeski theories and hairy black holes", Phys. Rev. D **99**, 124004 (2019).
[77] S. Chakraborty and N. Dadhich, "Limits on stellar structures in Lovelock theories of gravity", Physics of the Dark Universe **30**, 100658 (2020).
[78] C. Zhang, M. Gammon, and R. B. Mann, "Stellar structure and stability of charged interacting quark stars and their scaling behavior", Phys. Rev. D **104**, 123007 (2021).

Appendix A

Newtonian stellar equilibrium

Consider a star modeled as a spherical, static, non-relativistic perfect fluid in equilibrium. Since the perfect fluid is incompressible and non-viscous, its dynamic is described by the **Euler equation** [5]:

$$\rho(\vec{x})\frac{d\vec{v}}{dt} = \rho(\vec{x})\left(\frac{\partial\vec{v}}{\partial t} + (\vec{v}\cdot\nabla)\vec{v}\right) = -\nabla P(\vec{x}) + \vec{f}(\vec{x}), \tag{A.1}$$

where $\vec{v}(\vec{x},t)$ is the flow velocity of the fluid and $\vec{f}$ is the external force density acting on each fluid element. In the static case, the flow velocity vanishes, $\vec{v}(\vec{x},t) = \vec{0}$. Therefore, equation (A.1) reduces to

$$\nabla P(\vec{x}) = \vec{f}(\vec{x}). \tag{A.2}$$

In our case, the only external force is gravitational, acting on a fluid element of mass $dm = \rho(\vec{x})\,dV$, where $\rho(\vec{x})$ is the mass density. The gravitational force is given by $d\vec{F}_g = -dm\vec{\nabla}\phi$, where ϕ is the Newtonian gravitational potential that satisfies the Poisson equation

$$\nabla^2\phi = 4\pi G\rho. \tag{A.3}$$

Thus, the force density is $\vec{f} = -\rho\nabla\phi$ and the equilibrium condition can be expressed by

$$\frac{dP}{dr} = -\rho\frac{d\phi}{dr}, \tag{A.4}$$

where we have assumed spherical symmetry.

Integrating the equation (A.3) from the center of the star to an arbitrary radius r, we obtain

$$\frac{d\phi}{dr} = \frac{4\pi G}{r^2}\int_0^r d\bar{r}\ \bar{r}^{\,2}\rho(\bar{r}) = \frac{G\mathcal{M}(r)}{r^2}, \tag{A.5}$$

where we have defined the **mass function** $\mathcal{M}(r)$ by

$$\mathcal{M}(r) = 4\pi\int_0^r d\bar{r}\ \bar{r}^2\rho(\bar{r}), \tag{A.6}$$

or

$$\frac{d\mathcal{M}}{dr} = 4\pi r^2\rho. \tag{A.7}$$

Physically, the function $\mathcal{M}(r)$ (in this non-relativistic context) represents the mass of the star within the radius r of the star. When we write (A.6), we assume that there is no point mass in the center, since we would have a Dirac delta that would cancel the integral.

Replacing the equation (A.5) in (A.4), we obtain the Newtonian hydrostatic equilibrium condition:

$$\frac{dP}{dr} = -\frac{G\mathcal{M}}{r^2}\rho. \tag{A.8}$$

Note that, since $\rho > 0$, the pressure is a monotonically decreasing function in the radial coordinate.

Appendix B

Derivation of the Sturm-Liouville problem for the radial perturbations in General Relativity

The line element for the radial perturbation problem is given by

$$ds^2 = -e^{\alpha}(dx^0)^2 + e^{\beta}dr^2 + r^2[d\theta^2 + \sin^2\theta d\varphi^2], \tag{B.1}$$

where $x^0 = ct$, $\alpha = \alpha(x^0, r)$ and $\beta = \beta(x^0, r)$ are the perturbed metric functions. We can write

$$\alpha(x^0, r) = \alpha_0(r) + \delta\alpha(x^0, r), \tag{B.2}$$

$$\beta(x^0, r) = \beta_0(r) + \delta\beta(x^0, r), \tag{B.3}$$

and similarly for the pressure P, the energy density ϵ and the baryon number density n.

The components $(0r)$ and (rr) of the Einstein tensor, when we evaluate the metric (B.1), are:

$$G_{0r} = \frac{1}{cr}\frac{\partial\beta}{\partial t}(x^0, r), \tag{B.4}$$

$$G_{rr} = -\frac{1}{r^2}\left[e^{\beta(x^0,r)} - r\frac{\partial\alpha}{\partial r}(x^0, r) - 1\right]. \tag{B.5}$$

At first order, we can write these components as follows

$$G_{0r} = \frac{1}{cr}\frac{\partial}{\partial t}(\beta_0 + \delta\beta) = \frac{1}{rc}\frac{\partial \delta\beta}{\partial t}, \tag{B.6}$$

$$\begin{aligned} G_{rr} &= -\frac{1}{r^2}\left[e^{\beta_0}e^{\delta\beta} - r\frac{\partial}{\partial r}(\alpha_0 + \delta\alpha) - 1\right] \\ &= -\frac{1}{r^2}\left[e^{\beta_0}(1+\delta\beta) - r\frac{\partial \alpha_0}{\partial r} - r\frac{\partial \delta\alpha}{\partial r} - 1\right] \\ &= (G_{rr})_0 - \frac{1}{r^2}e^{\beta_0}\delta\beta + \frac{1}{r}\frac{\partial \delta\alpha}{\partial r}, \end{aligned} \tag{B.7}$$

where

$$(G_{rr})_0 = -\frac{1}{r^2}\left[e^{\beta_0} - r\frac{\partial \alpha_0}{\partial r} - 1\right] \tag{B.8}$$

is the (rr) component of the non-perturbed Einstein tensor.

The covariant components of the 4-velocity (3.5.16) and (3.5.17) are:

$$u_0 = -ce^{\alpha_0/2}\left(1 + \frac{1}{2}\delta\alpha\right), \tag{B.9}$$

$$u_r = e^{\beta_0 - \alpha_0/2}\dot{\delta r}. \tag{B.10}$$

Thus, the components $(0r)$ and (rr) of the energy-momentum tensor (3.2.7) are

$$\begin{aligned} T_{0r} &= (\epsilon_0 + P_0 + \delta\epsilon + \delta P)\frac{u_0}{c}\frac{u_r}{c} + Pg_{0r} \\ &= -\frac{1}{c}(\epsilon_0 + P_0 + \delta\epsilon + \delta P)e^{\alpha_0/2}\left(1 + \frac{1}{2}\delta\alpha\right)e^{\beta_0 - \alpha_0/2}\dot{\delta r} \\ &= -\frac{1}{c}(\epsilon_0 + P_0)e^{\beta_0}\dot{\delta r}, \end{aligned} \tag{B.11}$$

$$\begin{aligned} T_{rr} &= (\epsilon_0 + P_0 + \delta\epsilon + \delta P)\frac{(u_r)^2}{c^2} + Pg_{rr} \\ &= \frac{1}{c^2}(\epsilon_0 + P_0 + \delta\epsilon + \delta P)e^{2\beta_0 - \alpha_0}\dot{\delta r}^2 + (P_0 + \delta P)e^{\beta_0}e^{\delta\beta} \\ &= (P_0 + \delta P)e^{\beta_0}(1 + \delta\beta) \\ &= P_0 e^{\beta_0} + P_0 e^{2\beta_0}\delta\beta + \delta P e^{\beta_0}. \end{aligned} \tag{B.12}$$

Consequently, the $(0r)$ component of the field equation reduces to

$$\frac{\partial \delta\beta}{\partial t} = -\frac{8\pi G}{c^4}r(\epsilon_0 + P_0)e^{\beta_0}\dot{\delta r}. \tag{B.13}$$

Integrating with respect to t, we obtain the equation for the evolution of the perturbation $\delta\beta$:

$$\delta\beta = -\frac{8\pi G}{c^4}(\epsilon_0 + P_0)re^{\beta_0}\delta r. \tag{B.14}$$

Note that the integration constant is zero because $\delta\beta = 0$ when $\delta r = 0$. Moreover, the equation for the perturbation $\delta\beta$ depends only on the equilibrium configuration and the displacement δr. Now, if we sum the equations (3.5.2) and (3.5.3), we found that

$$\frac{d\alpha_0}{dr} + \frac{d\beta_0}{dr} = \frac{8\pi G}{c^4}(\epsilon_0 + P_0)re^{\beta_0}. \tag{B.15}$$

Thus, we can write equation (B.14) as follows:

$$\delta\beta = -\frac{8\pi G}{c^4}(\epsilon_0 + P_0)re^{\beta_0}\delta r = -\left(\frac{d\alpha_0}{dr} + \frac{d\beta_0}{dr}\right)\delta r. \tag{B.16}$$

This equation allow us to write the equations for the evolution of the perturbations δn, δP and $\delta\epsilon$ in terms only of the fields of the equilibrium configuration and the radial displacement δr since

$$\begin{aligned} r^{-2}e^{-\beta_0/2}(r^2e^{\beta_0/2}\delta r)' + \frac{1}{2}\delta\beta &= r^{-2}e^{-\beta_0/2}(r^2e^{\beta_0/2}\delta r)' - \frac{1}{2}\left(\frac{d\alpha_0}{dr} + \frac{d\beta_0}{dr}\right)\delta r \\ &= \frac{1}{2}\beta_0'\delta r + r^{-2}(r^2\delta r)' - \frac{1}{2}\alpha_0'\delta r - \frac{1}{2}\beta_0'\delta r \\ &= \left(r^{-2}(r^2\delta r)' - \frac{1}{2}\alpha_0'\delta r\right)\frac{e^{\alpha_0/2}}{e^{\alpha_0/2}} \\ &= \left(r^{-2}(r^2\delta r)'e^{-\alpha_0/2} + (e^{-\alpha_0/2})'\delta r\right)e^{\alpha_0/2} \\ &= r^{-2}(r^2\delta re^{-\alpha_0/2})'e^{\alpha_0/2}. \end{aligned} \tag{B.17}$$

Replacing the above equation in equations (3.5.28), (3.5.32) and (3.5.37), we can write them as follows:

$$\delta n = -n_0r^{-2}(r^2\delta re^{-\alpha_0/2})'e^{\alpha_0/2} - n_0'\delta r, \tag{B.18}$$

$$\delta P = -\Gamma P_0r^{-2}(r^2\delta re^{-\alpha_0/2})'e^{\alpha_0/2} - P_0'\delta r, \tag{B.19}$$

$$\delta\epsilon = -(\epsilon_0 + P_0)r^{-2}(r^2\delta re^{-\alpha_0/2})'e^{\alpha_0/2} - \epsilon_0'\delta r. \tag{B.20}$$

On the other hand, using equations (B.7) and (B.12) in the (rr) component of

the field equation, we can write

$$(G_{rr})_0 - \frac{1}{r^2}e^{\beta_0}\delta\beta + \frac{1}{r}\frac{\partial\delta\alpha}{\partial r} = \frac{8\pi G}{c^4}\left(P_0 e^{\beta_0} + P_0 e^{\beta_0}\delta\beta + \delta P e^{\beta_0}\right), \tag{B.21}$$

$$-\frac{1}{r^2}e^{\beta_0}\delta\beta + \frac{1}{r}\frac{\partial\delta\alpha}{\partial r} = \frac{8\pi G}{c^4}\left(P_0 e^{\beta_0}\delta\beta + \delta P e^{\beta_0}\right), \tag{B.22}$$

where in the last line, the field equation $(G_{rr})_0 = \frac{8\pi G}{c^4}P_0 e^{\beta_0}$ for the equilibrium configuration was used.

Using equation (B.14) to remove $\delta\beta$ and (B.19) to remove δP from the equation (B.22), we obtain

$$\frac{8\pi G}{c^4 r}(\epsilon_0 + P_0)e^{2\beta_0}\delta r + \frac{1}{r}\frac{\partial\delta\alpha}{\partial r} = -\frac{8\pi G}{c^4}\left(\frac{8\pi G}{c^4}P_0(\epsilon_0 + P_0)re^{2\beta_0}\delta r + \Gamma P_0 r^{-2}(r^2\delta r e^{-\alpha_0/2})' e^{\alpha_0/2+\beta_0} + P_0'\delta r e^{\beta_0}\right), \tag{B.23}$$

$$\frac{1}{r}\frac{\partial\delta\alpha}{\partial r} = -\frac{8\pi G}{c^4}(\epsilon_0 + P_0)e^{2\beta_0}\delta r\left(\frac{8\pi G}{c^4}P_0 r + \frac{1}{r}\right) - \frac{8\pi G}{c^4}\Gamma P_0 r^{-2}(r^2\delta r e^{-\alpha_0/2})' e^{\alpha_0/2+\beta_0} - \frac{8\pi G}{c^4}P_0'\delta r e^{\beta_0}, \tag{B.24}$$

$$\frac{\partial\delta\alpha}{\partial r} = -\frac{8\pi G}{c^4}(\epsilon_0 + P_0)e^{2\beta_0}\delta r\left(\frac{8\pi G}{c^4}P_0 r^2 + 1\right) - \frac{8\pi G}{c^4}\Gamma P_0 r^{-1}(r^2\delta r e^{-\alpha_0/2})' e^{\alpha_0/2+\beta_0} - \frac{8\pi G}{c^4}P_0' r\delta r e^{\beta_0}. \tag{B.25}$$

From equation (3.5.4), note that

$$\begin{aligned}
&-\frac{8\pi G}{c^4}(\epsilon_0 + P_0)e^{2\beta_0}\delta r\left(\frac{8\pi G}{c^4}P_0 r^2 + 1\right) - \frac{8\pi G}{c^4}P_0' r\delta r e^{\beta_0} \\
&= -\frac{8\pi G}{c^4}(\epsilon_0 + P_0)e^{2\beta_0}\delta r\left(\frac{8\pi G}{c^4}P_0 r^2 + 1\right) - \frac{16\pi G}{c^4}P_0' r\delta r e^{\beta_0} + \frac{8\pi G}{c^4}P_0' r\delta r e^{\beta_0} \\
&= -\frac{8\pi G}{c^4}(\epsilon_0 + P_0)e^{2\beta_0}\delta r\left(\frac{8\pi G}{c^4}P_0 r^2 + 1\right) + \frac{8\pi G}{c^4}(\epsilon_0 + P_0)\alpha_0' r\delta r e^{\beta_0} + \frac{8\pi G}{c^4}P_0' r\delta r e^{\beta_0} \\
&= -\frac{8\pi G}{c^4}(\epsilon_0 + P_0)e^{\beta_0}\delta r\left[\frac{8\pi G}{c^4}e^{\beta_0}P_0 r^2 + e^{\beta_0} - \alpha_0' r\right] + \frac{8\pi G}{c^4}P_0' r\delta r e^{\beta_0} \\
&= -\frac{8\pi G}{c^4}(\epsilon_0 + P_0)e^{\beta_0}\delta r\left[\frac{8\pi G}{c^4}e^{\beta_0}P_0 r^2 + e^{\beta_0} + 1 - e^{\beta_0} - \frac{8\pi G}{c^4}r^2 P_0 e^{\beta_0}\right] + \frac{8\pi G}{c^4}P_0' r\delta r e^{\beta_0} \\
&= \frac{8\pi G}{c^4}\left[P_0' r - \epsilon_0 - P_0\right]e^{\beta_0}\delta r.
\end{aligned} \tag{B.26}$$

Replacing equation (B.26) in equation (B.25), we obtain the equation for the evolution of the perturbation $\delta\alpha$:

$$\frac{\partial\delta\alpha}{\partial r} = -\frac{8\pi G}{c^4}\Gamma P_0 r^{-1} e^{\alpha_0/2+\beta_0}(r^2 e^{-\alpha_0/2}\delta r)' + \frac{8\pi G}{c^4}\left[P_0' r - \epsilon_0 - P_0\right] e^{\beta_0}\delta r. \quad \text{(B.27)}$$

Momentum conservation

Consider the conservation law of the energy-momentum tensor (3.2.25). Using the form of this tensor for a perfect fluid (3.2.7), we find that

$$\partial_\nu(\epsilon + P)u^\mu u^\nu + (\epsilon + P)a^\mu + (\epsilon + P)u^\mu \nabla_\nu u^\nu + c^2 g^{\mu\nu}\partial_\nu P = 0, \quad \text{(B.28)}$$

where $a^\mu = u^\nu \nabla_\nu u^\mu$ is the 4-acceleration of the fluid. Taking the r component of this equation, the first and third terms vanish, since u^r is of first order in the perturbation and both $\partial_\nu(\epsilon + P)u^\nu$ and $\nabla_\nu u^\nu$ are also of first order because they are zero in the equilibrium configuration. Thus, equation (B.28) reduces to

$$(\epsilon + P)a^r + c^2 e^{-\beta} P' = 0. \quad \text{(B.29)}$$

Let us determine the a^r component of the 4-acceleration, to first order:

$$\begin{aligned} a^r &= u^0 \nabla_0 u^r + u^r \nabla_r u^r \\ &\approx u^0 \left(\frac{1}{c}\frac{\partial u^r}{\partial t} + \Gamma^r{}_{0\lambda} u^\lambda\right) \\ &= \frac{u^0}{c}\frac{\partial u^r}{\partial t} + \Gamma^r{}_{00}(u^0)^2 + \Gamma^r{}_{0r} u^0 u^r. \end{aligned} \quad \text{(B.30)}$$

But,

$$\Gamma^r{}_{00} = \frac{1}{2} e^{\alpha-\beta}\frac{\partial\alpha}{\partial r}, \quad \Gamma^r{}_{0r} = \frac{1}{2}\frac{\partial\beta}{\partial t}. \quad \text{(B.31)}$$

Therefore, the last term of equation (B.30) is of second order. Replacing the expressions (3.5.16) and (3.5.17) for the components u^0 and u^r, respectively, in

equation (B.30), we obtain

$$\begin{aligned} a^r &\approx e^{-\alpha_0}\left(1-\frac{1}{2}\delta\alpha\right)\ddot{\delta r} + \frac{c^2}{2}e^{-\beta_0}e^{\delta\alpha}e^{-\delta\beta}\left(1-\delta\alpha\right)\frac{\partial}{\partial r}\left(\alpha_0+\delta\alpha\right) \\ &\approx e^{-\alpha_0}\ddot{\delta r} + \frac{c^2}{2}e^{-\beta_0}(1+\delta\alpha)(1-\delta\beta)(1-\delta\alpha)(\alpha_0'+\delta\alpha') \\ &\approx e^{-\alpha_0}\ddot{\delta r} + \frac{c^2}{2}e^{-\beta_0}(1-\delta\beta)\alpha_0' + \frac{c^2}{2}e^{-\beta_0}\delta\alpha'. \end{aligned} \tag{B.32}$$

Thus, equation (B.29) can be written to first order as follows

$$(\epsilon_0+P_0)a^r + (\delta\epsilon+\delta P)a^r + c^2e^{-\beta_0}(1-\delta\beta)(P_0'+\delta P') = 0, \tag{B.33}$$

$$\begin{aligned} &(\epsilon_0+P_0)\left[e^{-\alpha_0}\ddot{\delta r} + \frac{c^2}{2}e^{-\beta_0}(1-\delta\beta)\alpha_0' + \frac{c^2}{2}e^{-\beta_0}\delta\alpha'\right] \\ &+\frac{c^2}{2}(\delta\epsilon+\delta P)e^{-\beta_0}\alpha_0' + c^2e^{-\beta_0}(1-\delta\beta)(P_0'+\delta P') = 0. \end{aligned} \tag{B.34}$$

Using equation (3.5.4) to express P_0' in terms of α_0', equation (B.34) reduces to

$$(\epsilon_0+P_0)e^{-\alpha_0}\ddot{\delta r} + \frac{c^2}{2}(\epsilon_0+P_0)e^{-\beta_0}\delta\alpha' + \frac{c^2}{2}(\delta\epsilon+\delta P)e^{-\beta_0}\alpha_0' + c^2e^{-\beta_0}\delta P' = 0. \tag{B.35}$$

Multiplying by e^{β_0}/c^2 on both sides of the equation, we obtain the equation for the evolution of δr:

$$\frac{1}{c^2}(\epsilon_0+P_0)e^{\beta_0-\alpha_0}\ddot{\delta r} + \frac{1}{2}(\epsilon_0+P_0)\delta\alpha' + \frac{1}{2}(\delta\epsilon+\delta P)\alpha_0' + \delta P' = 0. \tag{B.36}$$

Now, our mission is to obtain an equation for the evolution of δr that depends explicitly on equilibrium configuration. For this purpose, replace equation (B.27) for $\delta\alpha'$ and equations (B.20) and (B.19) for $\delta\epsilon$ and δP, respectively,

$$\begin{aligned} &\frac{1}{c^2}(\epsilon_0+P_0)e^{\beta_0-\alpha_0}\ddot{\delta r} \\ &= \frac{4\pi G}{c^4}(\epsilon_0+P_0)\left[\Gamma P_0 r^{-1}e^{\alpha_0/2+\beta_0}(r^2e^{-\alpha_0/2}\delta r)' - \left(P_0'r-\epsilon_0-P_0\right)e^{\beta_0}\delta r\right] \\ &\quad + \frac{1}{2}\left[(\epsilon_0+P_0)r^{-2}(r^2\delta re^{-\alpha_0/2})'e^{\alpha_0/2} + \Gamma P_0 r^{-2}(r^2\delta re^{-\alpha_0/2})'e^{\alpha_0/2}\right. \\ &\quad \left.+\epsilon_0'\delta r + P_0'\delta r\right]\alpha_0' + \left[\Gamma P_0 r^{-2}(r^2\delta re^{-\alpha_0/2})'e^{\alpha_0/2} + P_0'\delta r\right]'. \end{aligned} \tag{B.37}$$

If we define the **renormalized displacement function**

$$\sigma := r^2 e^{-\alpha_0/2}\delta r, \tag{B.38}$$

we can write equation (B.37) as follows

$$\begin{aligned}
&\frac{1}{c^2}(\epsilon_0 + P_0)r^{-2}e^{\beta_0-\alpha_0/2}\ddot{\sigma} \\
&= \frac{4\pi G}{c^4}(\epsilon_0 + P_0)\left[\Gamma P_0 r^{-1}e^{\alpha_0/2+\beta_0}\sigma' - (P_0' r - \epsilon_0 - P_0)\, r^{-2}e^{\alpha_0/2+\beta_0}\sigma\right] \\
&\quad + \frac{1}{2}\left[(\epsilon_0 + P_0)r^{-2}\sigma' e^{\alpha_0/2} + \Gamma P_0 r^{-2}\sigma' e^{\alpha_0/2} + (\epsilon_0' + P_0')r^{-2}e^{\alpha_0/2}\sigma\right]\alpha_0' \\
&\quad + \left[\Gamma P_0 r^{-2}\sigma' e^{\alpha_0/2} + P_0' r^{-2}e^{\alpha_0/2}\sigma\right]'.
\end{aligned} \tag{B.39}$$

Multiplying both sides by $e^{\alpha_0+\beta_0/2}$, follow by an extensive calculation, equation (B.39) reduces to

$$W\ddot{\sigma} = (Q\sigma')' + R\sigma, \tag{B.40}$$

where the coefficients are given by

$$W = \frac{1}{c^2}(\epsilon_0 + P_0)r^{-2}e^{\alpha_0/2+3\beta_0/2}, \tag{B.41}$$

$$Q = \Gamma P_0 r^{-2}e^{3\alpha_0/2+\beta_0/2}, \tag{B.42}$$

$$R = e^{3\alpha_0/2+\beta_0/2}\left[\frac{(P_0')^2}{\epsilon_0 + P_0}r^{-2} - 4P_0' r^{-3} - \frac{8\pi G}{c^4}(\epsilon_0 + P_0)P_0 r^{-2}e^{\beta_0}\right]. \tag{B.43}$$